Gravitational Labs for Nuclear Physics

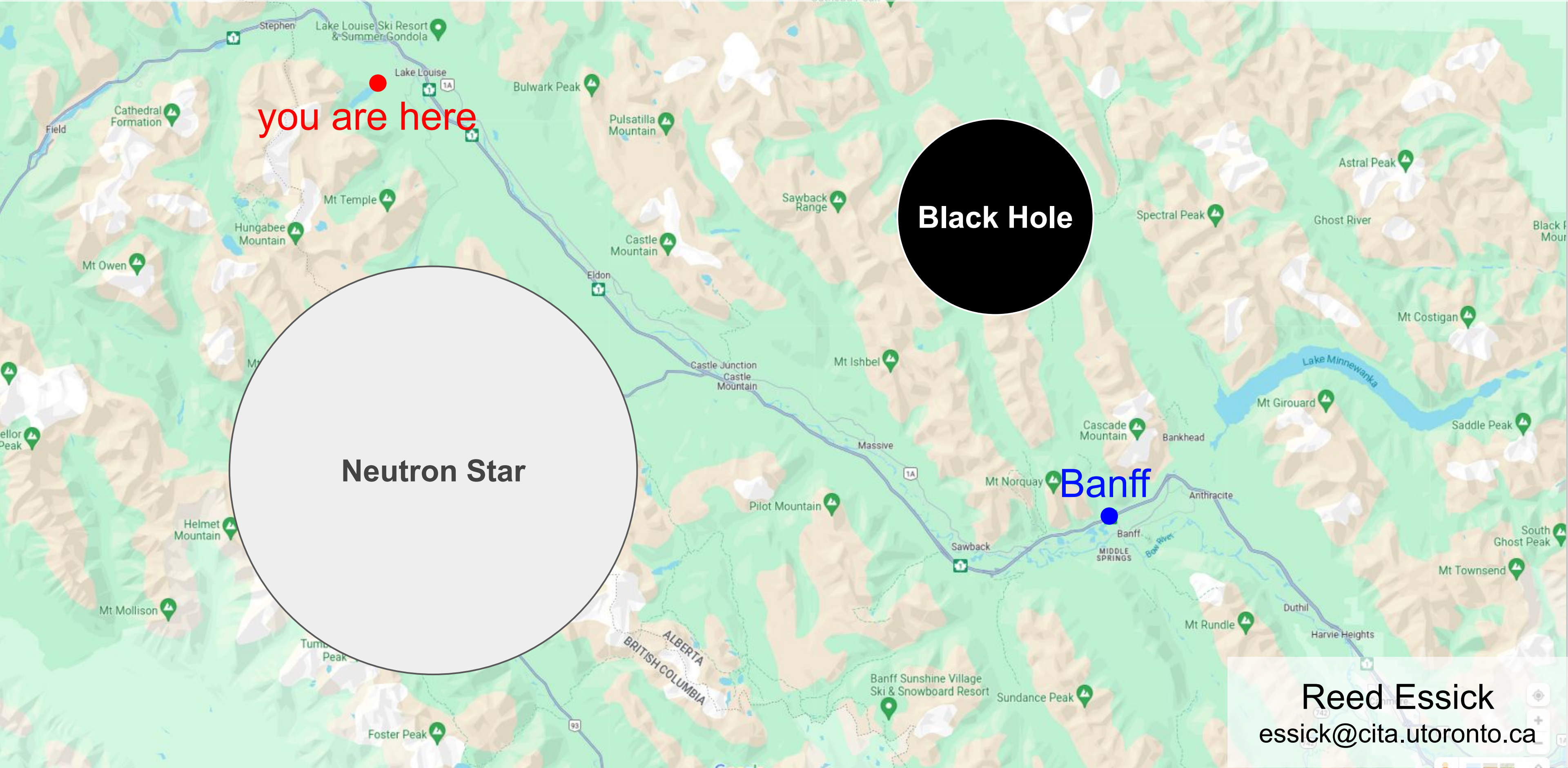

Reed Essick
essick@cita.utoronto.ca

Introduction to Gravitational Waves (GWs), Compact Binaries, and Neutron Stars

Overview of **LIGO-Virgo-KAGRA Observations**

Inferences of the **Equation of State** (EoS)

- Nonparametric EoS Representations
- Connections with Nuclear Theory and Experiment

Future **Prospects**

Introduction to Gravitational Waves (GWs), Compact Binaries, and Neutron Stars

Overview of **LIGO-Virgo-KAGRA Observations**

Inferences of the **Equation of State** (EoS)

Nonparametric EoS Representations

Connections with Nuclear Theory and Experiment

Future **Prospects**

Gravitational Waves and Compact Binaries

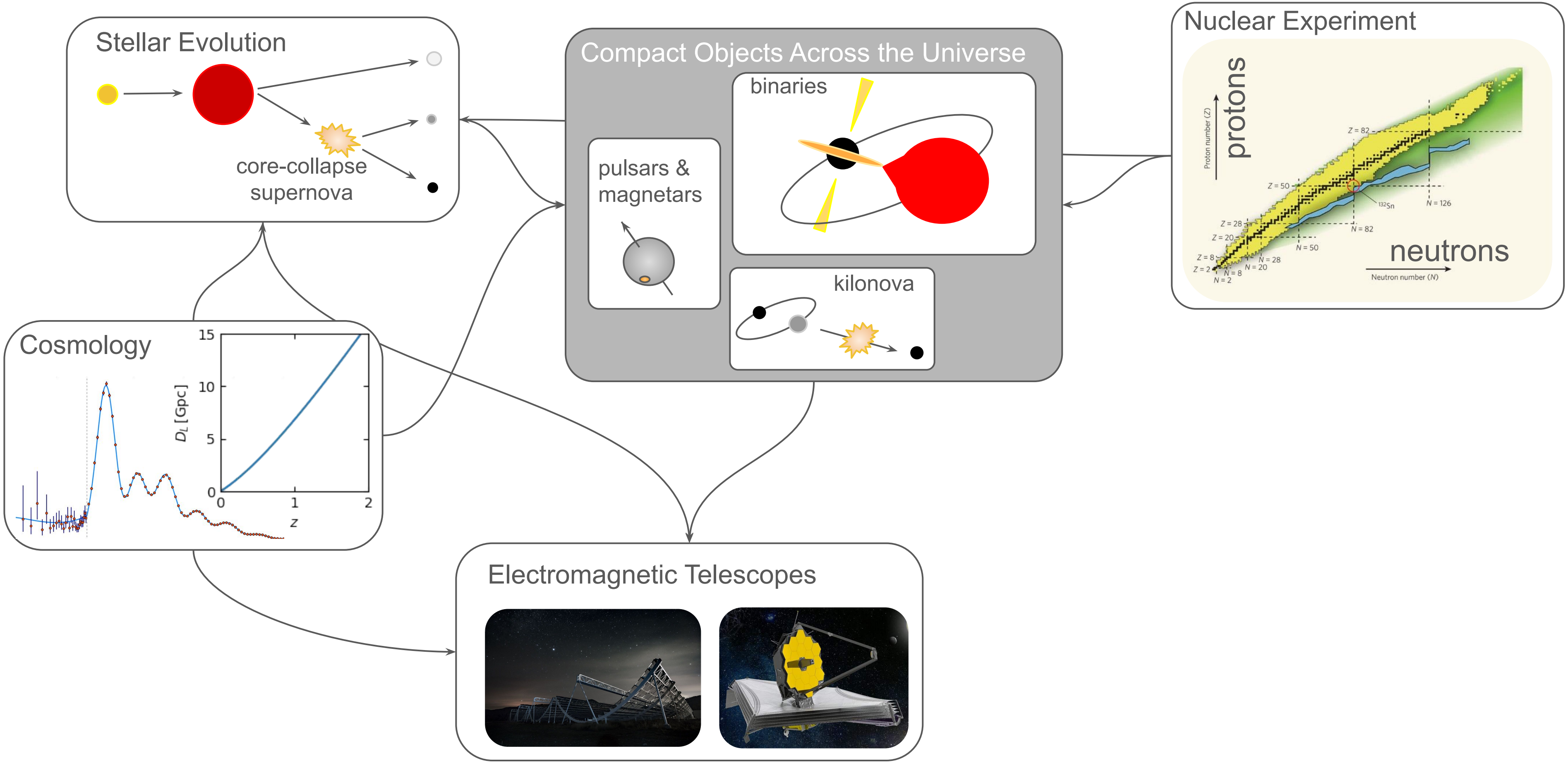

Gravitational Waves and Compact Binaries

Abbott+**Essick**+ (2016)

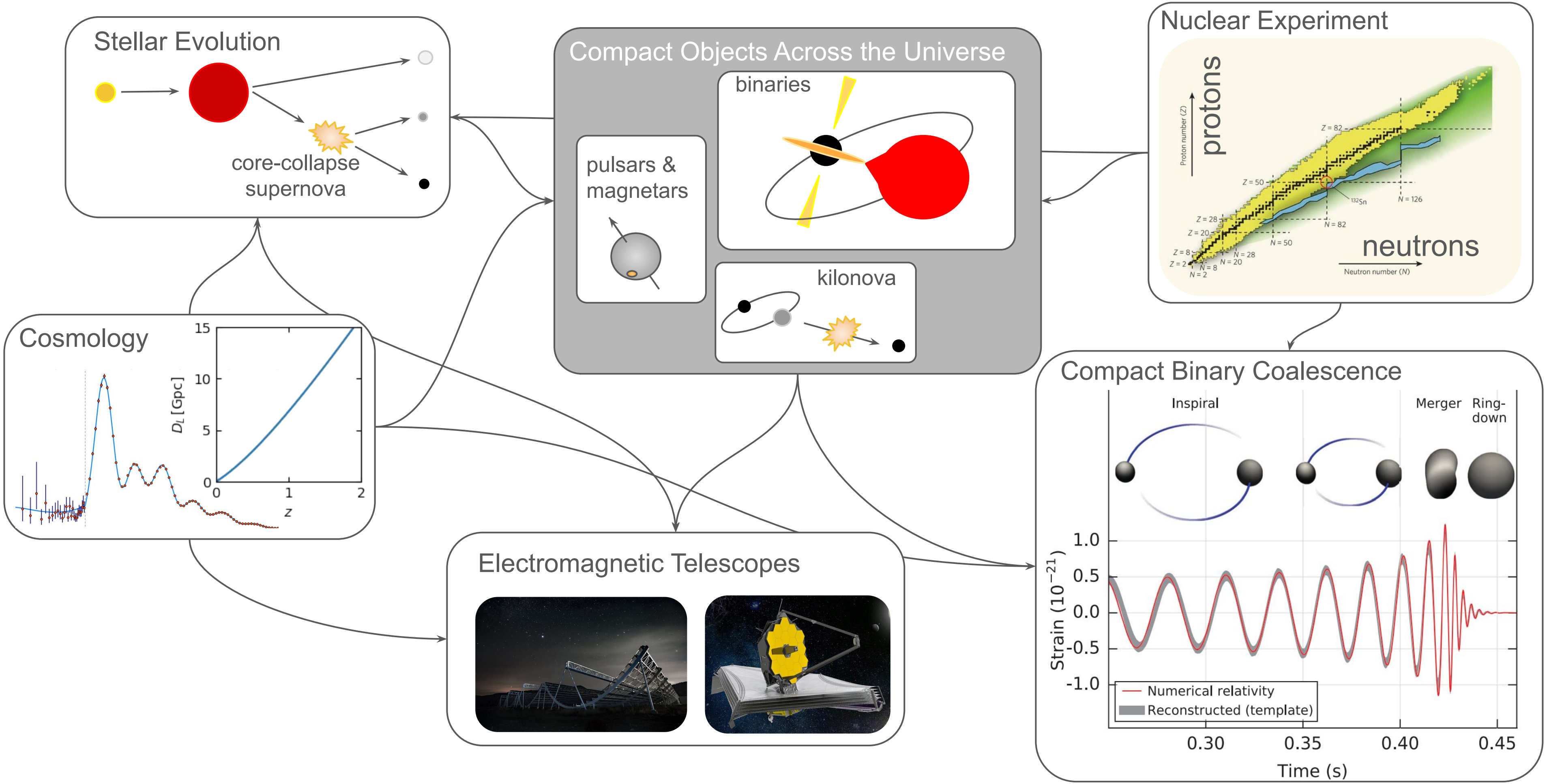

Current Interferometers (LIGO, Virgo, KAGRA)

Abbott+**Essick**+ (2016)

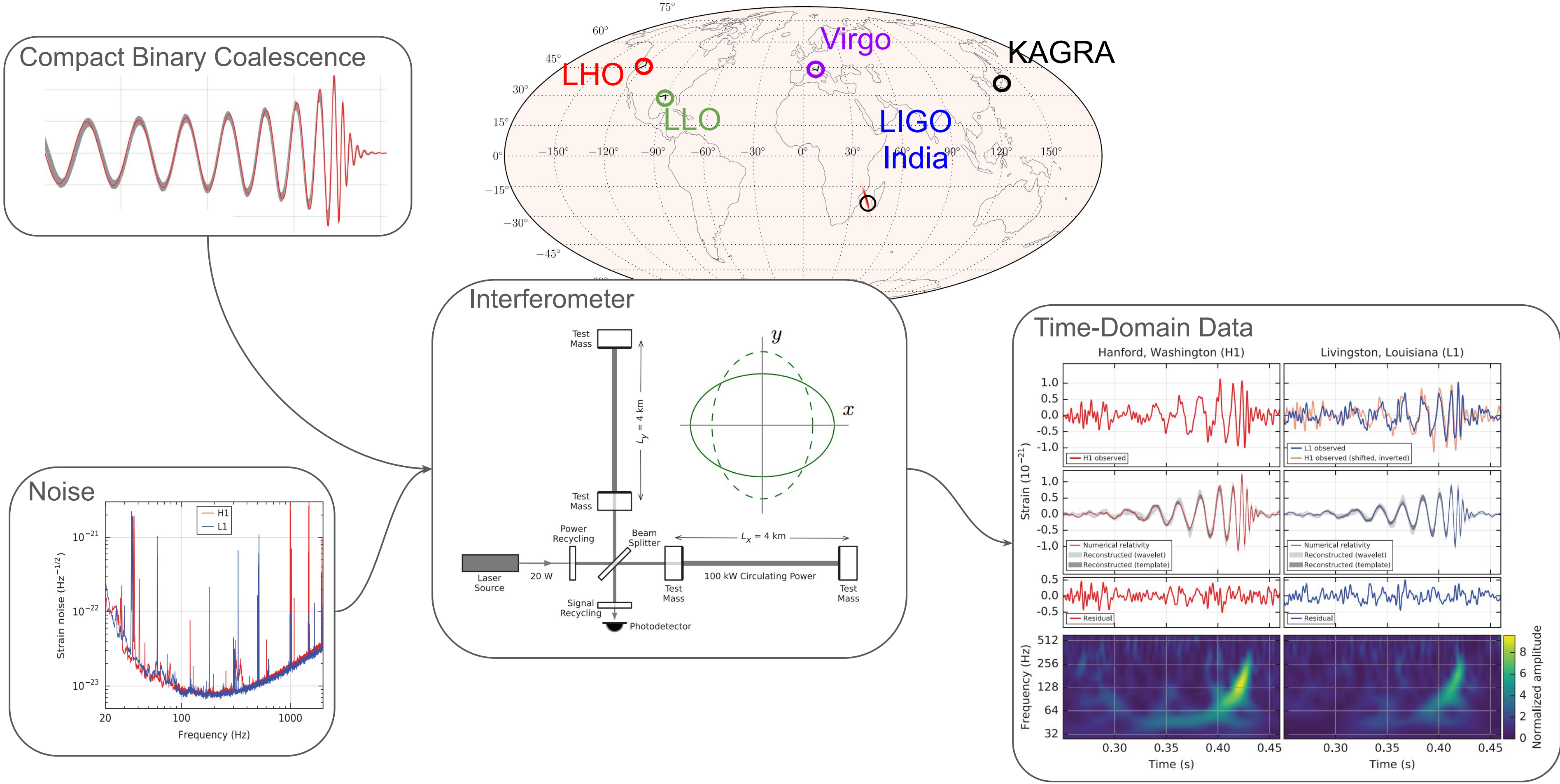

How Physical Properties Affect the Gravitational Waveform

The waveform depends on binary

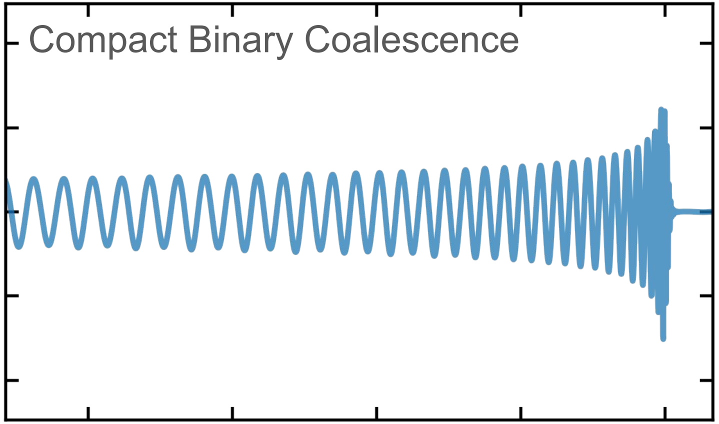

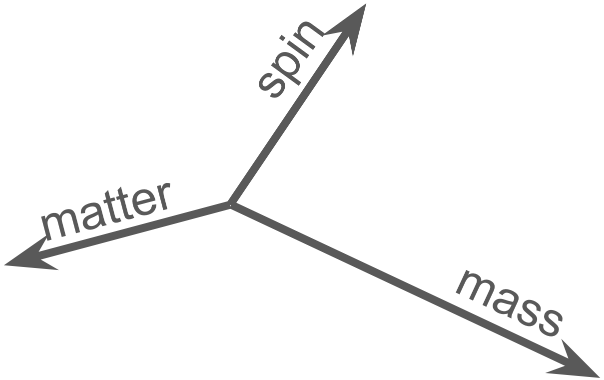

How Physical Properties Affect the Gravitational Waveform: masses

The waveform depends on binary

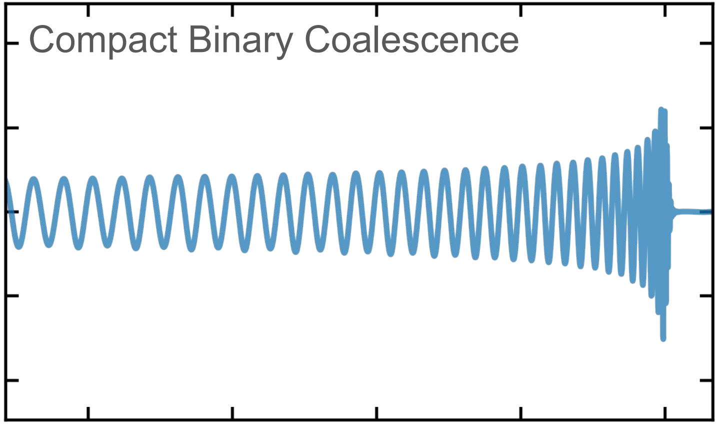

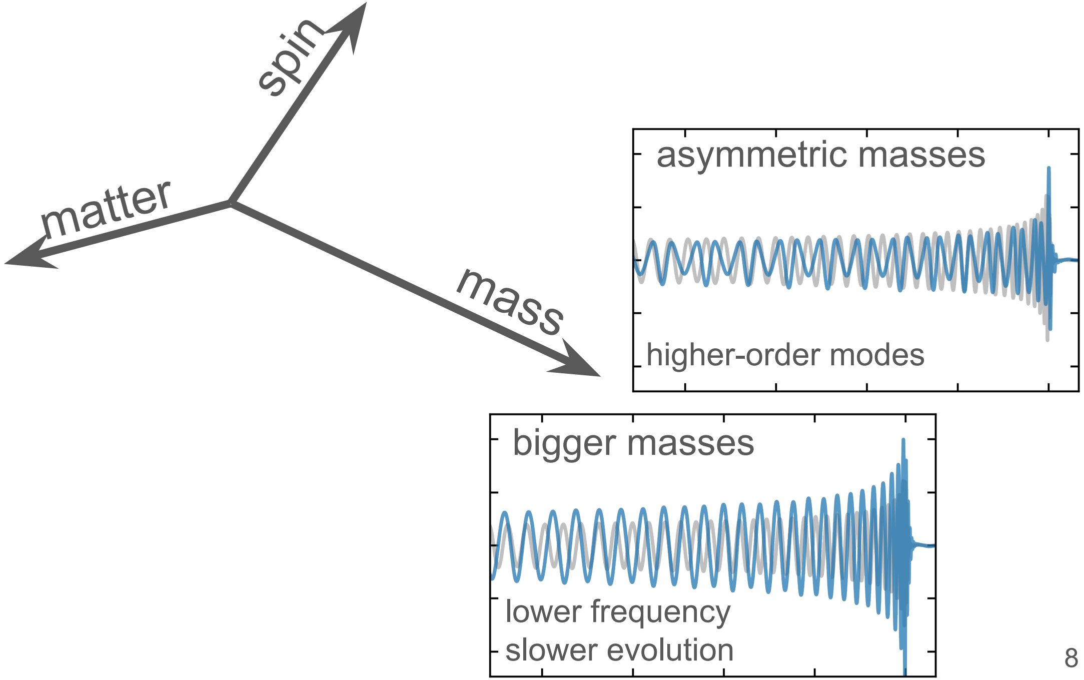

How Physical Properties Affect the Gravitational Waveform: spins

The waveform depends on binary

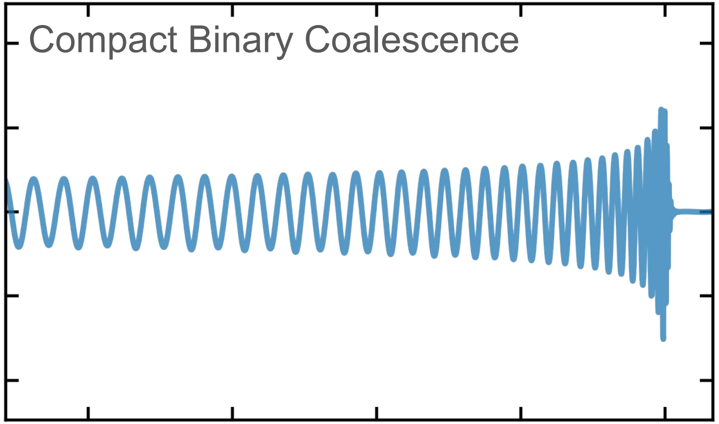

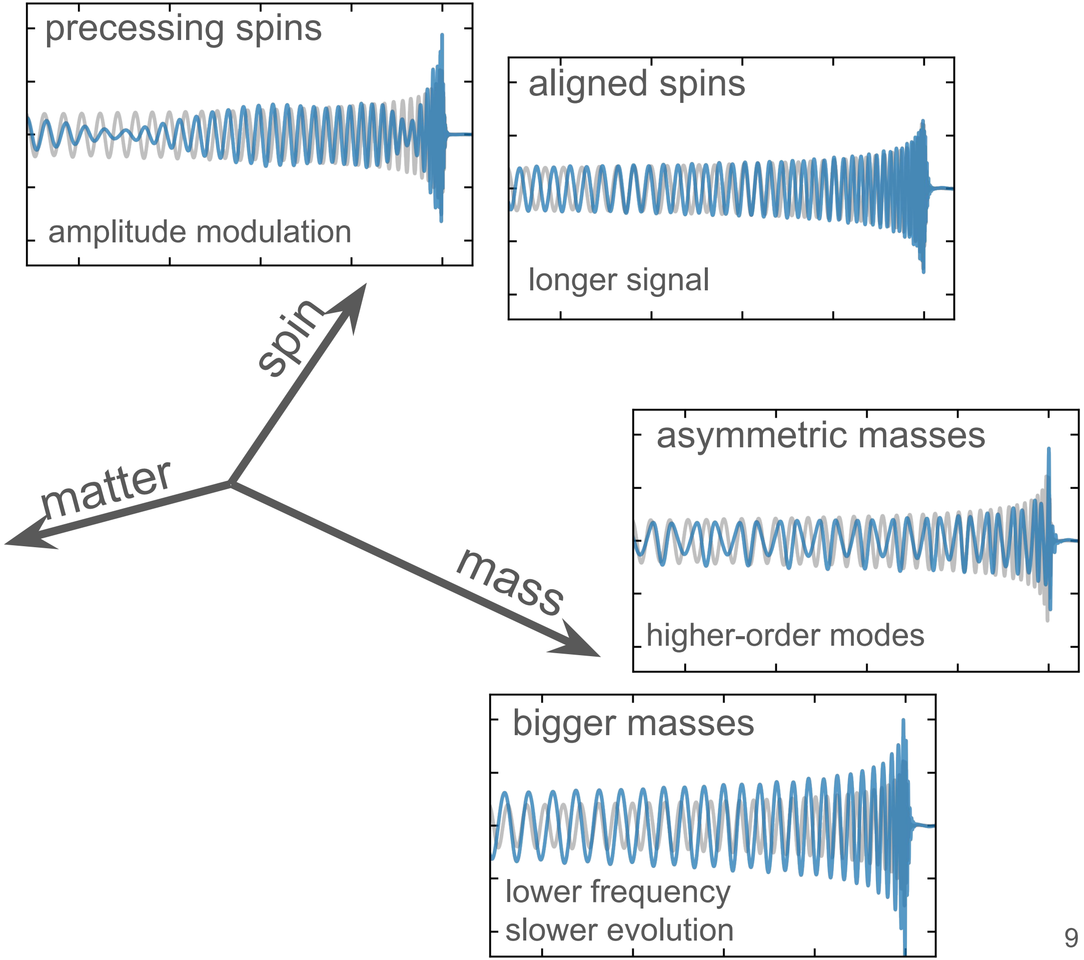

How Physical Properties Affect the Gravitational Waveform: tides

The waveform depends on binary

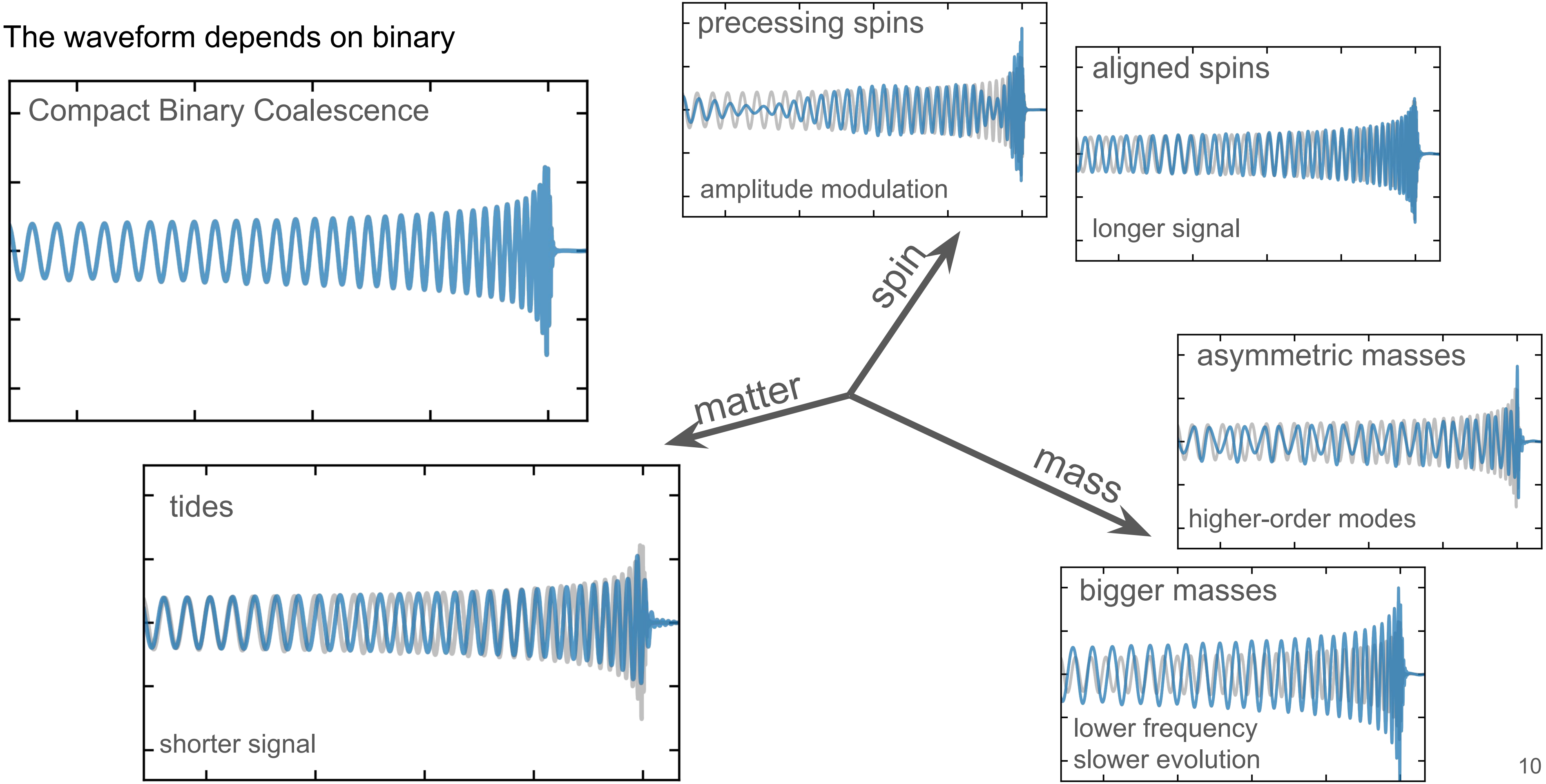

Neutron Star Structure and the Phase Plane

we don't know what particles exist in the cores of neutron stars

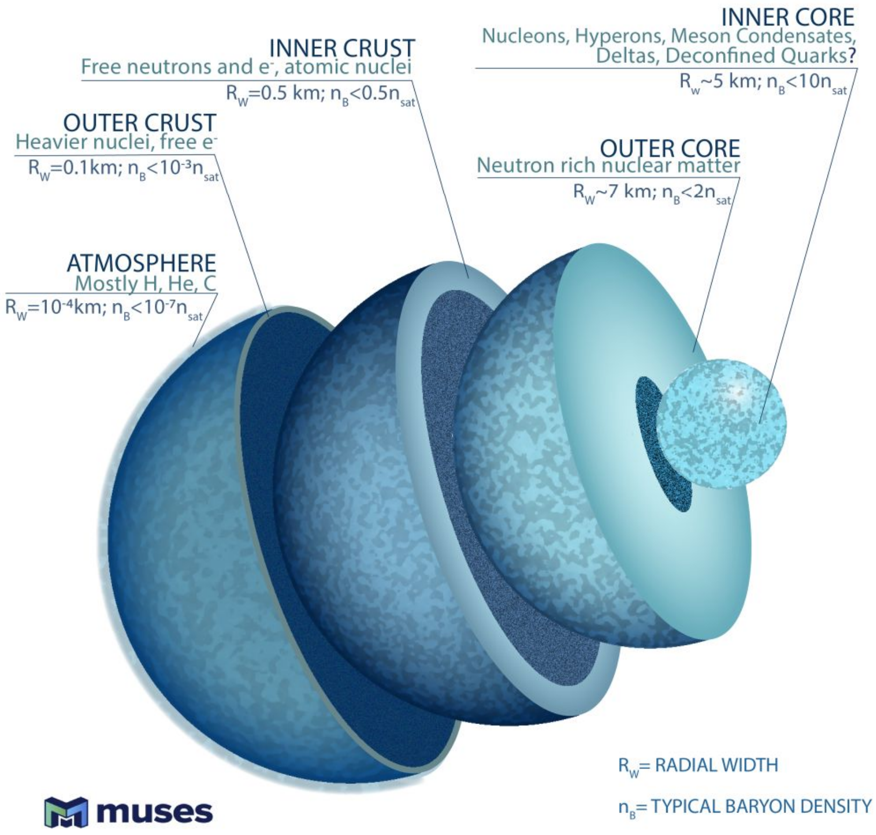

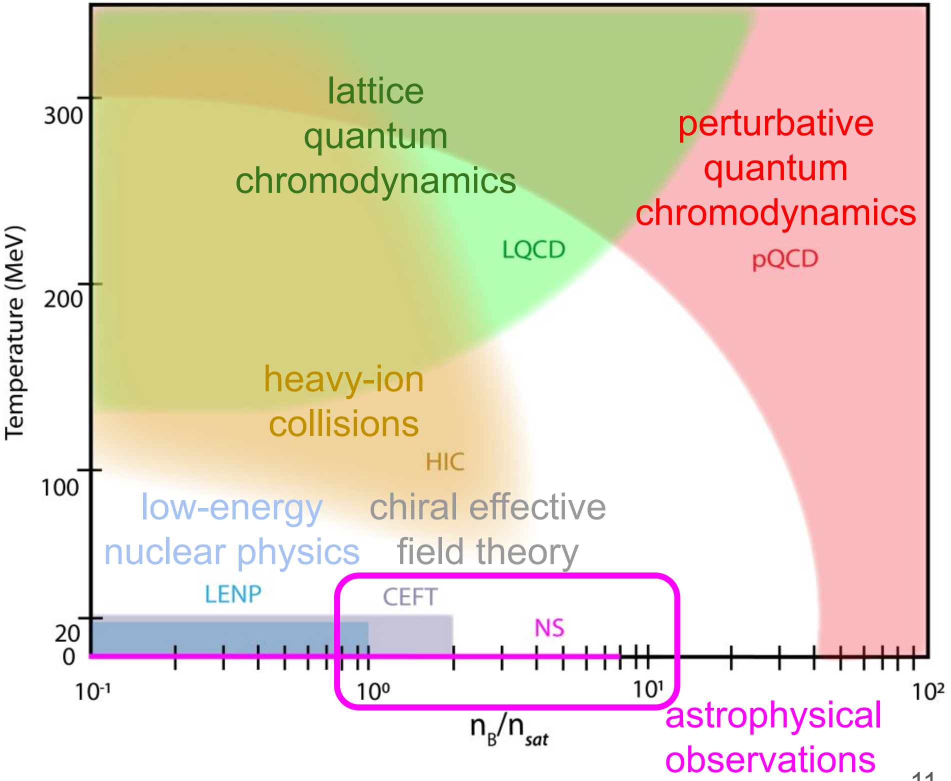

Introduction to Gravitational Waves (GWs), Compact Binaries, and Neutron Stars

Overview of **LIGO-Virgo-KAGRA Observations**

Inferences of the **Equation of State** (EoS)

Nonparametric EoS Representations

Connections with Nuclear Theory and Experiment

Future **Prospects**

Overview of LIGO-Virgo-KAGRA Observations: public data

gracedb.ligo.org

GraceDB | LVK Public Ale...

gracedb.ligo.org/superevents/public/O4/

GraceDB Public Alerts Latest Search Documentation Login

Please log in to view full database contents.

LIGO/Virgo/KAGRA Public Alerts

- More details about public alerts are provided in the LIGO/Virgo/KAGRA Alerts User Guide.
- Retractions are marked in red. Retraction means that the candidate was manually vetted and is no longer considered a candidate of interest.
- Less-significant events are marked in grey, and are not manually vetted. Consult the LVK Alerts User Guide for more information on significance in O4.
- Less-significant events are not shown by default. Press "**Show All Public Events**" to show significant and less-significant events.

O4 Significant Detection Candidates: **81** (92 Total - 11 Retracted)

O4 Low Significance Detection Candidates: **1610** (Total)

Show All Public Events

Page 1 of 7. next last »

SORT: EVENT ID (A-Z)

Event ID	Possible Source (Probability)	Significant	UTC	GCN	Location	FAR
S240109a	BBH (99%)	Yes	Jan. 9, 2024 05:04:31 UTC	GCN Circular Query Notices | VOE		1 per 4.3136 years
S240107b	BBH (97%), Terrestrial (3%)	Yes	Jan. 7, 2024 01:32:15 UTC	GCN Circular Query Notices | VOE		1.8411 per year
S240104bl	BBH (>99%)	Yes	Jan. 4, 2024 16:49:32 UTC	GCN Circular Query Notices | VOE		1 per 8.9137e+08 years
S231231ag	BBH (>99%)	Yes	Dec. 31, 2023 15:40:16 UTC	GCN Circular Query Notices | VOE		1 per 3.7932e+06 years

emfollow.docs.ligo.org/userguide

IGWN | Public Alerts Use...

emfollow.docs.ligo.org/userguide/

IGWN | Public Alerts User Guide Search userguide

Primer on public alerts for astronomers from the LIGO, Virgo, and KAGRA gravitational-wave observatories.

LIGO/Virgo/KAGRA Public Alerts User Guide

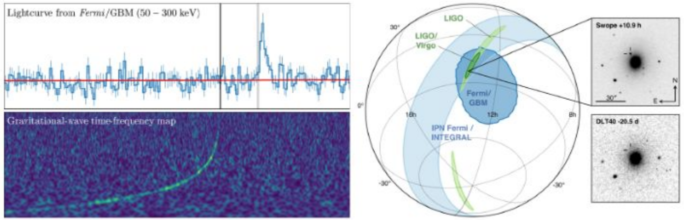

Welcome to the LIGO/Virgo/KAGRA Public Alerts User Guide! This document is intended for both professional astronomers and science enthusiasts who are interested in receiving alerts and real-time data products related to gravitational-wave (GW) events.

Four sites (LHO, LLO, Virgo, KAGRA) together form a global network of ground-based GW detectors. The LIGO Scientific Collaboration, the Virgo Collaboration, and the KAGRA Collaboration jointly analyze the data in real time to detect and localize transients from compact binary mergers and other sources. When a signal candidate is found, an alert is sent to astronomers in order to search for counterparts (electromagnetic waves or neutrinos).

LIGO/Virgo/KAGRA alerts are public. Alerts are distributed through NASA's General Coordinates Network (GCN, https://gcn.nasa.gov) and Scalable Cyberinfrastructure to support Multi-Messenger Astrophysics (SCiMMA, https://scimma.org). There are two types of alerts: human-readable GCN Circulars and machine-readable Notices. This document provides a brief overview of the procedures for vetting and sending GW alerts, describes their contents and format, and includes instructions and sample code for receiving Notices and decoding GW sky maps.

Overview of LIGO-Virgo-KAGRA Observations: public data

gwosc.org

Overview of LIGO-Virgo-KAGRA Observations: past & present

Abbott+**Essick+** (2023)

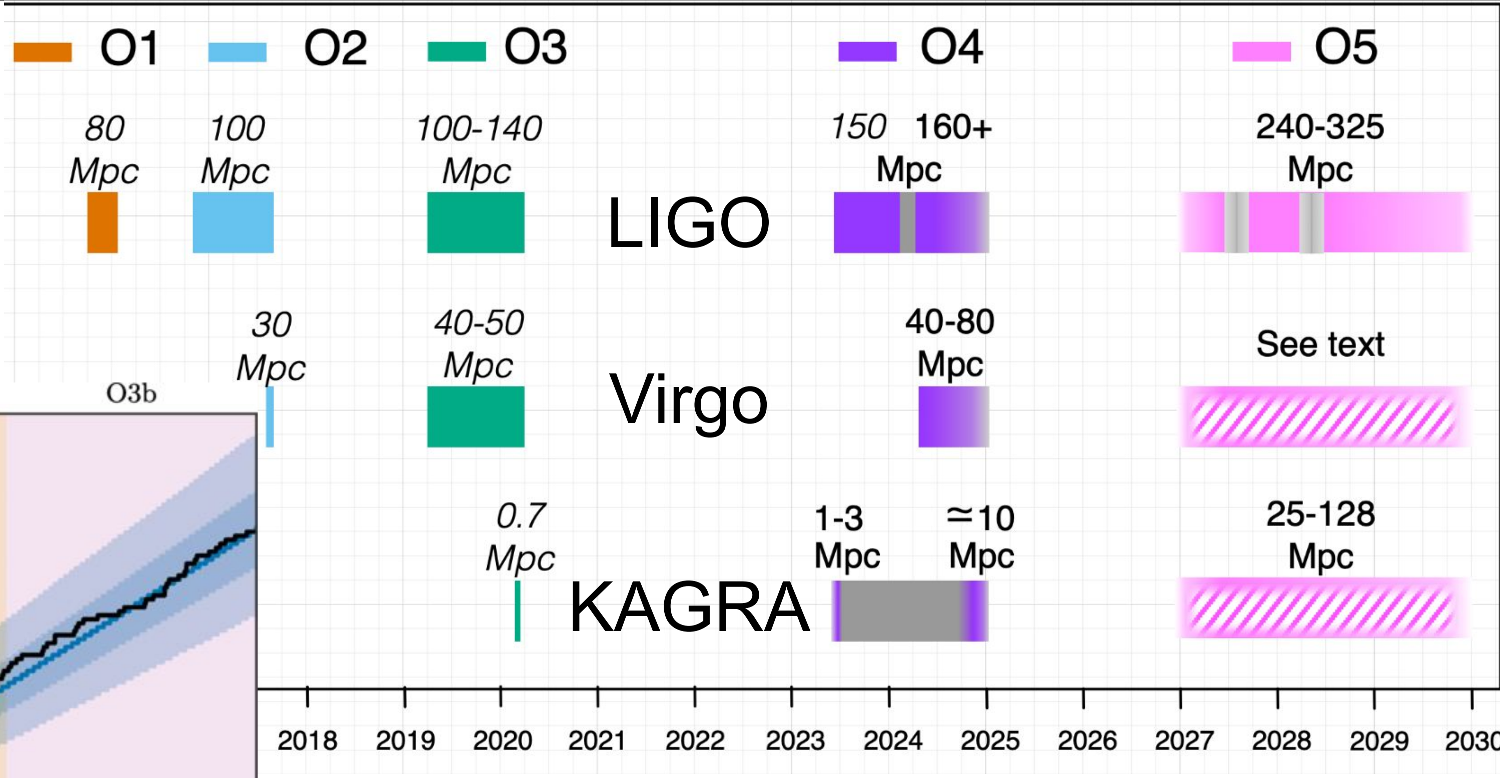

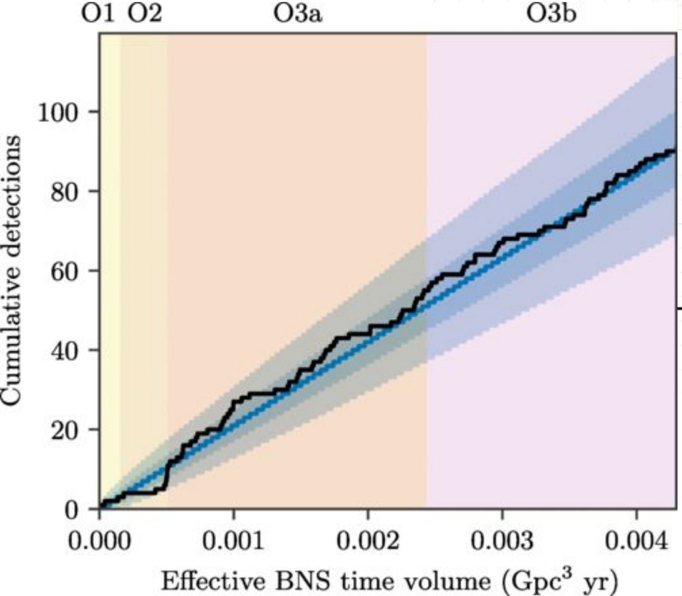

Overview of LIGO-Virgo-KAGRA Observations: detections

Geller+ (2023)

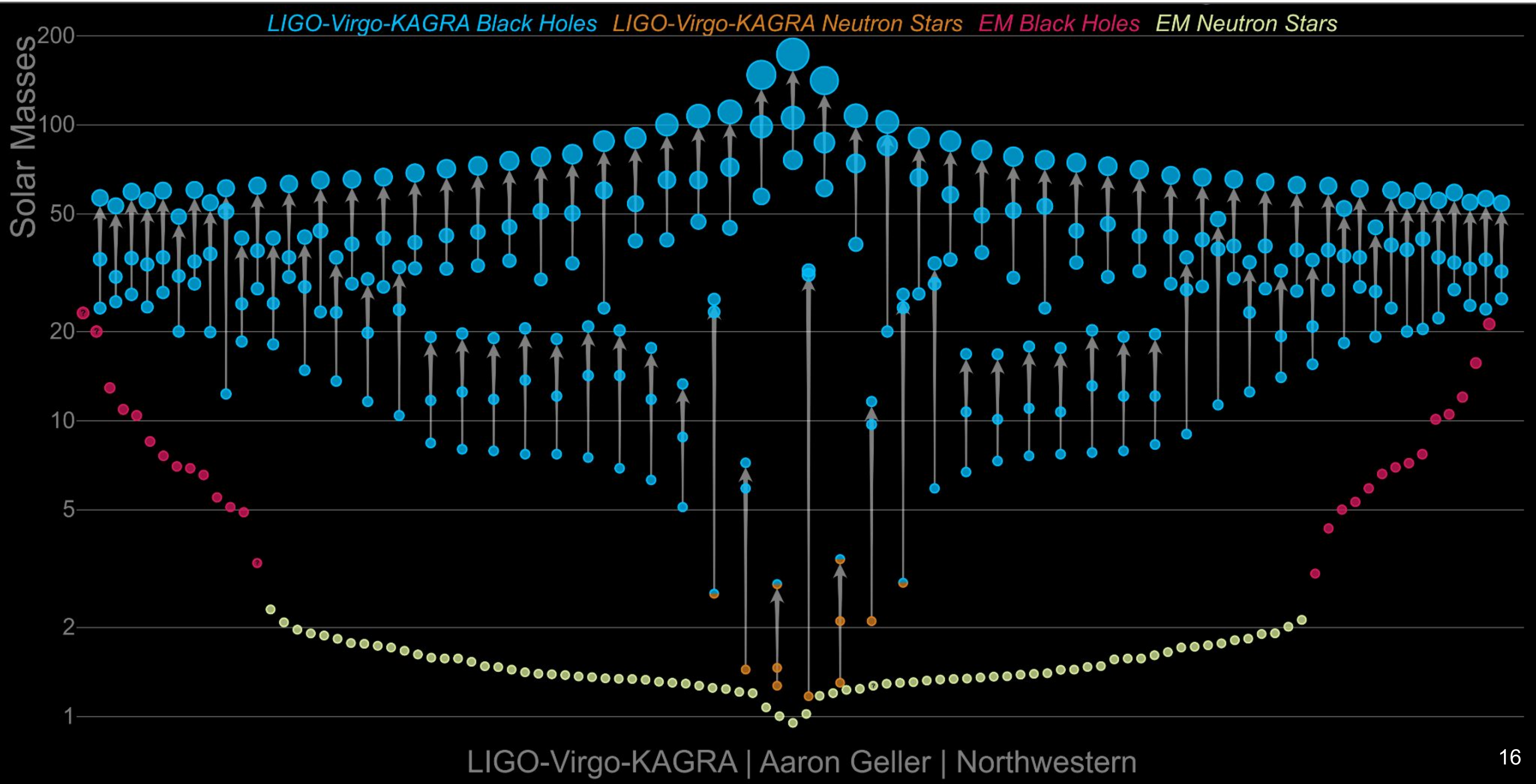

Overview of LIGO-Virgo-KAGRA Observations: masses

Farah+**Essick+** (2022)

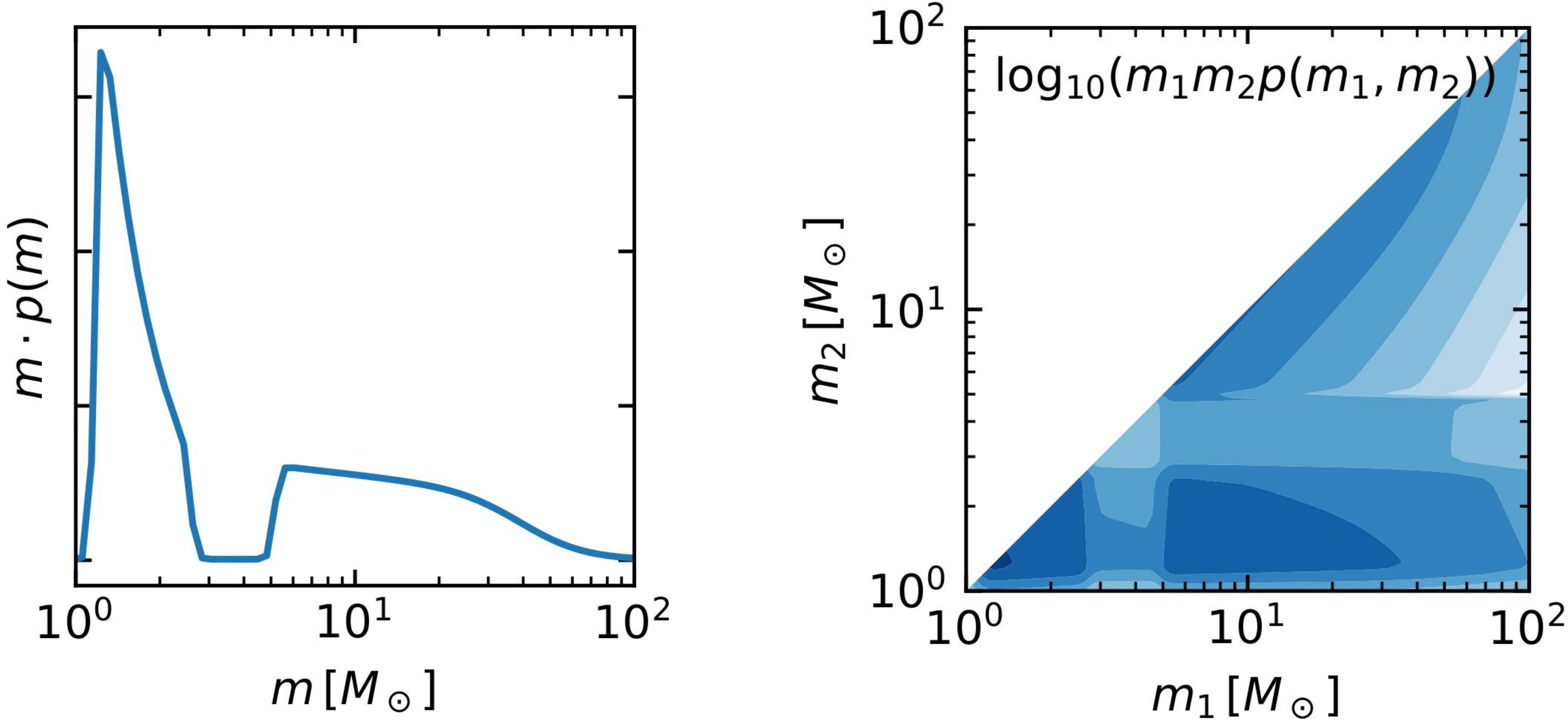

Overview of LIGO-Virgo-KAGRA Observations: masses (BBH)

Abbott+**Essick+** (2021)

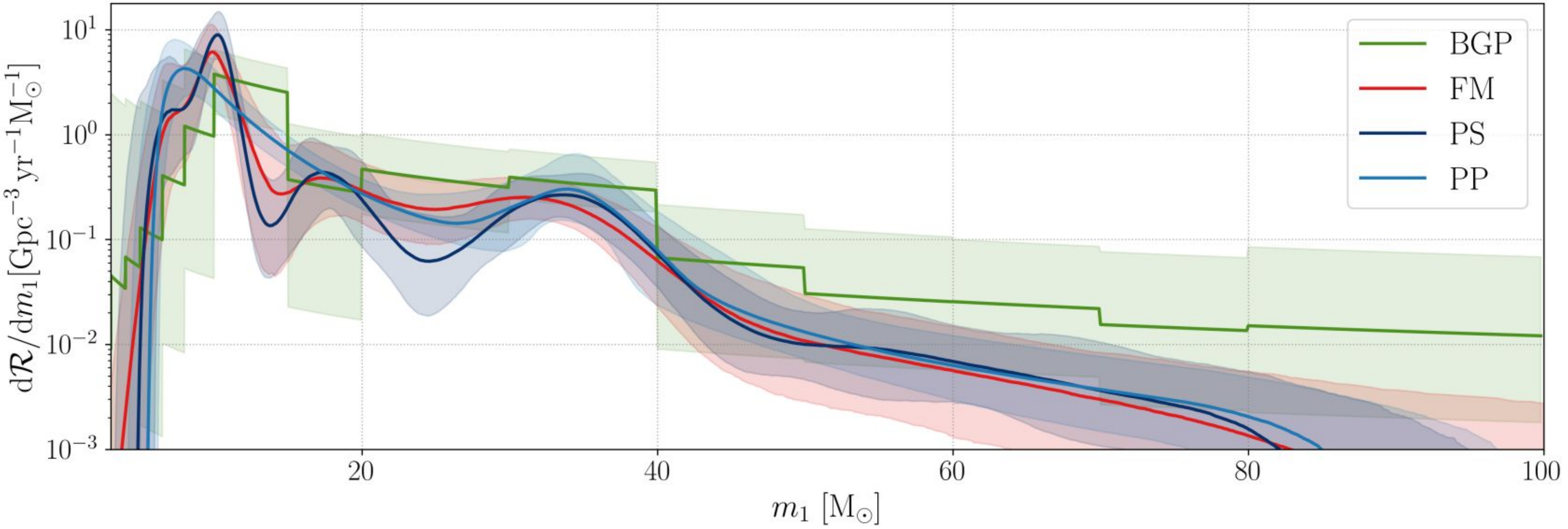

Introduction to Gravitational Waves (GWs), Compact Binaries, and Neutron Stars

Overview of **LIGO-Virgo-KAGRA Observations**

Inferences of the **Equation of State** (EoS)

- Nonparametric EoS Representations
- Connections with Nuclear Theory and Experiment

Future **Prospects**

Inference of the NS EoS: nonparametric results

Current *Theory Agnostic* Constraints

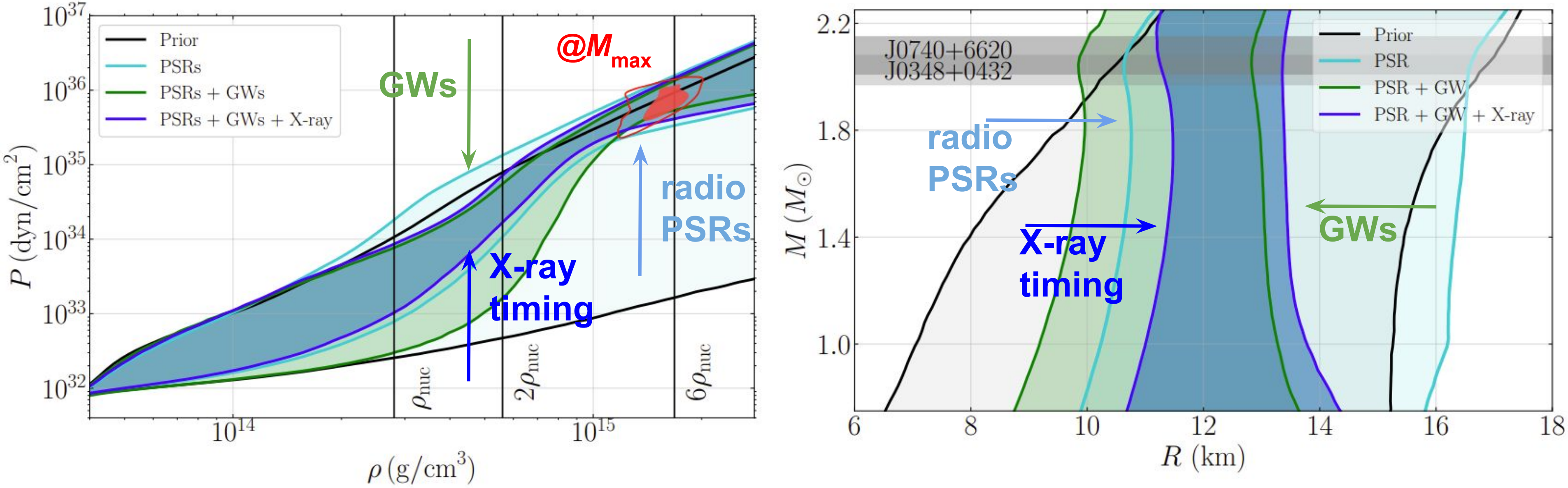

Inference of the NS EoS: nonparametric results

Legred+**Essick**+ (2021)

Current *Theory Agnostic* Constraints

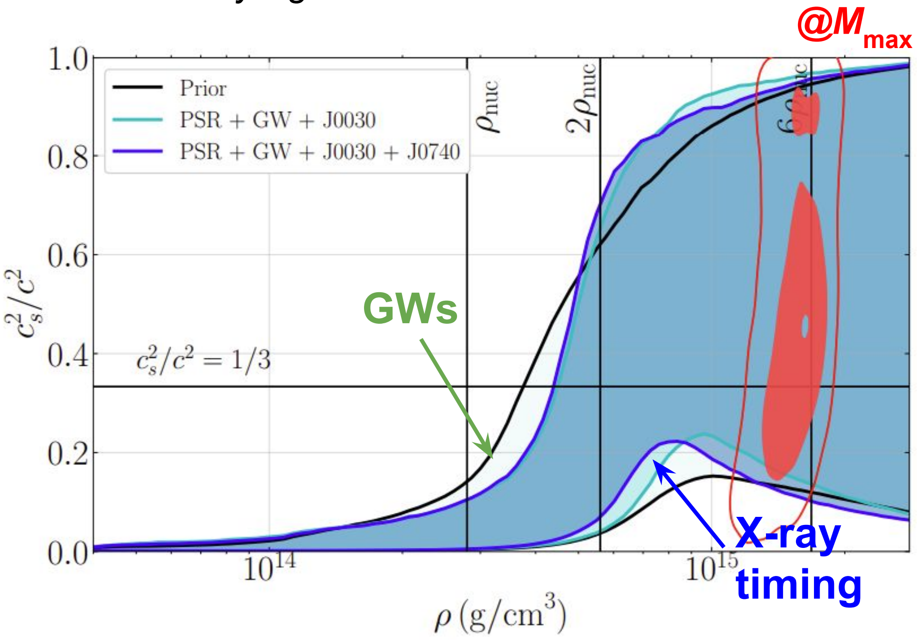

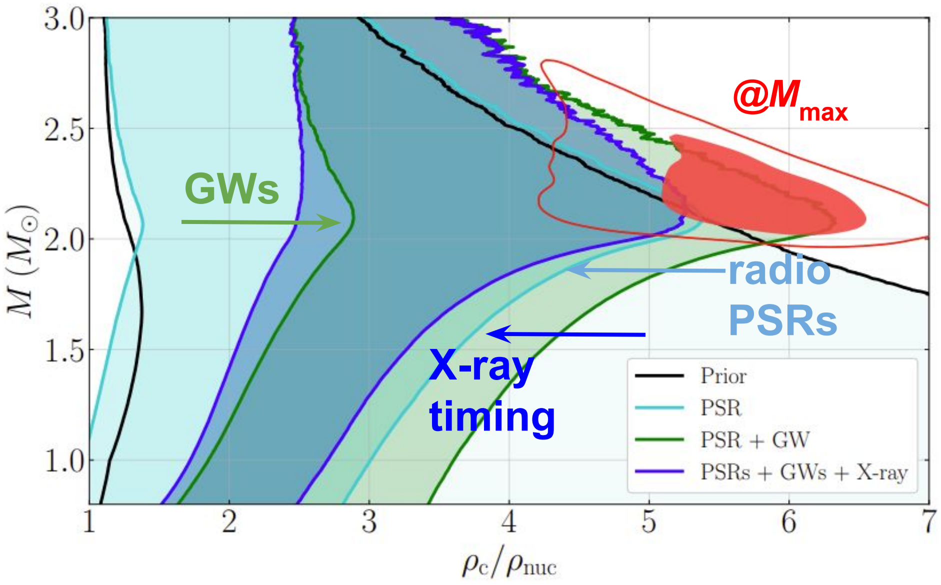

supranuclear sound speed almost certainly exceeds the conformal limit
→strongly-coupled interactions

maximum central density is likely ~6ρ_{nuc}

Inference of the NS EoS: nonparametric results

Legred+**Essick**+ (2021)

	Observable	Prior	w/ PSRs	w/o J0740+6620	w/J0740+6620	
					Miller+	Riley+
Properties of the EoS	$\boxed{M_{\max}\ [\mathrm{M}_\odot]}$	$1.47^{+0.71}_{-1.37}$	$2.24^{+0.48}_{-0.24}$	$2.20^{+0.30}_{-0.19}$	$\boxed{2.21^{+0.31}_{-0.21}}$	$2.19^{+0.27}_{-0.19}$
	$p(\rho_{\rm nuc})$ [10^{33}dyn/cm^2]	$2.25^{+5.81}_{-2.15}$	$6.07^{+7.53}_{-5.93}$	$4.05^{+3.59}_{-3.74}$	$4.30^{+3.37}_{-3.80}$	$4.15^{+3.50}_{-3.76}$
	$p(2\rho_{\rm nuc})$ [10^{34}dyn/cm^2]	$1.22^{+4.86}_{-1.21}$	$6.00^{+4.79}_{-5.99}$	$3.75^{+2.36}_{-2.98}$	$4.38^{+2.46}_{-2.96}$	$3.90^{+2.11}_{-2.88}$
	$p(6\rho_{\rm nuc})$ [10^{35}dyn/cm^2]	$2.43^{+4.70}_{-2.43}$	$7.51^{+6.77}_{-5.15}$	$8.33^{+5.22}_{-4.14}$	$7.41^{+5.87}_{-4.18}$	$7.82^{+5.47}_{-3.53}$
	$\max\{c_s^2/c^2\} \mid \rho \le \rho_c(M_{\max})$	$0.76^{+0.24}_{-0.37}$	$0.72^{+0.28}_{-0.26}$	$0.84^{+0.16}_{-0.28}$	$0.75^{+0.25}_{-0.24}$	$0.80^{+0.20}_{-0.26}$
	$\rho(\max\{c_s^2/c^2\})$ [10^{15}g/cm^3]	$1.38^{+1.65}_{-1.34}$	$0.97^{+0.64}_{-0.70}$	$1.13^{+0.64}_{-0.63}$	$1.01^{+0.63}_{-0.53}$	$1.10^{+0.63}_{-0.58}$
	$p(\max\{c_s^2/c^2\})$ [10^{35}dyn/cm^2]	$1.65^{+8.16}_{-1.65}$	$2.68^{+5.18}_{-2.68}$	$3.52^{+6.90}_{-3.48}$	$2.77^{+5.81}_{-2.70}$	$3.26^{+6.51}_{-3.15}$
Properties defined for both NSs and BHs	$\boxed{R_{1.4}\ [\mathrm{km}]}$	$8.09^{+5.68}_{-3.96}$	$13.54^{+2.61}_{-3.13}$	$12.25^{+1.13}_{-1.33}$	$\boxed{12.56^{+1.00}_{-1.07}}$	$12.34^{+1.01}_{-1.25}$
	$R_{2.0}$ [km]	$5.90^{+6.97}_{-0.00}$	$13.18^{+3.02}_{-2.90}$	$12.05^{+1.18}_{-1.45}$	$12.41^{+1.00}_{-1.10}$	$12.09^{+1.07}_{-1.17}$
	$\Delta R \equiv R_{2.0} - R_{1.4}$ [km]	$0.48^{+1.28}_{-6.67}$	$-0.07^{+1.00}_{-1.04}$	$-0.17^{+0.85}_{-0.83}$	$-0.12^{+0.83}_{-0.85}$	$-0.20^{+0.82}_{-0.88}$
	$\Lambda_{1.4}$	24^{+841}_{-24}	795^{+1262}_{-708}	442^{+235}_{-274}	507^{+234}_{-242}	457^{+219}_{-256}
	$\Lambda_{2.0}$	0^{+54}_{-0}	66^{+184}_{-66}	34^{+35}_{-27}	44^{+34}_{-30}	35^{+32}_{-24}
Properties defined only for NSs	$\rho_c(1.4\,\mathrm{M}_\odot)$ [10^{14}g/cm^3]	$8.4^{+12.5}_{-6.0}$	$5.7^{+3.2}_{-3.1}$	$7.2^{+2.6}_{-1.7}$	$6.7^{+1.7}_{-1.3}$	$7.1^{+2.1}_{-1.5}$
	$\rho_c(2.0\,\mathrm{M}_\odot)$ [10^{14}g/cm^3]	$9.0^{+5.7}_{-6.3}$	$8.5^{+4.8}_{-5.3}$	$10.5^{+4.1}_{-3.8}$	$9.7^{+3.6}_{-3.1}$	$10.4^{+3.6}_{-3.5}$
	$\rho_c(M_{\max})$ [10^{15}g/cm^3]	$2.4^{+0.9}_{-2.0}$	$1.4^{+0.5}_{-0.6}$	$1.6^{+0.3}_{-0.4}$	$1.5^{+0.3}_{-0.4}$	$1.6^{+0.3}_{-0.3}$

$M_{max} \sim 2.21 \pm 0.25\ M_\odot$

$R(1.4M_\odot) \sim 12.5 \pm 1$ km

at 90% credibility

Introduction to Gravitational Waves (GWs), Compact Binaries, and Neutron Stars

Overview of **LIGO-Virgo-KAGRA Observations**

Inferences of the **Equation of State** (EoS)

- Nonparametric EoS Representations
- Connections with Nuclear Theory and Experiment

Future **Prospects**

Inference of the NS EoS: incorporating low-density nuclear theory

Essick+ (2020)

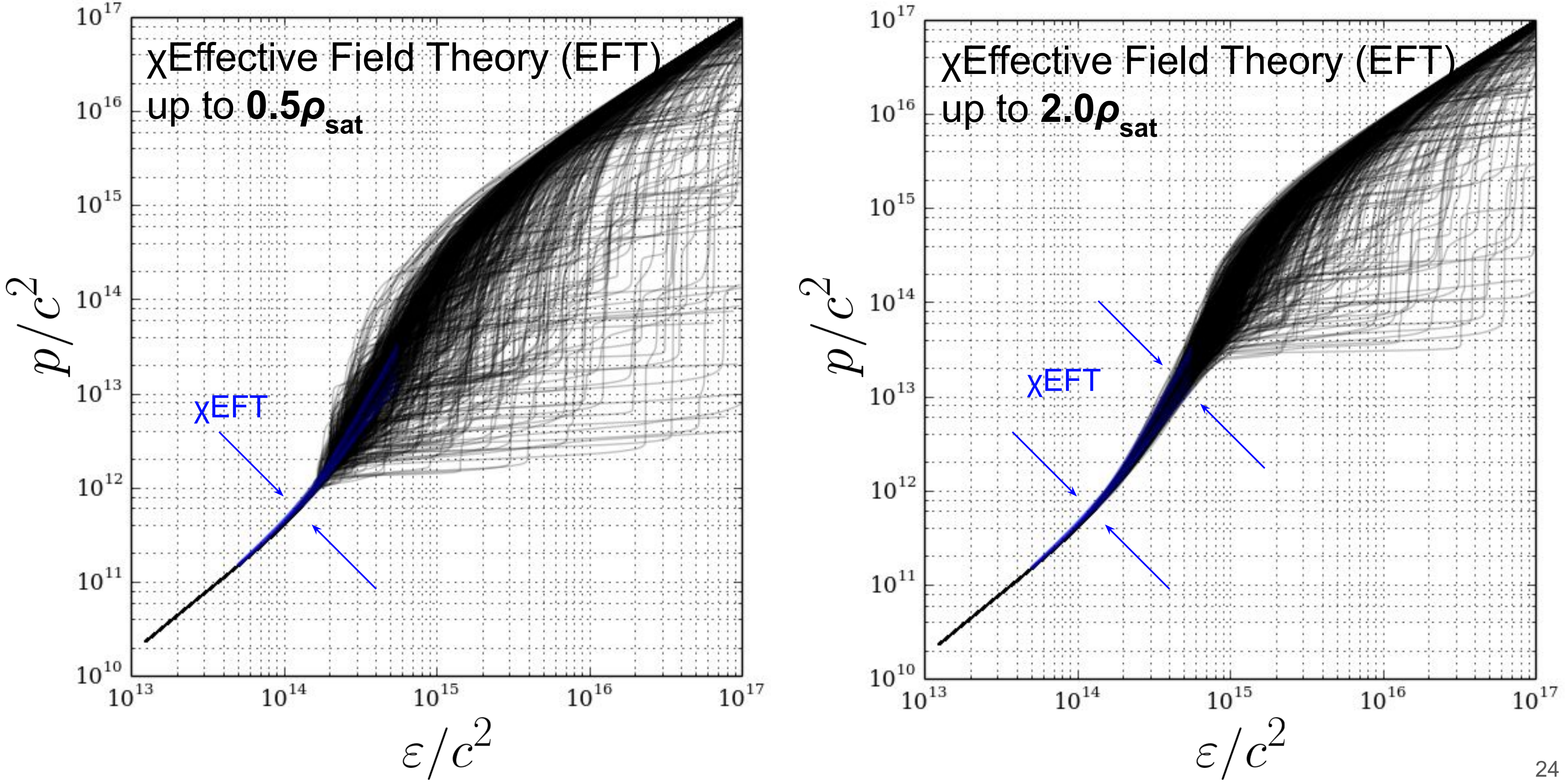

Inference of the NS EoS: incorporating low-density nuclear theory

Essick+ (2020)

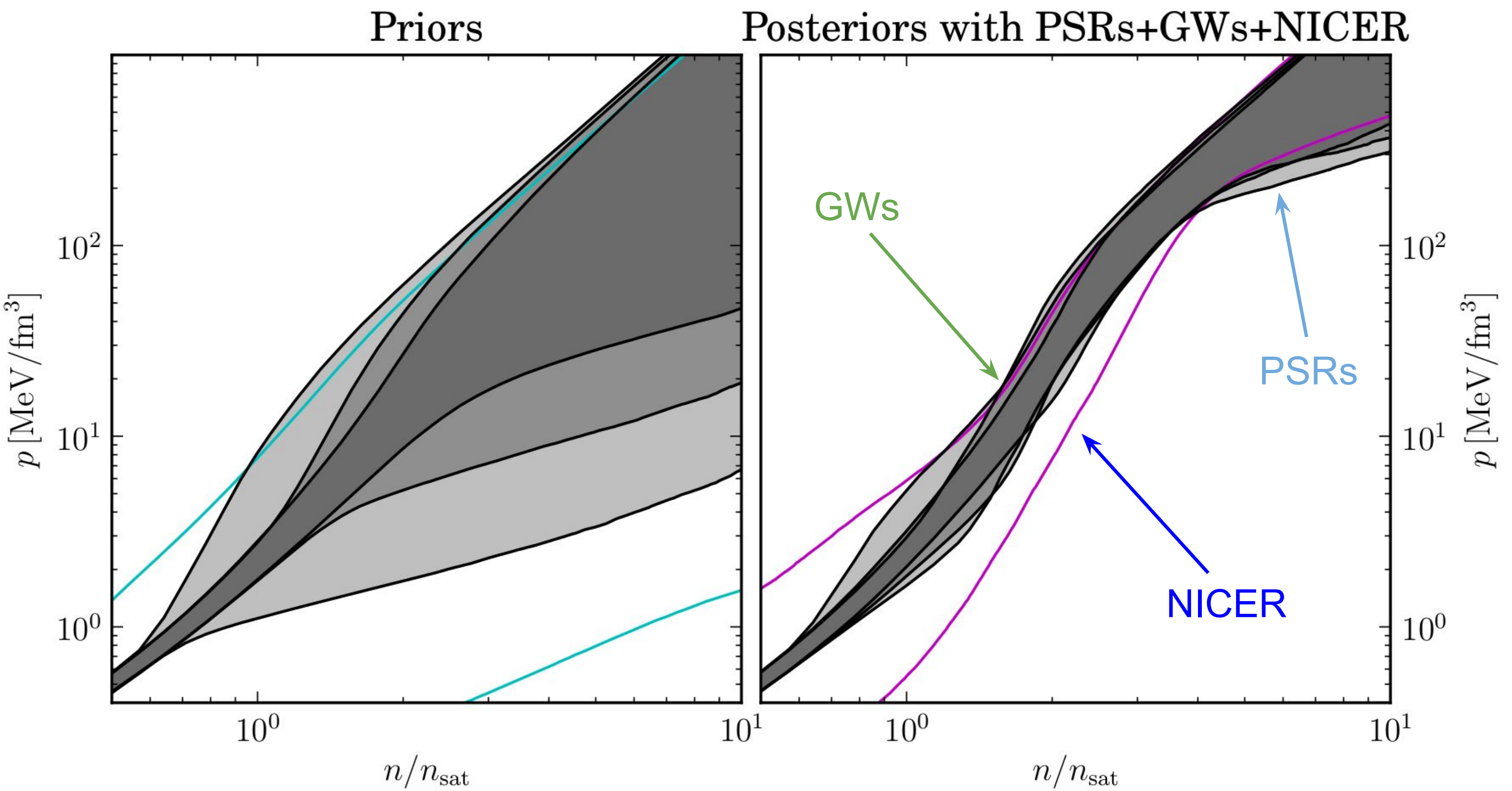

Inference of the NS EoS: comparing low-density theories

Essick+ (2020)

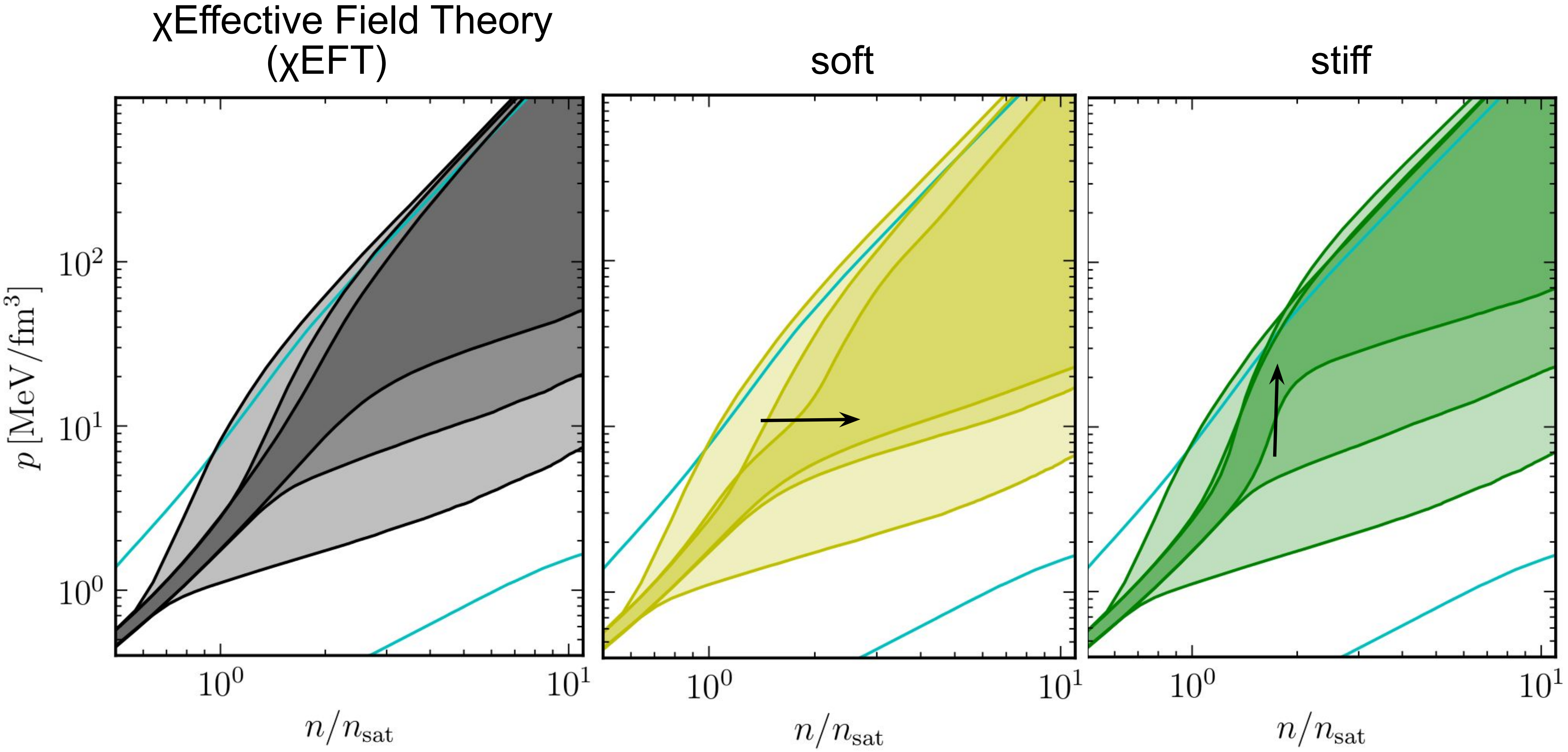

Inference of the NS EoS: comparing low-density theories

Essick+ (2020)

PSR+GW

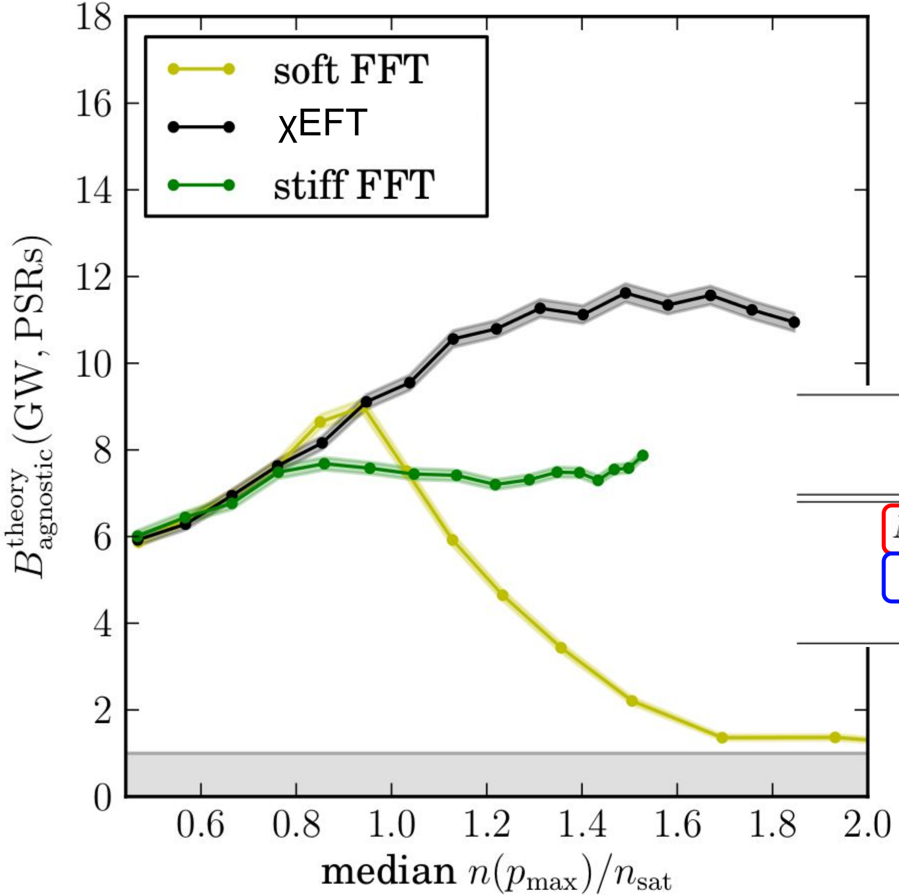

Quantity	Marginalized $\mathrm{QMC}^{(2018)}_{\mathrm{N^2LO,l}}$		Completely Agnostic	
	PSRs+GWs	+NICER	PSRs+GWs	+NICER
$M_{\max}$ $[M_\odot]$	$2.19^{+0.24}_{-0.18}$	$2.24^{+0.31}_{-0.23}$	$2.20^{+0.24}_{-0.18}$	$2.22^{+0.30}_{-0.20}$
$R_{1.4}$ [km]	$11.40^{+1.38}_{-1.04}$	$12.54^{+0.71}_{-0.63}$	$10.95^{+2.00}_{-1.37}$	$12.32^{+1.09}_{-1.47}$
$\Lambda_{1.4}$	260^{+270}_{-140}	494^{+201}_{-166}	228^{+319}_{-134}	451^{+241}_{-279}

$M_{\max} \sim 2.24 \pm 0.25\ M_\odot$

$R(1.4M_\odot) \sim 12.5 \pm 0.7$ km

at 90% credibility

Inference of the NS EoS: low-density nuclear experiment

Connection to "new" experimental probes: Neutron Skin Thickness ($R_{\rm skin}$)

Reed+(2021) infer $L \gtrsim 100$ MeV based on $R_{\rm skin} = 0.29 \pm 0.07$ fm. Suggest this implies $R_{1.4} \gtrsim 14$ km.

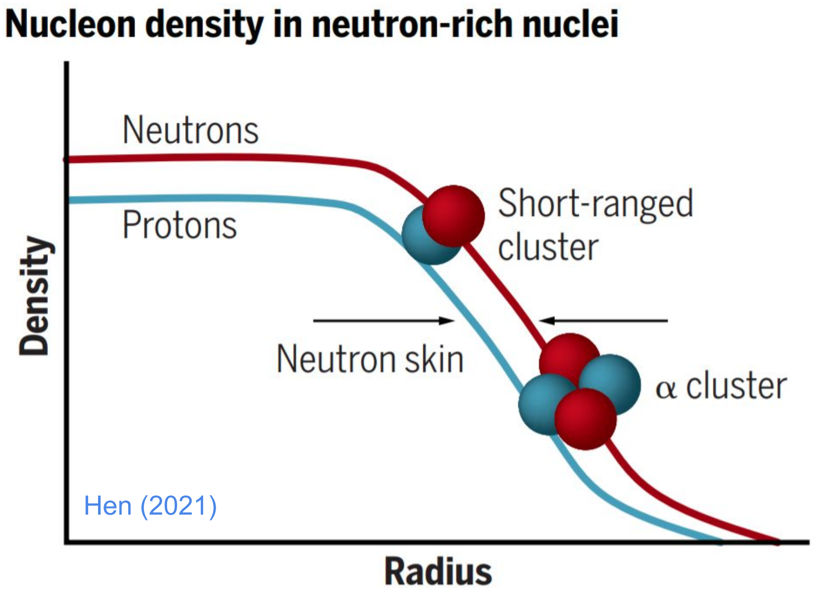

Scattering experiments (PREX) measure this

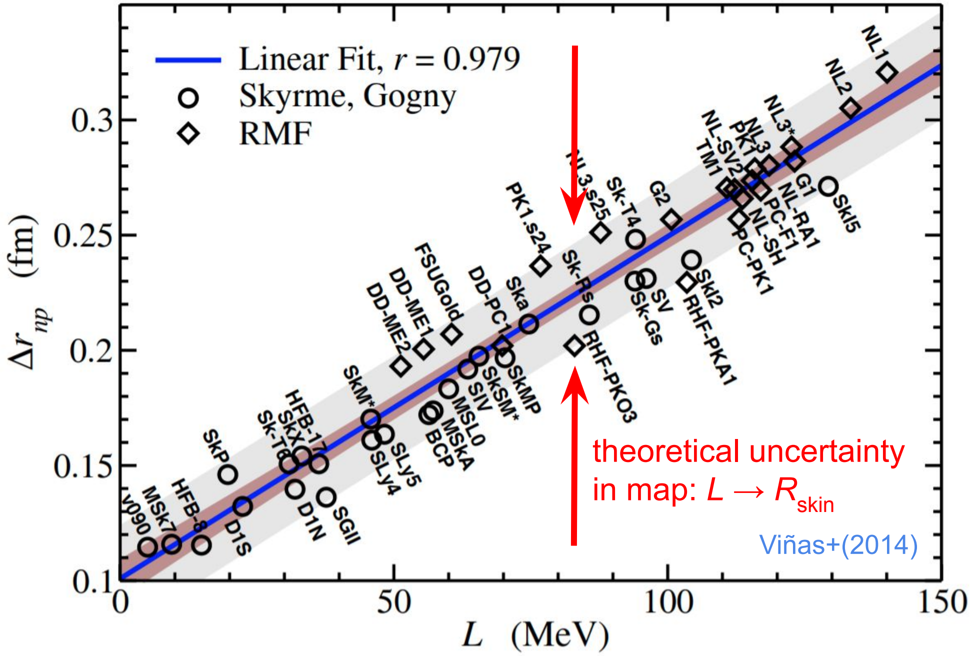

we constrain this with astrophysical observations

Inference of the NS EoS

Essick+ (2021)
Essick+ (2021)

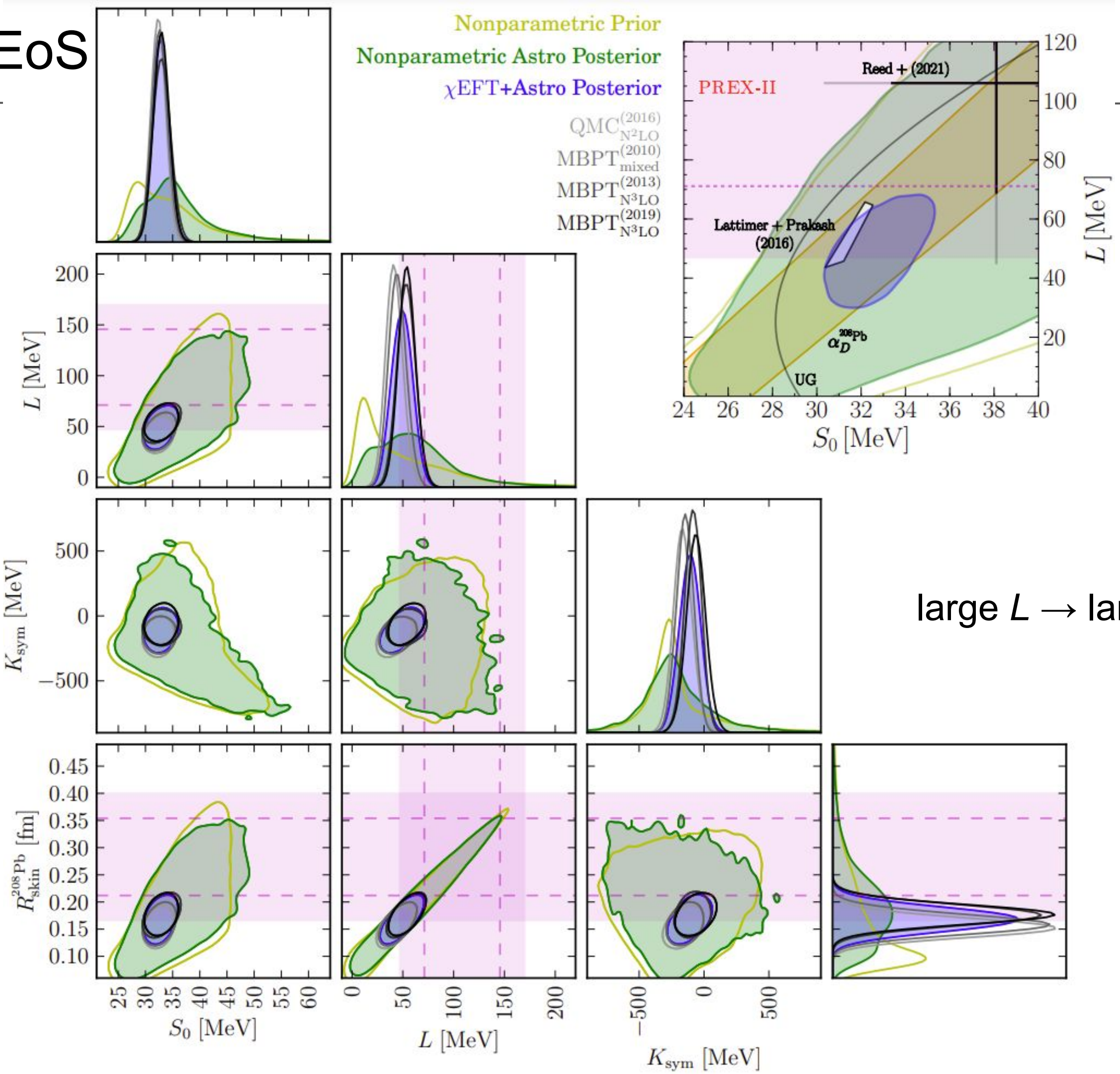

We can also extract "nuclear parameters" directly from nonparametric EoS without the need for parametrized EoS models

large $L \rightarrow$ large $p(n_{sat})$

Inference of the NS EoS

current R_{skin} uncertainty

R_{skin} uncertainty improved by a factor of 2

hypothetical perfect R_{skin} measurement

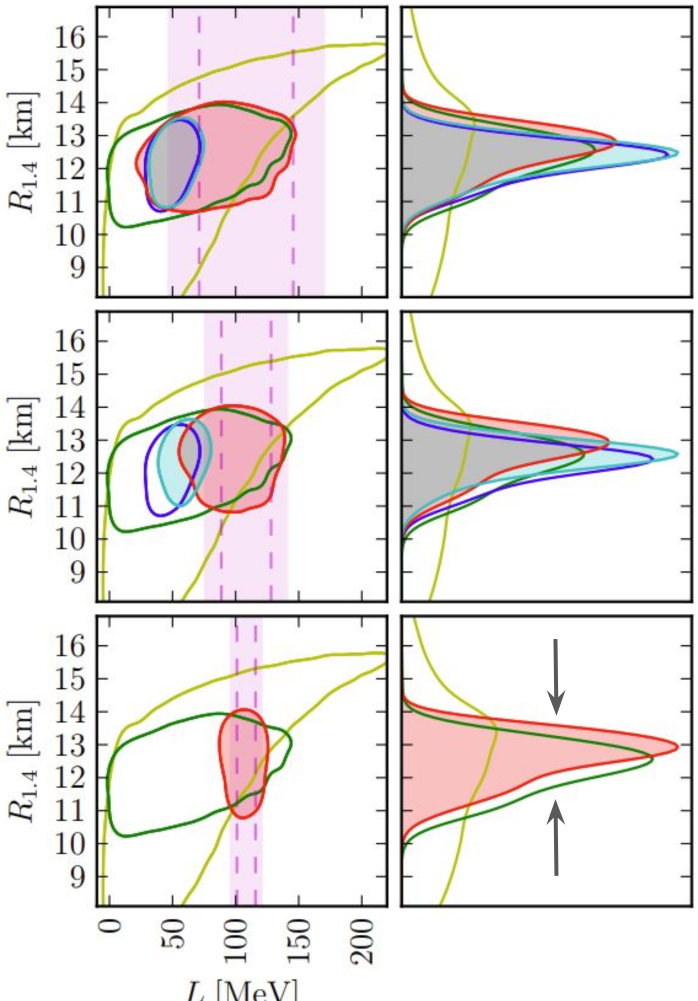

nonparametric prior
nonparametric astro-only posterior
χEFT+astro posterior
nonparametric astro+R_{skin} posterior
χEFT+astro+R_{skin} posterior

improved precision in nuclear experiments is unlikely to affect our knowledge of NS radii without improved theoretical calculations

Inference of the NS EoS: low-density nuclear experiment

Essick+ (2021)
Essick+ (2021)

astro data can distinguish between nuclear theories at high densities

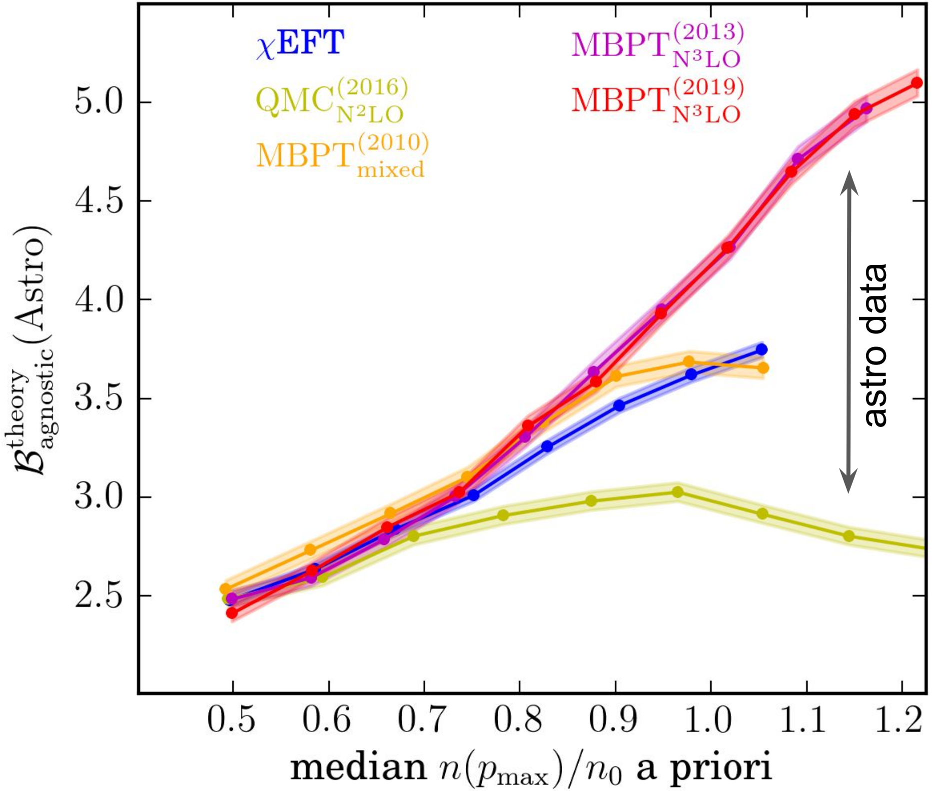

nuclear experiments probe lower densities

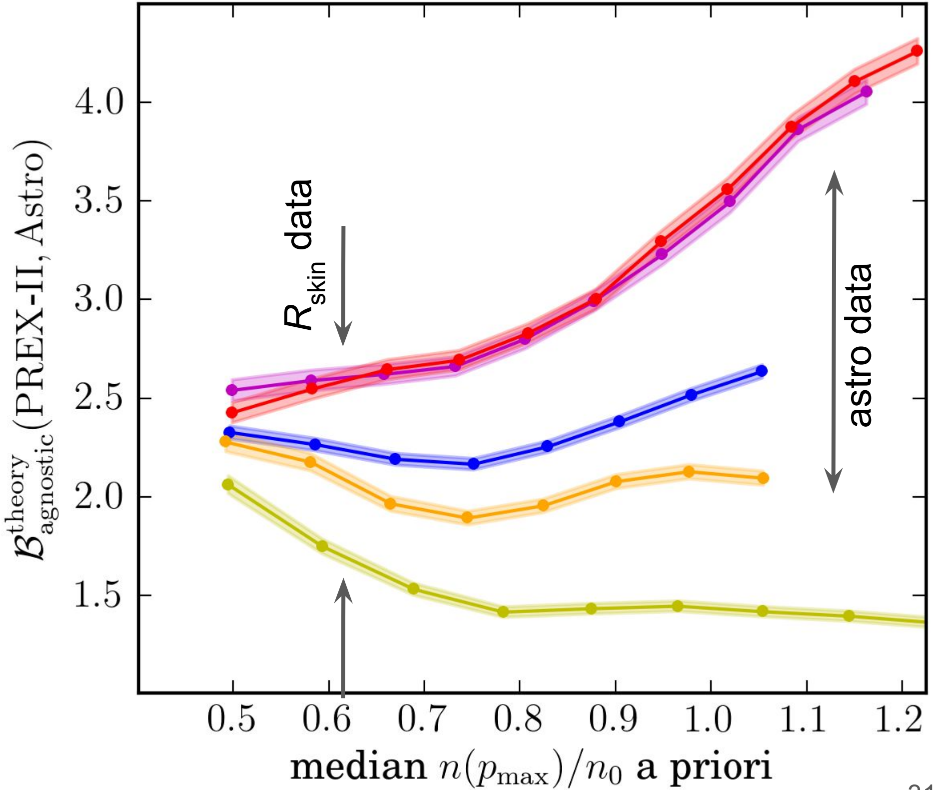

Inference of the NS EoS: low-density nuclear experiment

Essick+ (2021)
Essick+ (2021)

100 MeV < L
30 MeV < L < 70 MeV
All L

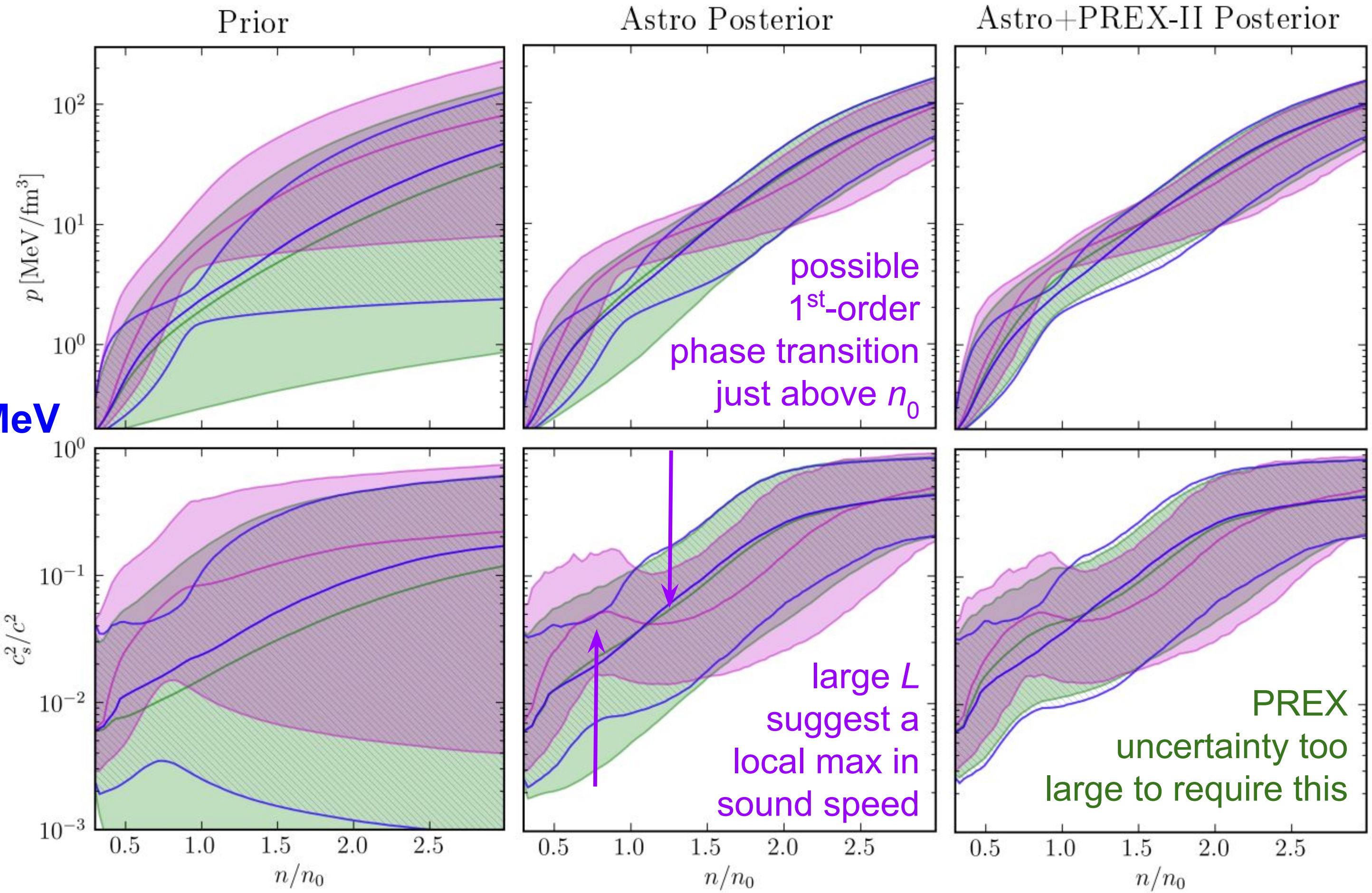

Introduction to Gravitational Waves (GWs), Compact Binaries, and Neutron Stars

Overview of **LIGO-Virgo-KAGRA Observations**

Inferences of the **Equation of State** (EoS)

- Nonparametric EoS Representations
- Connections with Nuclear Theory and Experiment

Future **Prospects**

Future Prospects: EoS constraints

Legred+**Essick**+ (2021)

nuclear experiment

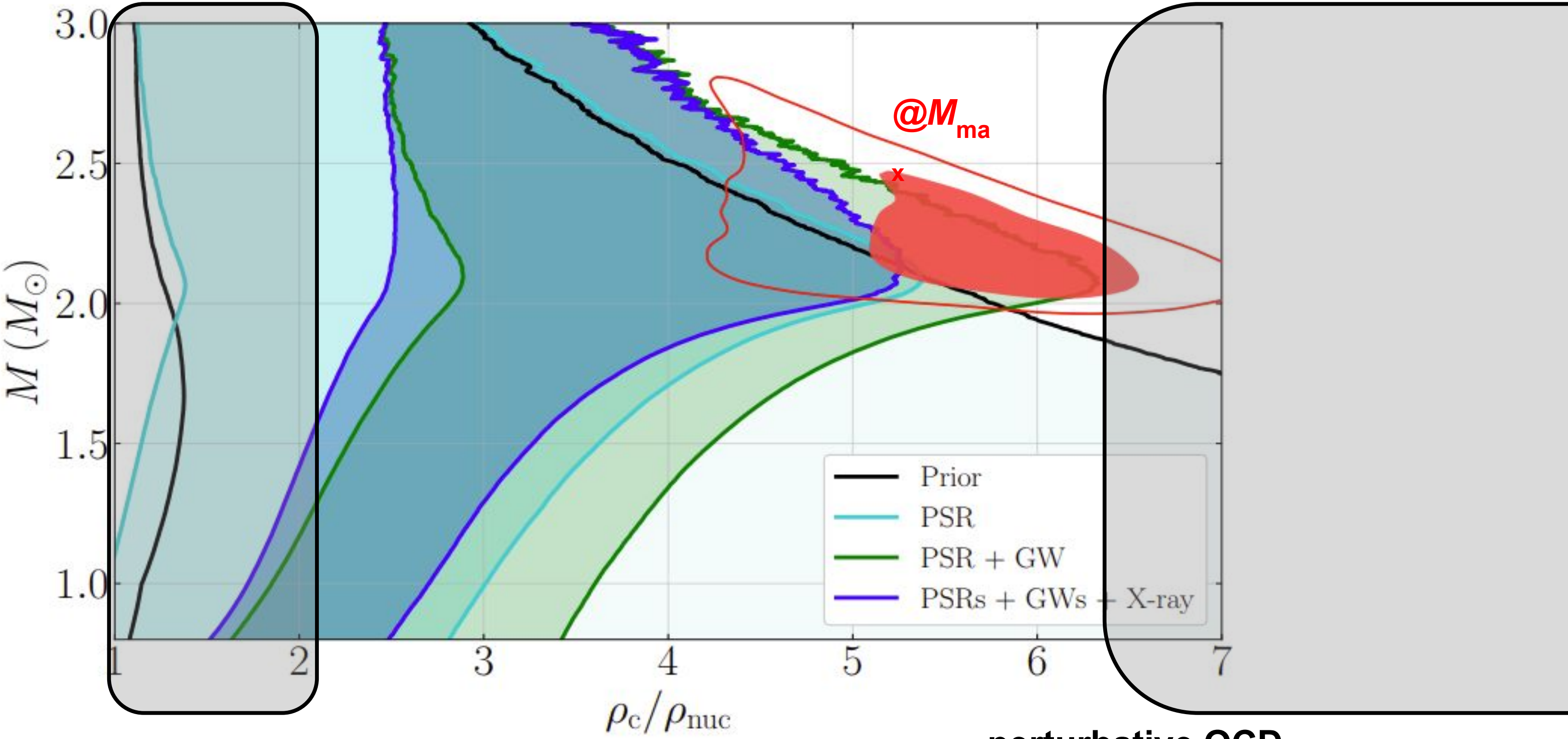

χEffective Field Theory

Lynn+ (2016)
Drischler+ (2020a), Drischler+ (2020b)

perturbative QCD

Komoltsev+Kurkela (2022)
Gorda+ (2022)
Komoltsev+ (2023)

Future Prospects: EoS Constraints

Legred+**Essick**+ (2021)

nuclear experiment

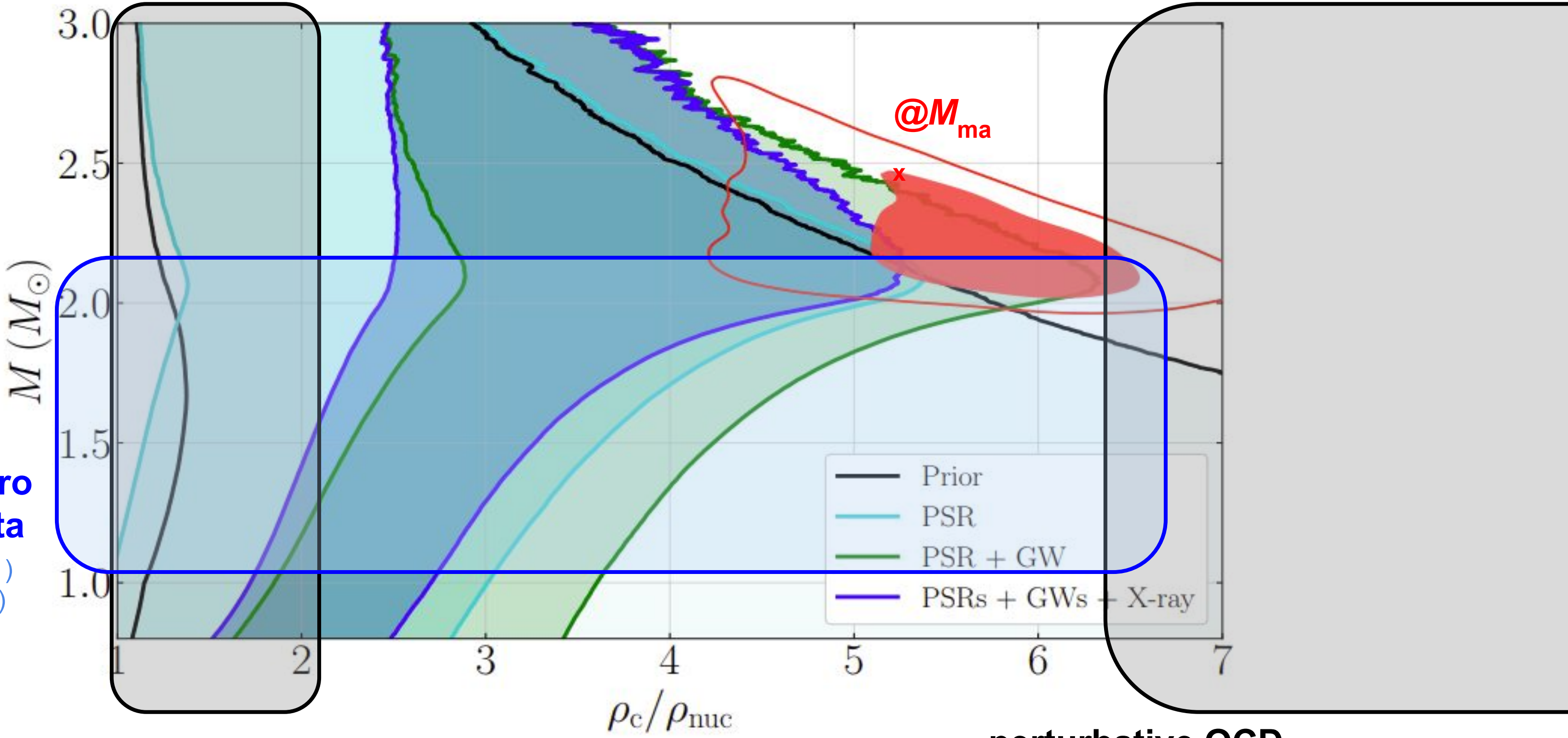

Astro Data

Abbott+**Essick**+ (2021)
Farah+**Essick**+ (2022)
Landry+Read (2021)

χEffective Field Theory

Lynn+ (2016)
Drischler+ (2020a), Drischler+ (2020b)

perturbative QCD

Komoltsev+Kurkela (2022)
Gorda+ (2022)
Komoltsev+ (2023)

Future Prospects: EoS Constraints

Legred+**Essick**+ (2021)

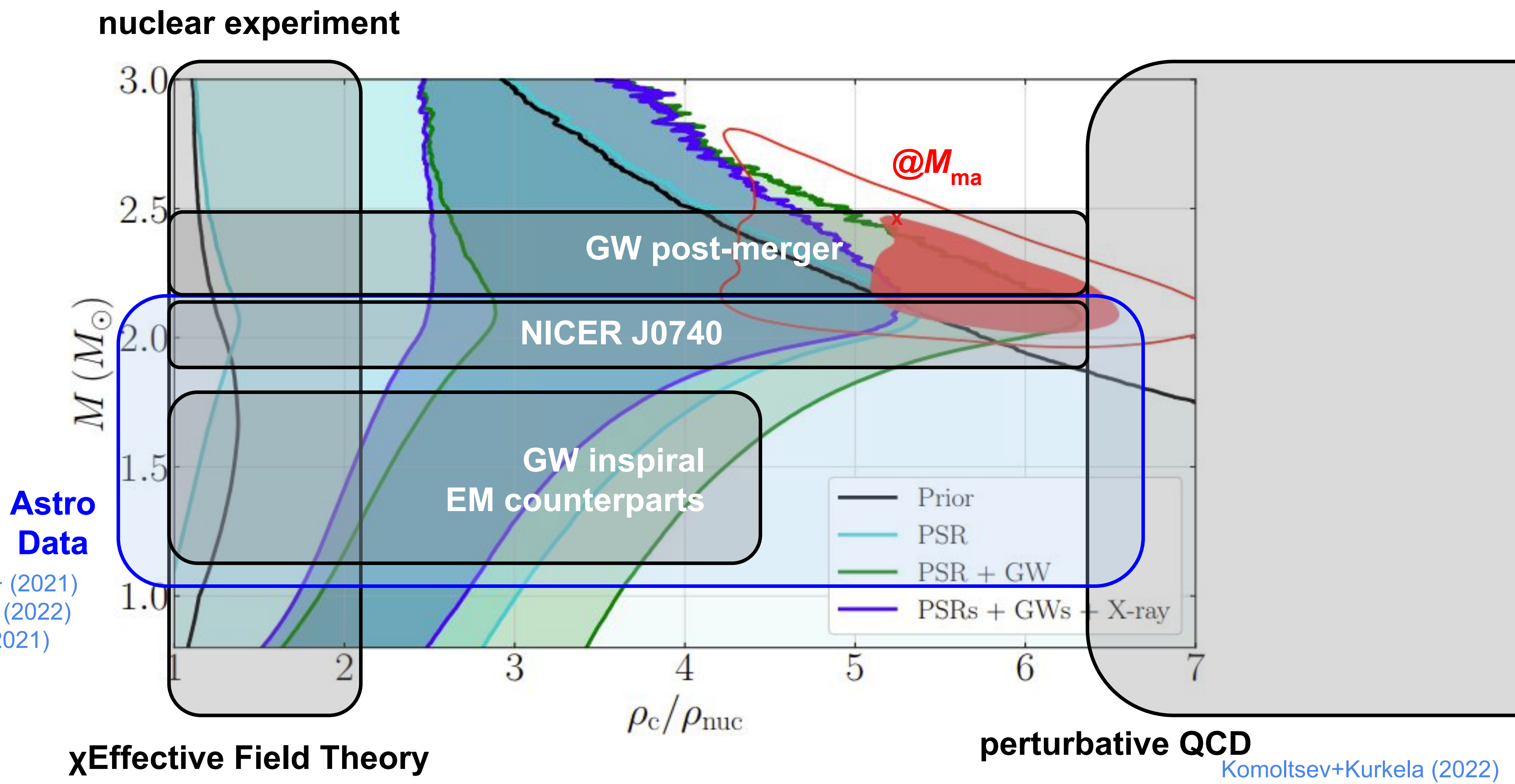

Abbott+**Essick**+ (2021)
Farah+**Essick**+ (2022)
Landry+Read (2021)

Lynn+ (2016)
Drischler+ (2020a), Drischler+ (2020b)

Komoltsev+Kurkela (2022)
Gorda+ (2022)
Komoltsev+ (2023)

Future Prospects: new detectors

Evans (2021)

Proposed ***next generation ground-based detectors*** may be 10x more sensitive and ***will see every binary black hole merger in the universe***

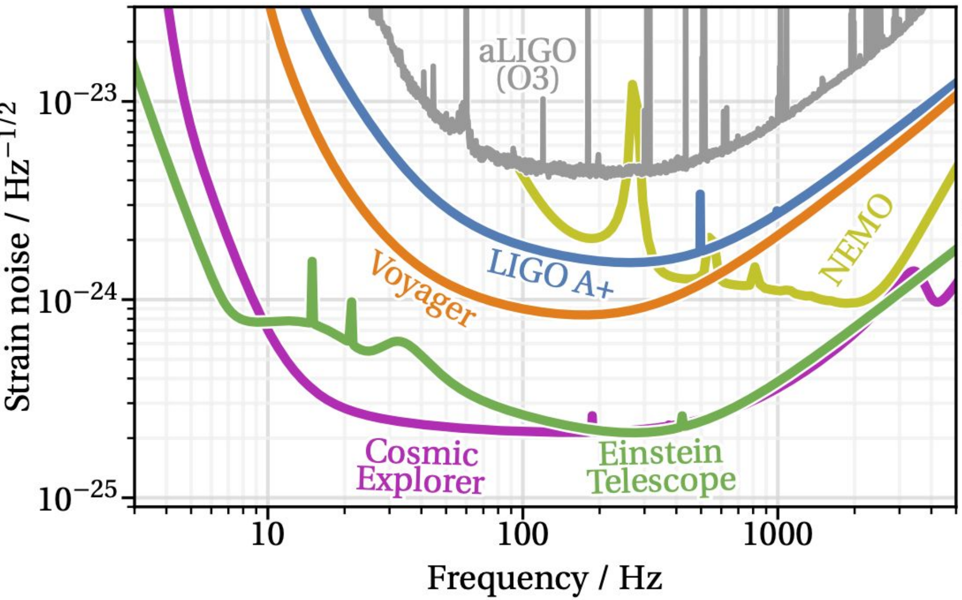

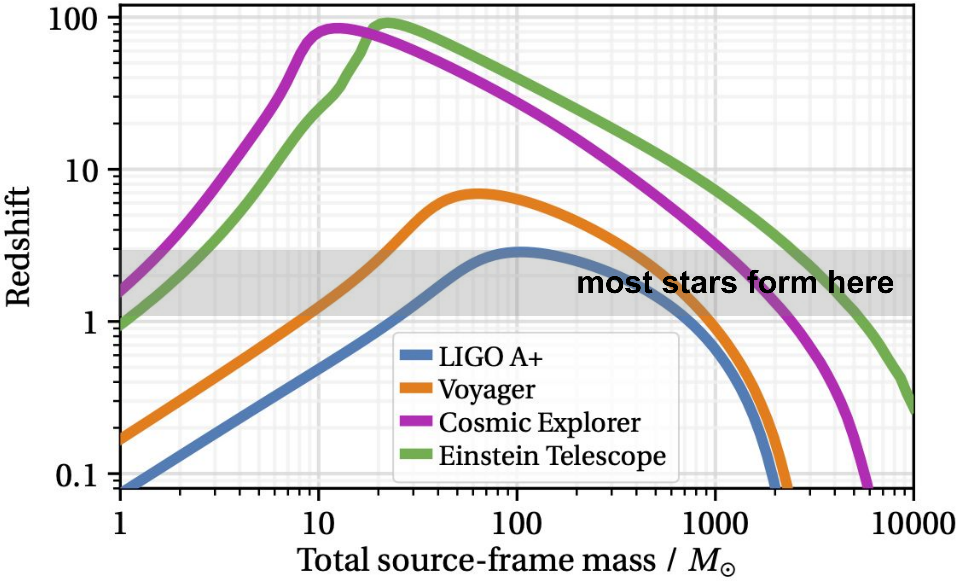

Can’t tell on an event-by-event level, but perhaps we can measure the fractions of each type of system within the population

$$f_{\mathrm{NS}} = p(\mathrm{NS}|m) = \frac{p(m|\mathrm{NS})p(\mathrm{NS})}{p(m|\mathrm{NS})p(\mathrm{NS}) + p(m|\mathrm{BH})p(\mathrm{BH})}$$

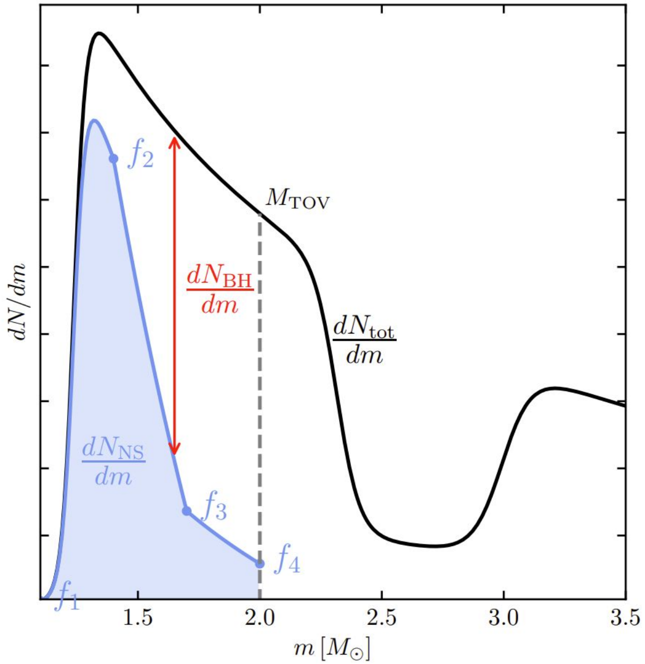

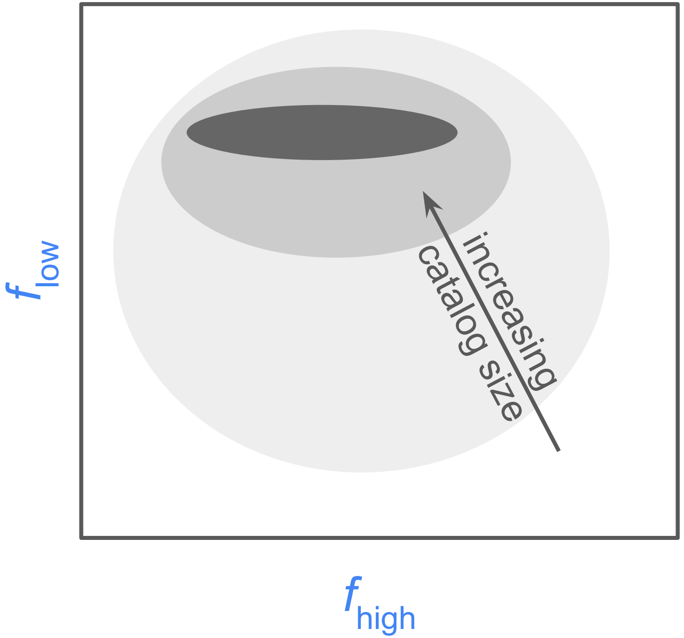

Future Prospects: cosmology with the mass distribution

Utkarsh Mali

Sharp features in the mass distribution can be used to measure H_0

$$m_{\rm det} = (1+z)m_{\rm src}$$
$$\approx \left(1 + \frac{H_0 D_L}{c}\right) m_{\rm src}$$

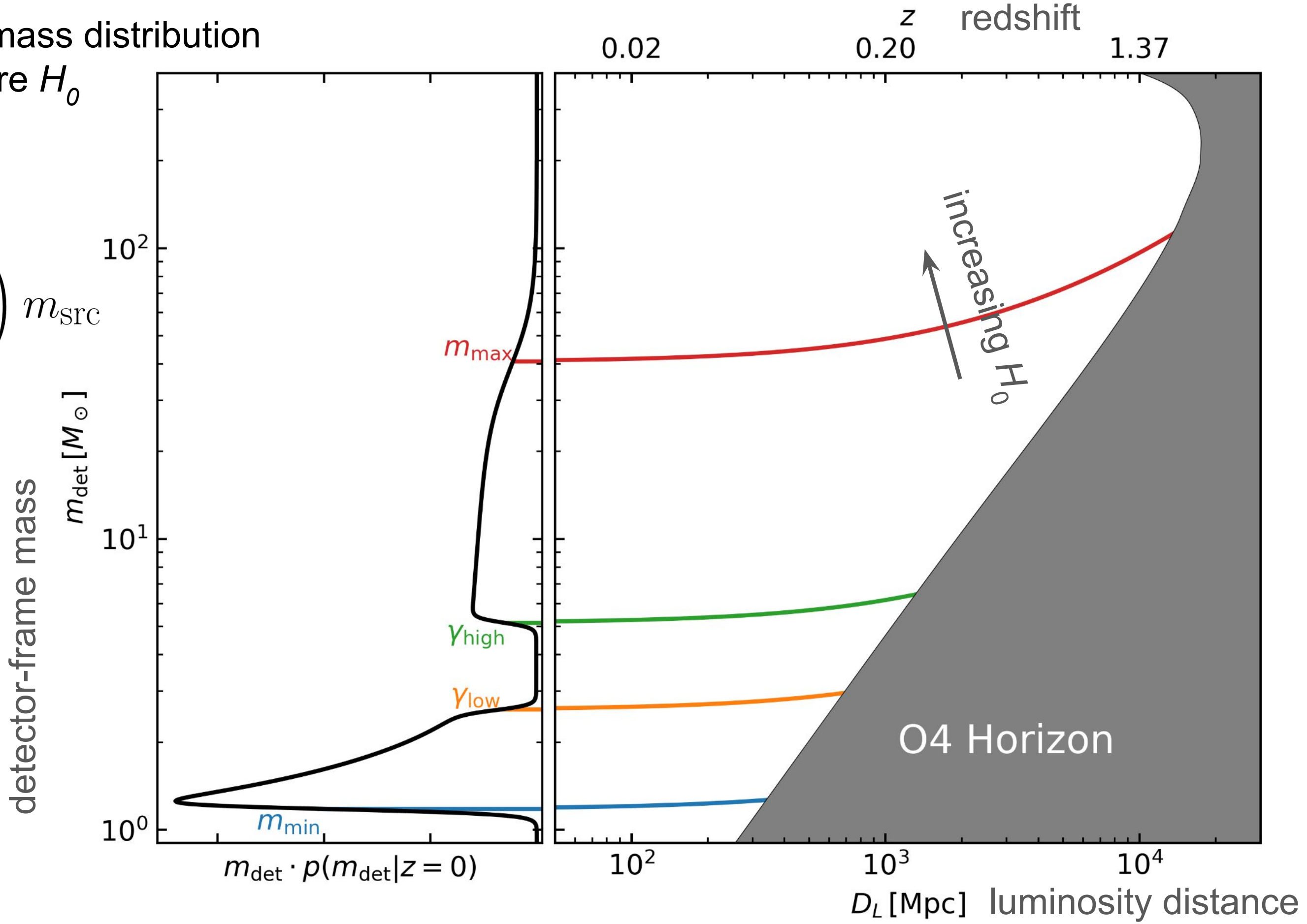

Future Prospects: large catalog studies

An isotropy measurement of the rate-density of compact binaries

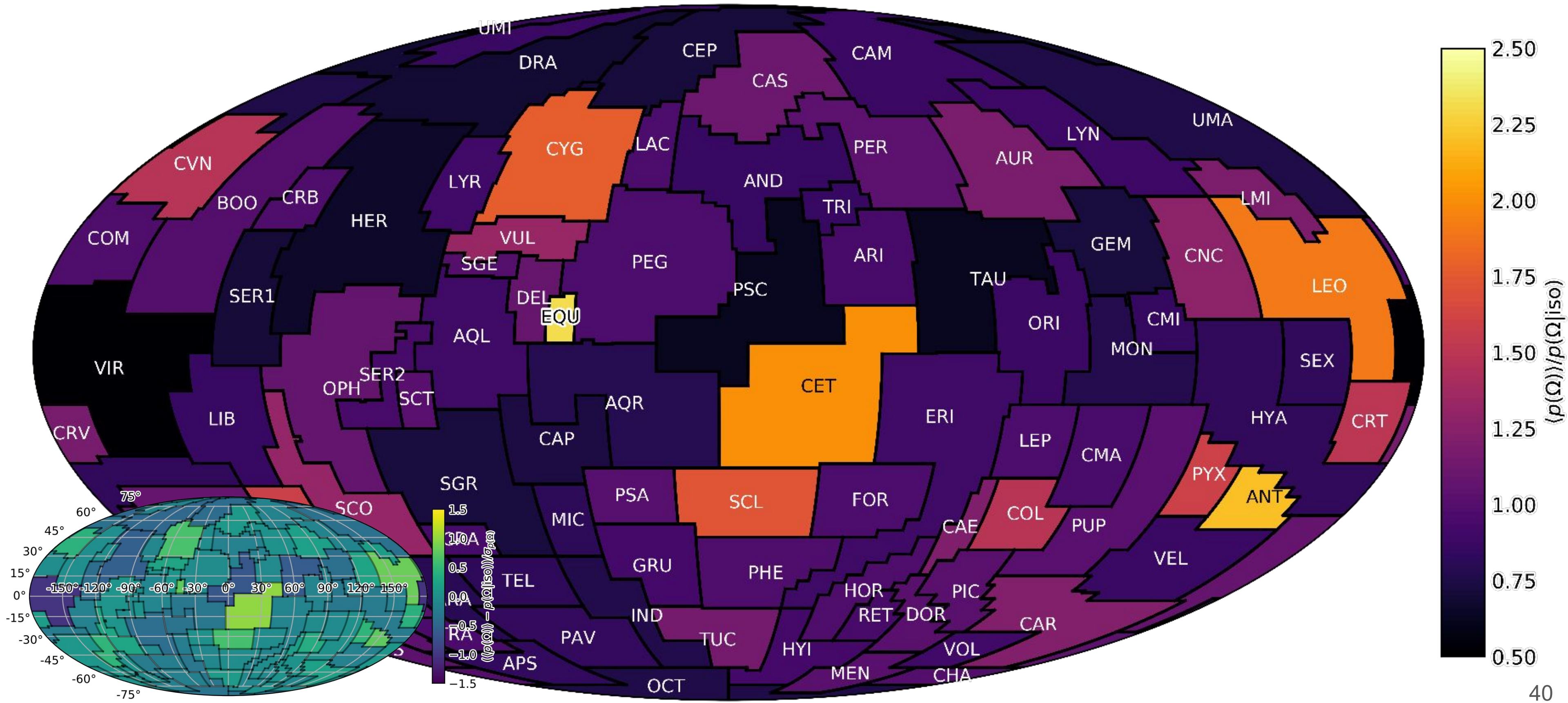

References

Reed Essick
essick@cita.utoronto.ca

Viñas+ (2015) Eur. Phys. J. A 50 27
Abbott+**Essick**+ (2016) Phys. Rev. Lett. 116 061102
Lynn+ (2016) Phys. Rev. Lett. 116 062501
Drischler+ (2020a) Phys. Rev. Lett. 125 202702
Drischler+ (2020b) Phys. Rev. C 102 054315
Essick+ (2020) Phys. Rev. C 102 055803
Abbott+**Essick**+ (2021) arXiv:2111.03634
Essick+ (2021a), Phys. Rev. Lett. 127 192701
Essick+ (2021b), Phys. Rev. C 104 065804
Evans (2021) arXiv:2109.09882
Hen (2021) Science 371, 6526
Landry & Read (2021) ApJ Lett. 921 L25
Legred+**Essick**+ (2021) Phys. Rev. D 104 063003
Reed+ (2021) arXiv:2101.03193
Farah+**Essick**+ (2022) ApJ 931 108
Gorda+ (2022) arXiv:2204.11877
Komoltsev & Kurkela (2022) Phys. Rev. Lett 128 202701
Abbott+**Essick**+ (2023) Phys. Rev. X 13 041039
Essick+ (2023) Phys. Rev. D 107 043016
Komoltsev (2023) arXiv:2312.14127
Kumar+**Essick**+ (2023) arXiv:2303.17021

Basic Physics of CBCs

$$\langle P \rangle = \frac{32G^4}{5c^5}\left(\frac{m_1^2 m_2^2 (m_1+m_2)}{a^5}\right)\cancel{\left(\frac{1}{(1-e^2)^{7/2}}\left(1+\frac{73}{24}e^2+\frac{37}{96}e^4\right)\right)}$$

General Relativity
"Larmor formula"

circular orbit : $e = 0$

$$E = -\frac{Gm_1m_2}{a}$$

Keplerian Orbit

$$\Omega^2 = \frac{G(m_1+m_2)}{a^3}$$

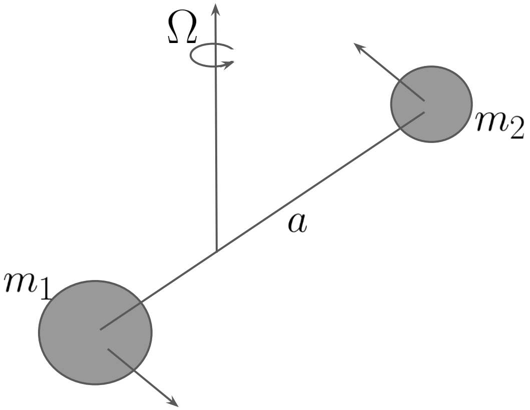

$$\langle P \rangle = -\frac{dE}{dt}$$

Post Newtonian Energy Balance

$$\boxed{f(m_1, m_2, \Omega) = g(m_1, m_2, \Omega)\frac{d\Omega}{dt}}$$

evolution of the orbital frequency is directly imprinted within GWs

$$h \sim e^{i(2\Omega)t}$$

Basic Physics of CBCs

$$\langle P \rangle = \frac{32 G^4}{5 c^5} \left(\frac{m_1^2 m_2^2 (m_1 + m_2)}{a^5} \right) \cancel{\left(\frac{1}{(1-e^2)^{7/2}} \left(1 + \frac{73}{24} e^2 + \frac{37}{96} e^4 \right) \right)}$$

General Relativity
“Larmor formula”

circular orbit : $e = 0$

$$E = -\frac{G m_1 m_2}{a}$$

Keplerian Orbit

$$\Omega^2 = \frac{G(m_1 + m_2)}{a^3}$$

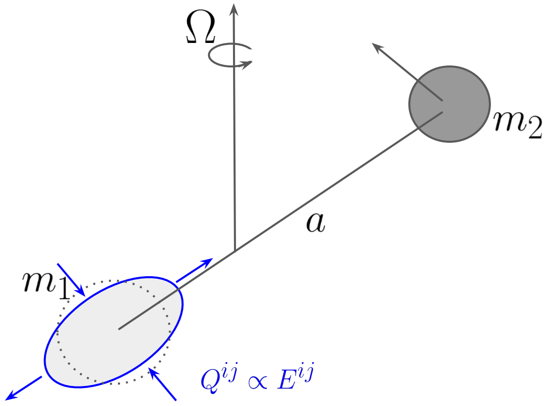

$$\langle P \rangle = -\frac{dE}{dt}$$

Post Newtonian Energy Balance

$$\boxed{f(m_1, m_2, \Omega) = g(m_1, m_2, \Omega) \frac{d\Omega}{dt}}$$

evolution of the orbital frequency is directly imprinted within GWs

$$h \sim e^{i(2\Omega)t}$$

adiabatic tides deform stars

changes **flux** and orbit’s **binding energy**

Basic Physics of CBCs

$$\langle P \rangle = -\frac{dE}{dt}$$

Post Newtonian Energy Balance Orbit

$$\boxed{f(m_1, m_2, \Omega) = g(m_1, m_2, \Omega)\frac{d\Omega}{dt}}$$

evolution of the orbital frequency is directly imprinted within GWs

$$h \sim e^{i(2\Omega)t}$$

adiabiatic tides $\Lambda(m) \sim k_2 \left(\frac{R(m)}{m}\right)^5$

$$\tilde{\Lambda} = \left(\frac{16}{13}\right) \frac{(m_1 + 12m_2)m_1^4\Lambda(m_1) + (m_2 + 12m_1)m_1^4\Lambda(m_2)}{(m_1 + m_2)^5}$$

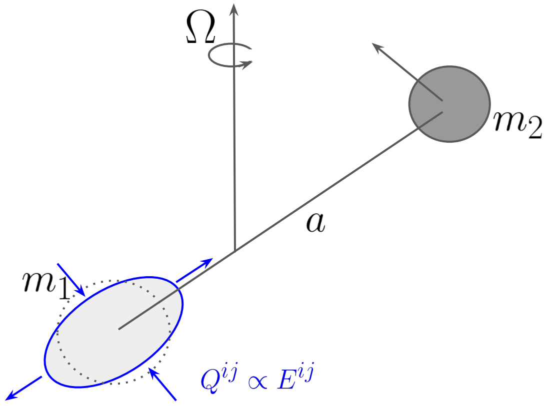

adiabatic tides deform stars

Basic Physics of CBCs

$$\langle P \rangle = -\frac{dE}{dt}$$

Post Newtonian Energy Balance Orbit

$$\boxed{f(m_1, m_2, \Omega) = g(m_1, m_2, \Omega)\frac{d\Omega}{dt}}$$

evolution of the orbital frequency is directly imprinted within GWs

$$h \sim e^{i(2\Omega)t}$$

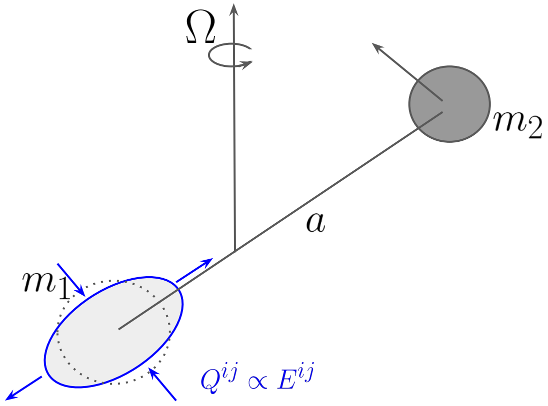

adiabatic tides deform stars

adiabiatic tides

linear tidal resonances
- Pratten+ (2021)

nonlinear tidal instabilities
- Weinberg+ (2016)
- Abbott+**Essick**+ (2019)

orbital energy transferred to stellar normal modes

post-merger signals
- Most+Raithel (2021)
- Weih+ (2020)

Basic Physics of CBCs

$$\phi(t) = \int_{-\infty}^{t} d\tau\, f(\tau)$$

orbital evolution gives time-domain phase

$$\psi(f) = i(2\pi f t - \phi(t)) - \pi/4$$

frequency-domain phase is related to time-domain phase (saddle point approximation)

$$\ln \mathcal{L} \sim \int df \frac{\mathcal{R}\{\tilde{d}^* \tilde{h}\}}{S}$$

$$\sim \int df \underbrace{\boxed{\frac{|\tilde{d}||\tilde{h}|}{S}}}_{\text{varies slowly}} \underbrace{\boxed{\cos(\Delta\psi)}}_{\text{oscillates rapidly}}$$

likelihood of GW data is an integral over a rapidly oscillating function of the difference of freq-domain phases

significant likelihood only when $\Delta\psi$ is small and/or varies slowly at all frequencies

IFO Detector Response

Essick & Isi (2023)

There are 6 degrees of freedom within the strain tensor, which are often grouped as follows based on their symmetry properties.

GR only predicts tensor modes.

$$h_{ij} = \begin{array}{c} \begin{array}{ccc} \quad x \quad & \quad\quad y \quad\quad & z \end{array} \\ \begin{bmatrix} h_b + h_+ & h_\times & h_x \\ h_\times & h_b - h_+ & h_y \\ h_x & h_y & h_l \end{bmatrix} \end{array}$$

tensor | vector | scalar

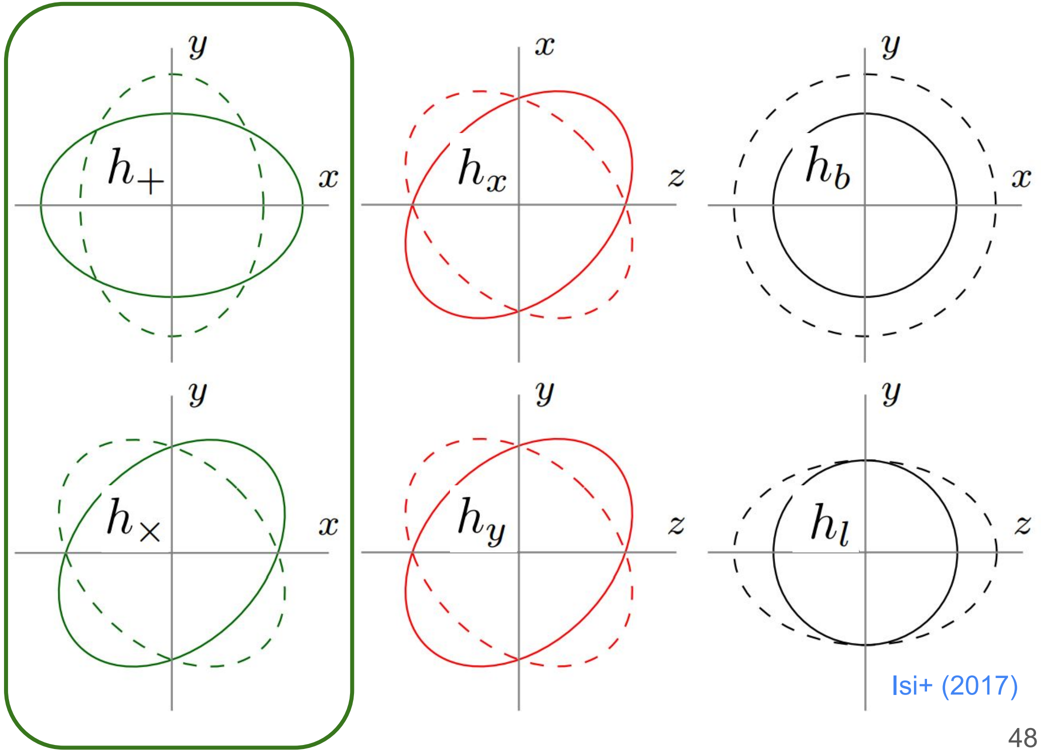

Isi+ (2017)

IFO Detector Response

Interferometers (IFOs) measure differences in the lengths of their arms by comparing the phase of light after it travels down the arms (i.e., comparing round-trip travel times). The phase from each arm depends on the strain projected along that arm.

$$\frac{\delta T}{T} \equiv D = \frac{h}{2}$$

where

$$h = h_{ij}\hat{e}^i\hat{e}^j$$

*assumes measurement is instantaneous $f \ll \frac{c}{2L}$

IFO Detector Response

Interferometers (IFOs) measure differences in the lengths of their arms by comparing the phase of light after it travels down the arms (i.e., comparing round-trip travel times). The phase from each arm depends on the strain projected along that arm.

$$\frac{\delta T}{T} \equiv D = \frac{h}{2} \qquad \text{where} \qquad h = h_{ij}\hat{e}^i\hat{e}^j$$

*assumes measurement is instantaneous $f \ll \frac{c}{2L}$

The IFO readout can is sensitive to

$$\frac{\delta T_x - \delta T_y}{T} = \boxed{\frac{1}{2}\left(\hat{e}^i_x\hat{e}^j_x - \hat{e}^i_y\hat{e}^j_y\right)} h_{ij}$$

which can be expressed in terms of the *Detector Tensor* D^{ij}, which acts as a *Transfer Function* between the astrophysical GW strain and the IFO readout.

IFO Detector Response

Essick & Isi (2023)

Current IFOs will respond to 5/6 polarizations: there is an unobservable linear combination of scalar modes.

$$\begin{array}{cc} & \begin{array}{ccc} x & y & z \end{array} \\ h_{ij} = & \begin{bmatrix} \boxed{h_b} + h_+ & h_\times & h_x \\ h_\times & \boxed{h_b} - h_+ & h_y \\ h_x & h_y & \boxed{h_l} \end{bmatrix} \end{array}$$

$$\boxed{\varepsilon_b + \varepsilon_l} = \mathbb{I}$$

*isotropic expansion/contraction.

This results in indistinguishable antenna patterns $F_p = D^{ij}(\varepsilon_p)_{ij}$ for the scalar modes.

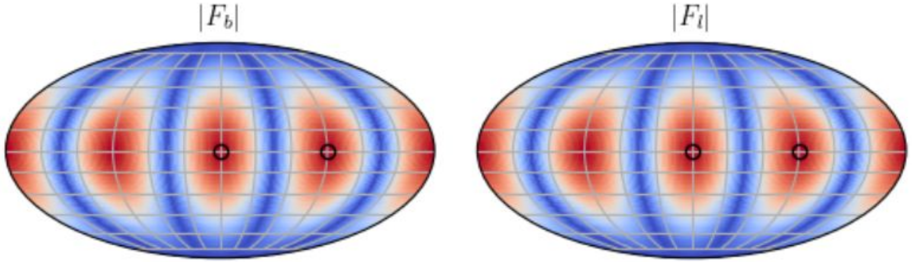

$$\underbrace{\boxed{\left(e_x^i e_x^j - e_y^i e_y^j\right)}}_{\sim D^{ij}} \mathbb{I}_{ij} = 1 - 1 = 0$$

IFO Detector Response

For high-frequency signals, the strain projected along the arm of the detector may change appreciably while the measurement is taking place.

$$f \sim f_{\mathrm{FSR}} \equiv \frac{c}{2L} \approx 37\,\mathrm{kHz}\left(\frac{4\,\mathrm{km}}{L}\right)$$

In this case, the response of each arm is more complicated

$$D(f, n_e) \equiv \frac{c}{8\pi i f L}\left(\frac{1 - e^{-2\pi i f(1-n_e)L/c}}{1 - n_e} - e^{-4\pi i f L/c}\frac{1 - e^{+2\pi i f(1+n_e)L/c}}{1 + n_e}\right)$$

where $n_e = \hat{n}_i \hat{e}^i$ and $\hat{n}_i$ is the GW's direction of propagation. We then construct

$$D^{ij} = D(f, n_k e^k_x) e^i_x e^j_x - D(f, n_l e^l_y) e^i_y e^j_y$$

See Essick+ (2017) for more discussion.

IFO Detector Response

This additional dependence on the GW's propagation direction breaks the degeneracy between scalar modes.

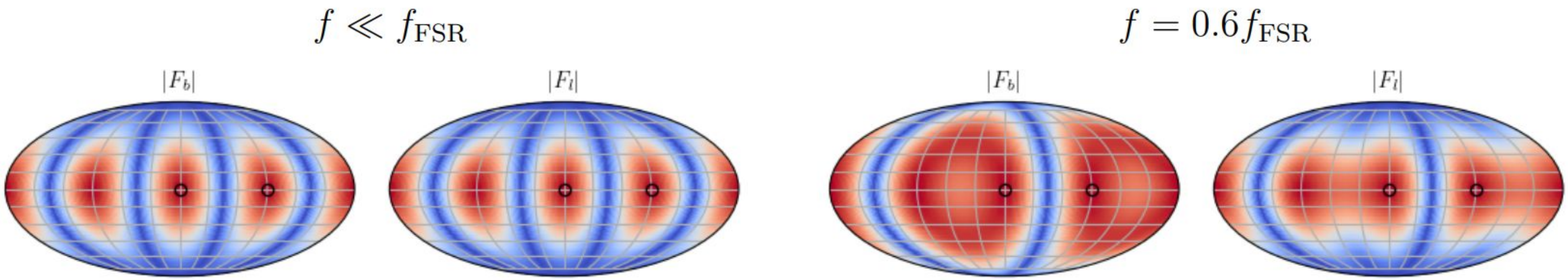

Figure 1. Mollweide projections of the magnitude of the detector response to the breathing mode and longitudinal mode as a function of the direction to the source at (*left*) $f \ll f_{\rm FSR}$ and (*right*) $f = 0.6 f_{\rm FSR}$, approximately ISCO for a 1+1 $M_\odot$ binary at $z \ll 1$ in a 40 km Cosmic Explorer.

As Essick+ (2017) shows, the long-wavelength approximation only begins to break down significantly for frequencies $f \gtrsim f_{\rm FSR}/2$. By this metric, then, ***only detectors with arms longer than ≈ 34 km would be able to distinguish between scalar polarizations near ISCO with low-mass (solar-mass) mergers***.

GW Data Quality: iDQ

Essick+ (2021)

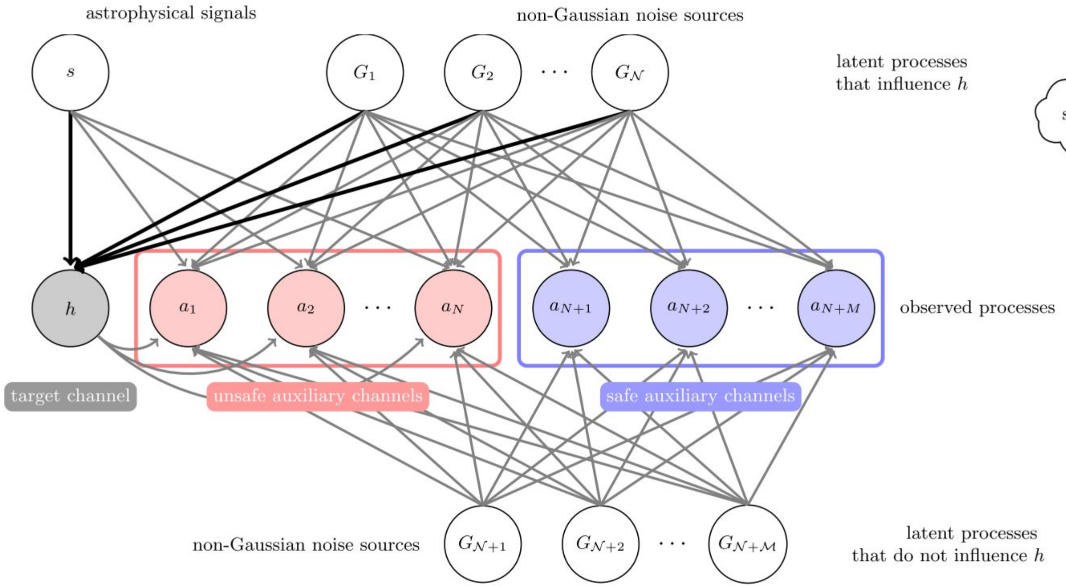

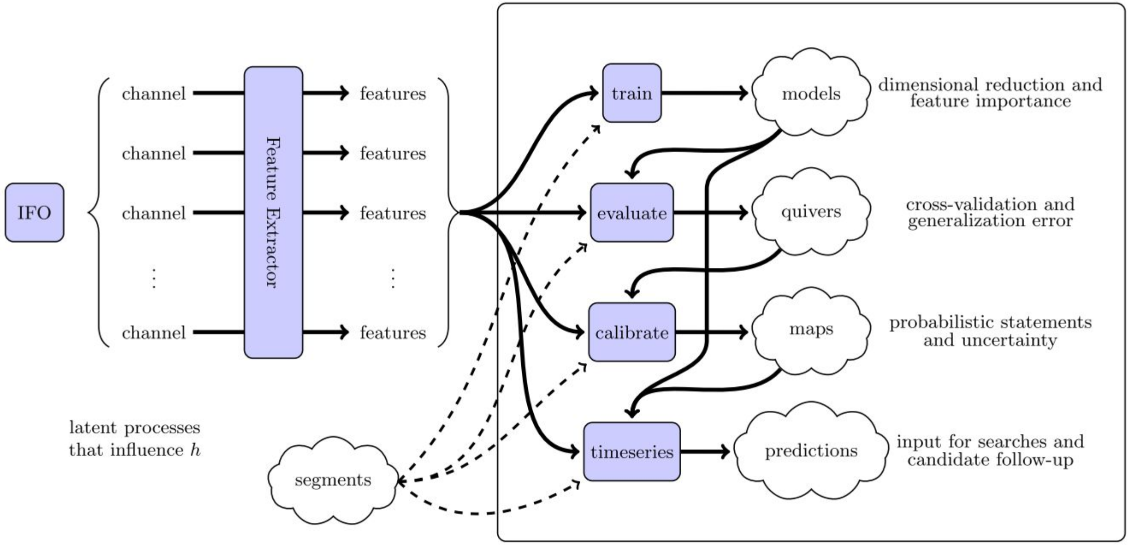

GW Data Quality: iDQ

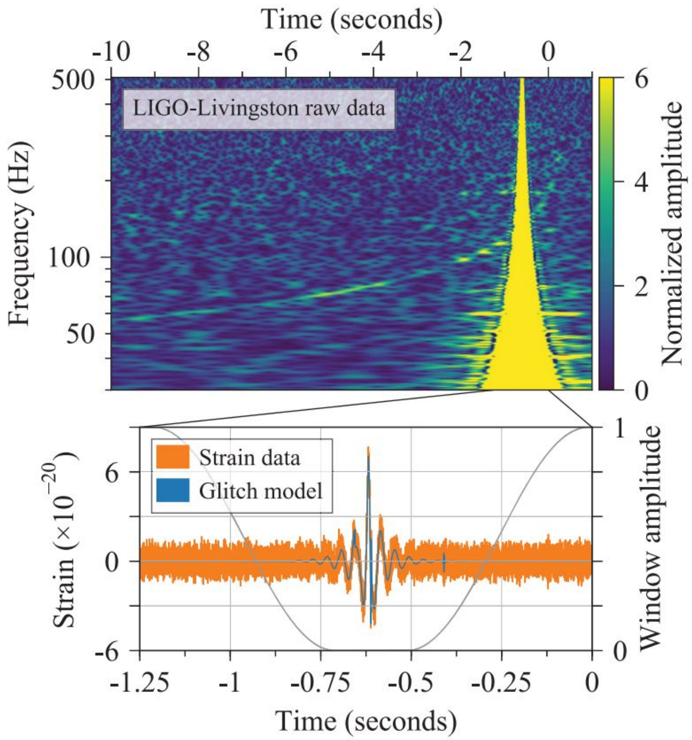

Abbott+**Essick+** (2017)

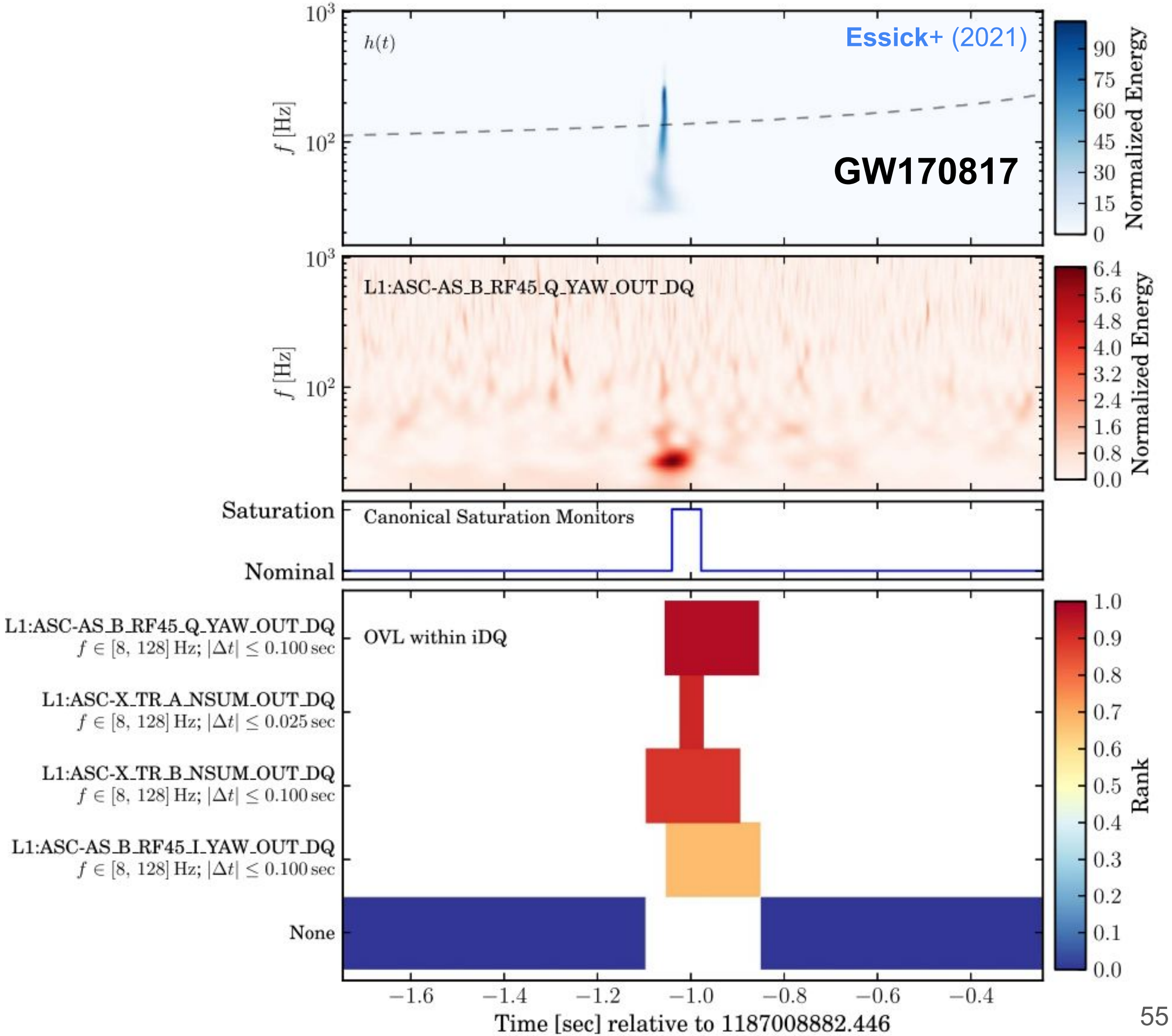

GW Data Quality: Coincidence Null-test for Poisson Processes

$$P(\Delta t \leq \tau | \lambda) = 1 - e^{-2\lambda\tau}$$

joint statistic from 208 channels

individually significant

randomly selected

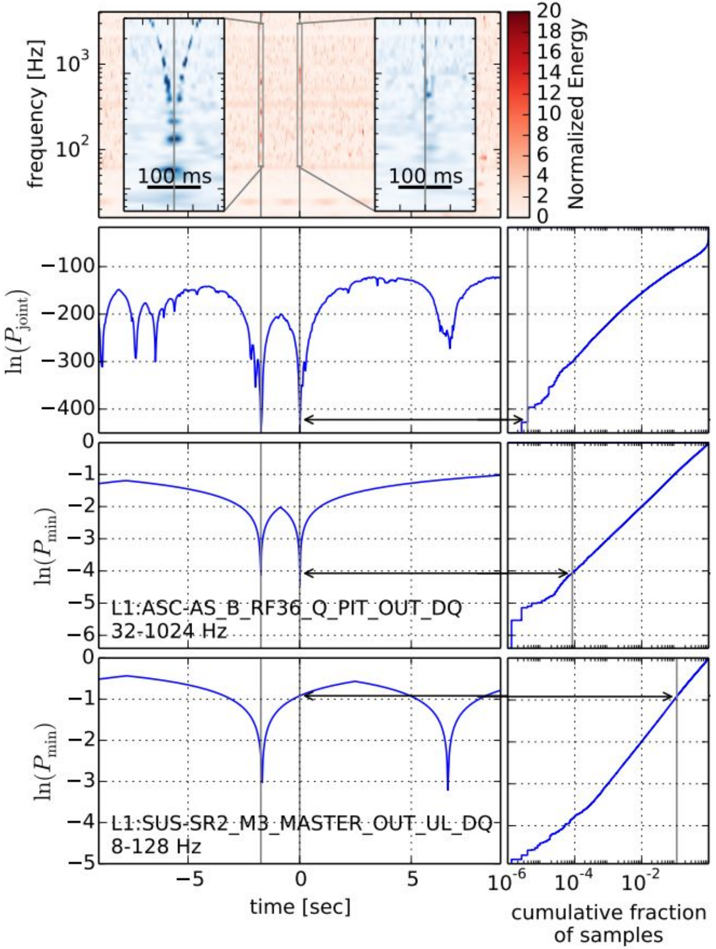

(astro)Calibration

Essick & Holz (2019)

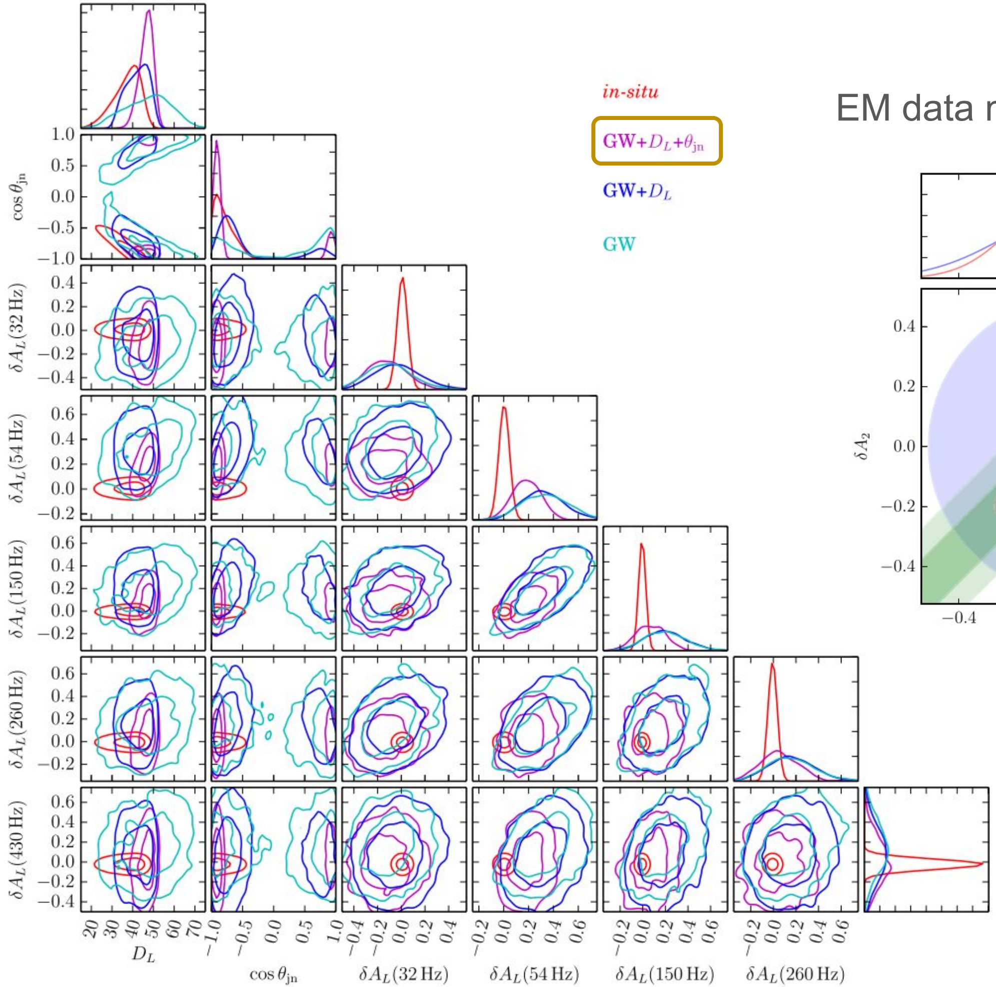

EM data must constrain both D_L and θ_{jn} to constrain δA

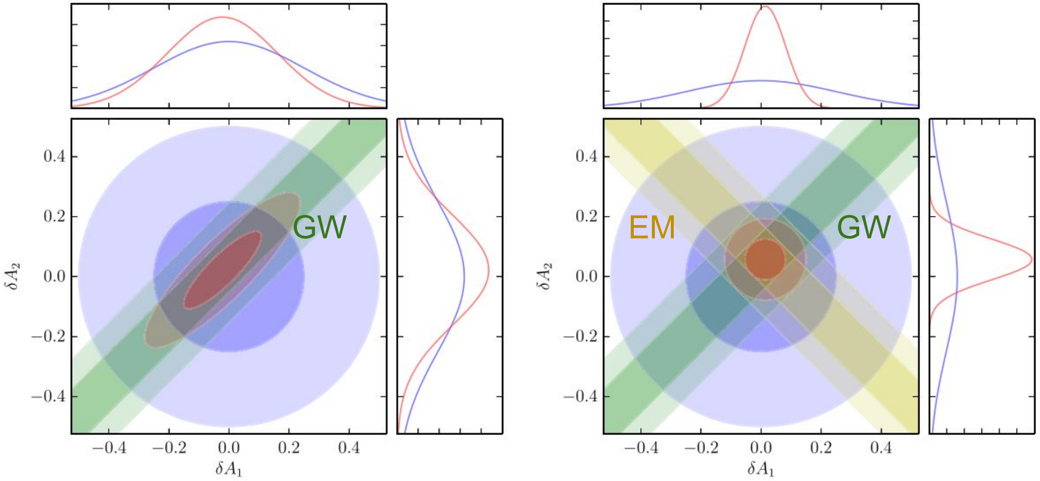

GW Calibration Uncertainty

Essick (2022)

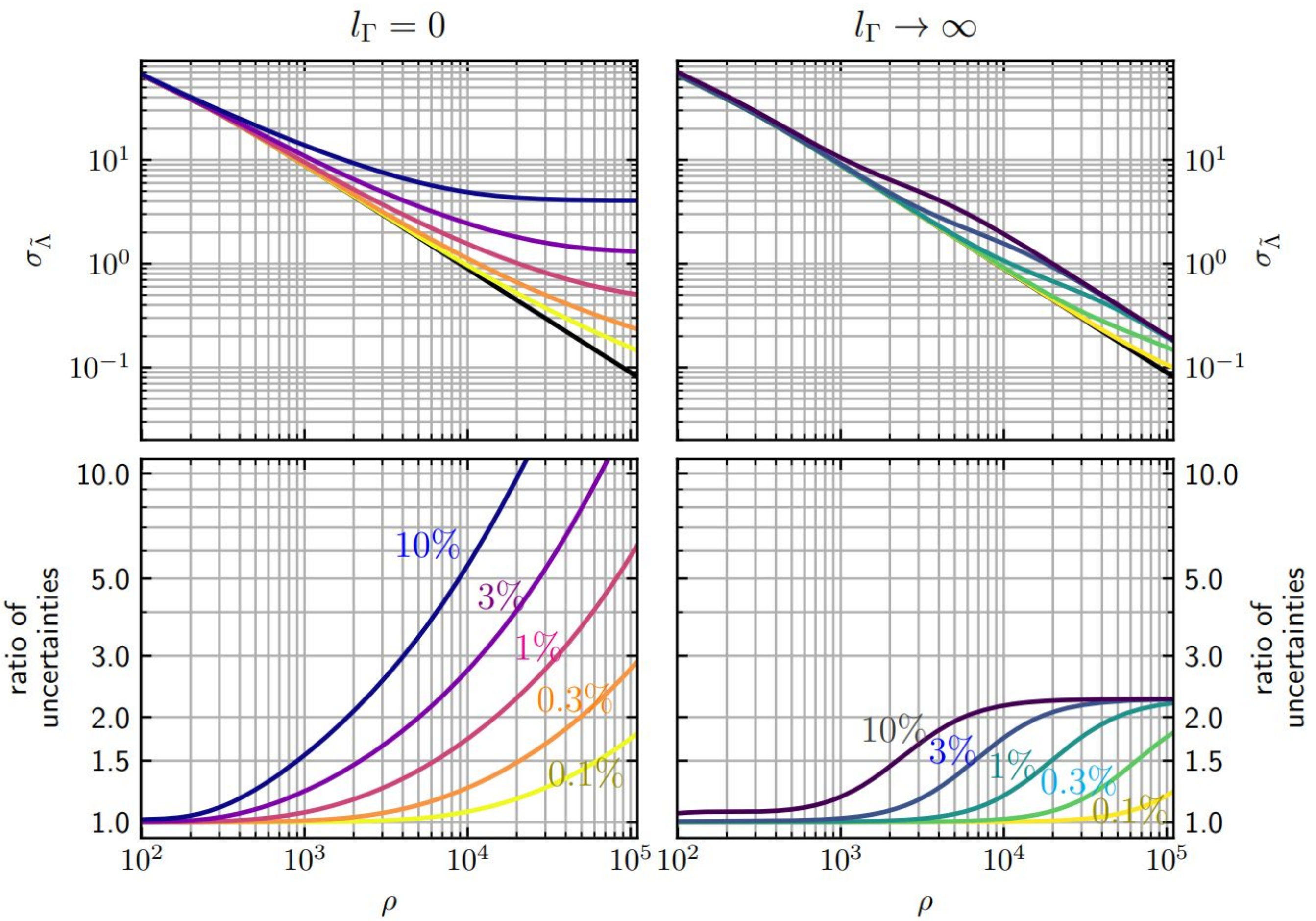

GW Calibration Uncertainty

Essick (2022)

TABLE I. Estimates of the precision of individual parameters for a 1.4+1.4 $M_\odot$ binary when $l_\Gamma = 0$ with projected design sensitivities of future IFOs. I show the uncertainty assuming no calibration error ($\sigma_\Gamma \rightarrow 0$) at a reference S/N of 10 as well as the lower limit set by nonzero calibration uncertainty. The lower limits scale linearly with the calibration uncertainty (and the square root of the frequency spacing), and I quote reference values for $\sigma_\Gamma\sqrt{\Delta f} = 0.01$. In addition to the uncertainty in the coalescence time (t_c), I approximate the corresponding uncertainty in the polar angle (localization precision) between the LIGO Hanford (LHO) and LLO detectors from triangulation ($\sigma_{\theta_{HL}} \approx \sqrt{2}(\sigma_{t_c}/10\,\mathrm{ms})$) [50].

IFO	quantity	$\mathcal{M}\,[M_\odot]$	η	$\tilde{\Lambda}$	t_c [ms]	θ_{HL}
aLIGO design [51]	$(\rho/10)\lim\limits_{\Gamma\rightarrow 0}\sigma_i$	$1.06 \cdot 10^{-4}$	$3.17 \cdot 10^{-3}$	$2.61 \cdot 10^{2}$	$3.14 \cdot 10^{-1}$	2.5°
Cosmic Explorer [52]		$7.46 \cdot 10^{-5}$	$2.24 \cdot 10^{-3}$	$5.09 \cdot 10^{+2}$	$5.66 \cdot 10^{-1}$	4.6°
$f \in [5, 1500]$ Hz	$\left(0.01/\sigma_\Gamma\sqrt{\Delta f}\right)\lim\limits_{\rho\rightarrow\infty}\sigma_i$	$1.44 \cdot 10^{-6}$	$4.31 \cdot 10^{-5}$	$4.27 \cdot 10^{-1}$	$1.03 \cdot 10^{-3}$	$30.0''$

NS Observables: Mass

M_{max}

Massive pulsars (PSRs)
J0740+6620 Cromartie+(2019)
Fonseca+(2021)

EoS
nuclear
microphysics

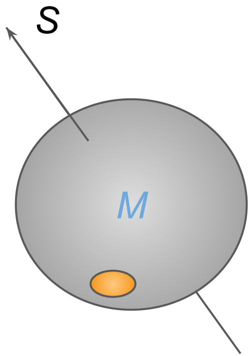

pulsar observations
radial velocity
Shapiro delay

NS Observables

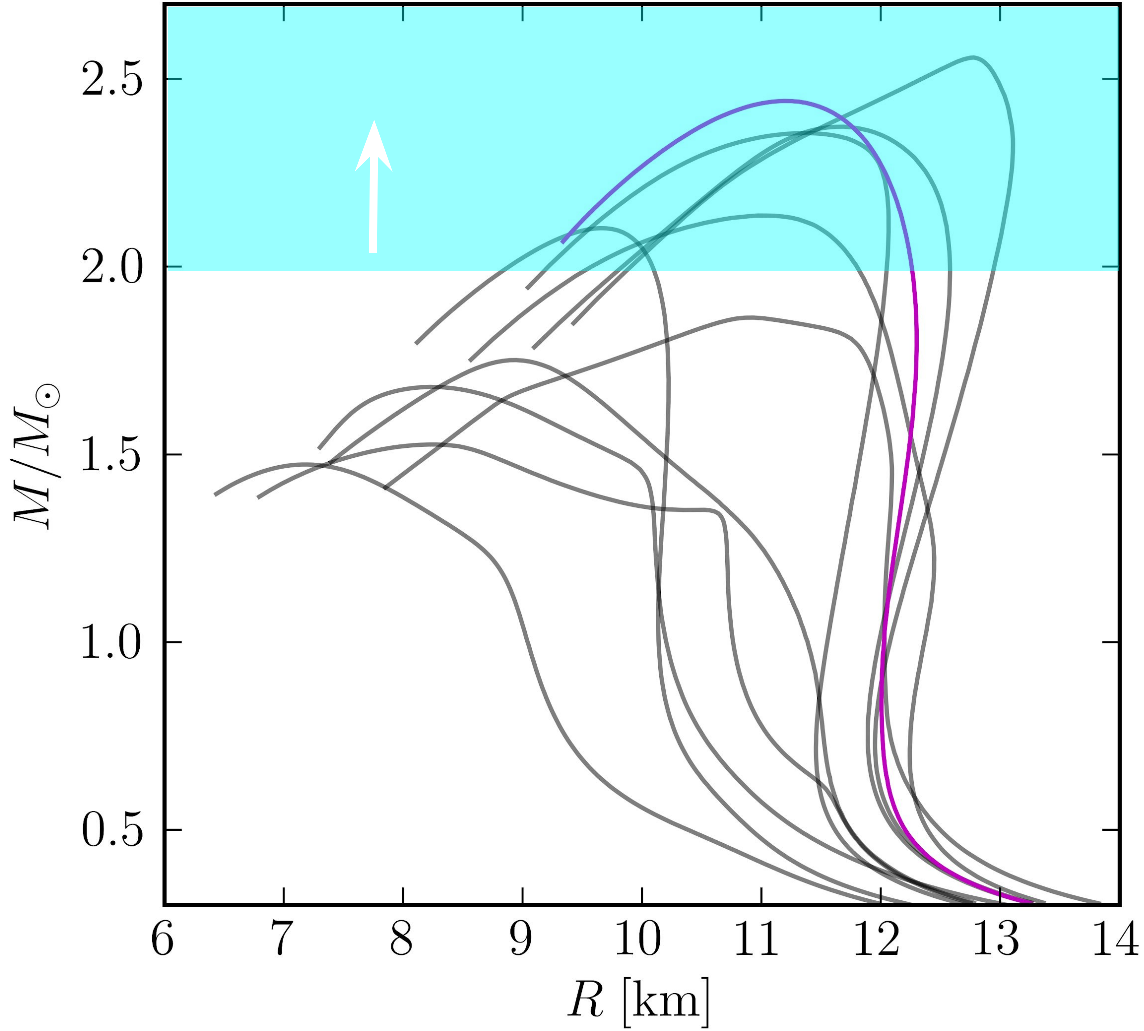

NS Observables: Mass and Radius

M_{max}

Massive pulsars (PSRs)
J0740+6620 Cromartie+(2019)
Fonseca+(2021)

EoS
nuclear
microphysics

$R(M)$

X-ray pulse timing (NICER)
J0030+0451 Miller+(2019)
J0740+6620 Miller+(2021)

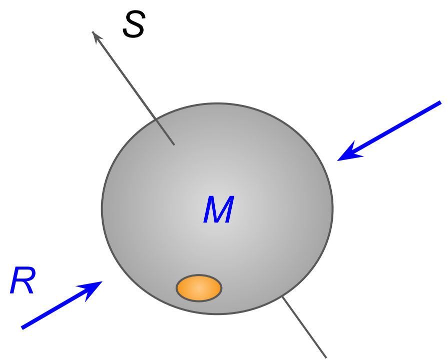

X-ray timing
Pulse profile modeling

NS Observables

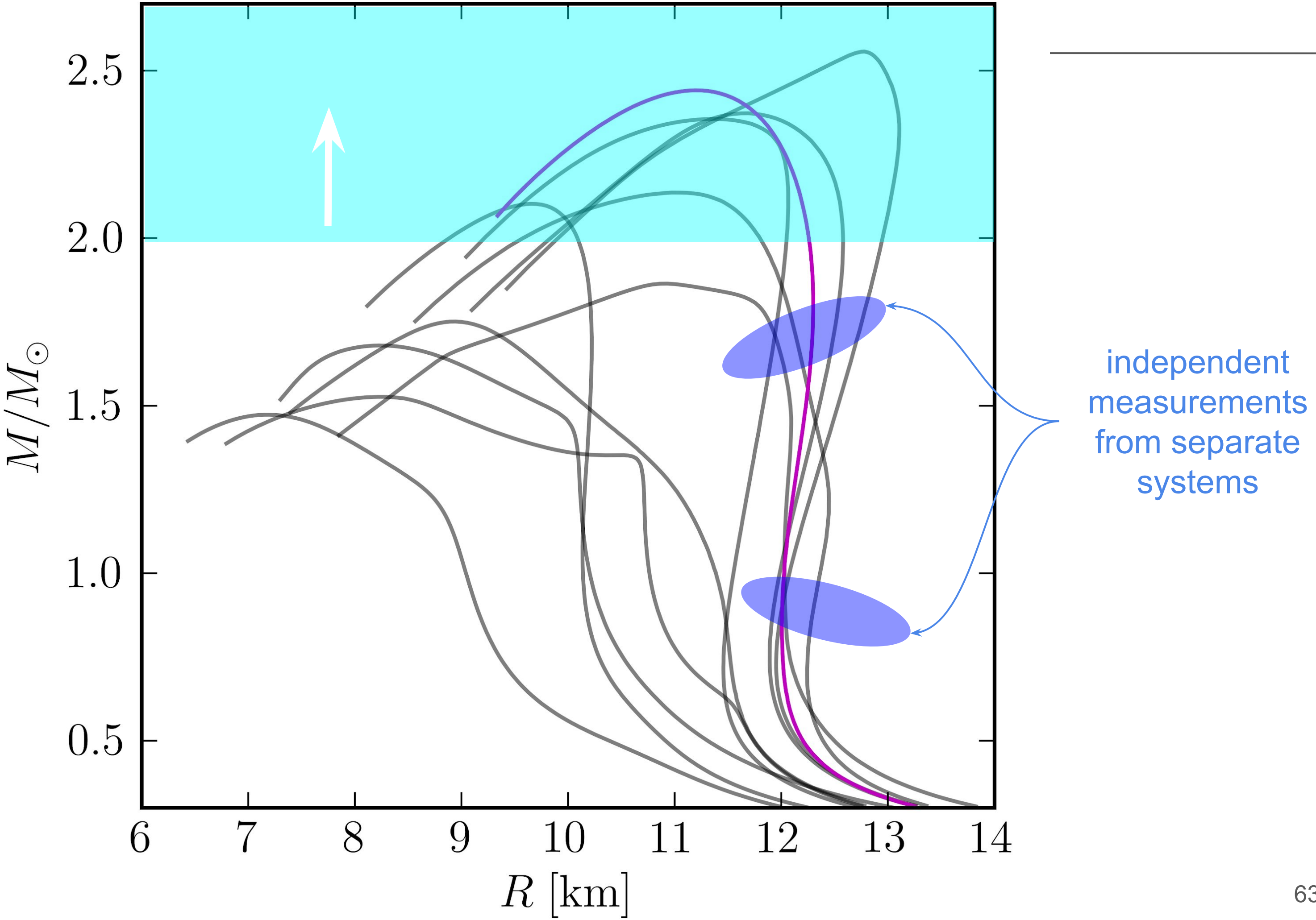

NS Observables: Mass and Tidal Deformability

dynamical tidal effects

M_{max}

Massive pulsars (PSRs)
J0740+6620 Cromartie+(2019)
Fonseca+(2021)

$\Lambda(M)$

Gravitational Waves
GW170817 Abbott+**Essick**+ (2019)
GW190425 Abbott+**Essick**+ (2020)

EoS
nuclear microphysics

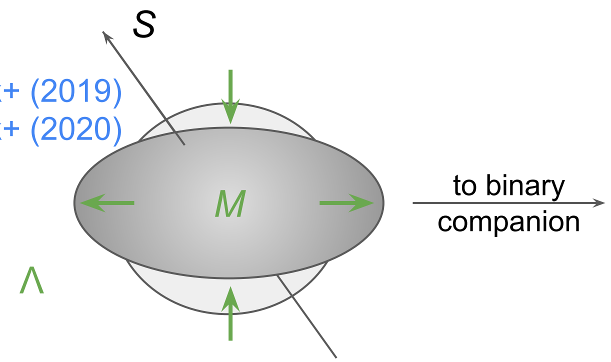

quasi-static tidal deformation

$R(M)$

X-ray pulse timing (NICER)
J0030+0451 Miller+(2019)
J0740+6620 Miller+(2021)

NS Observables

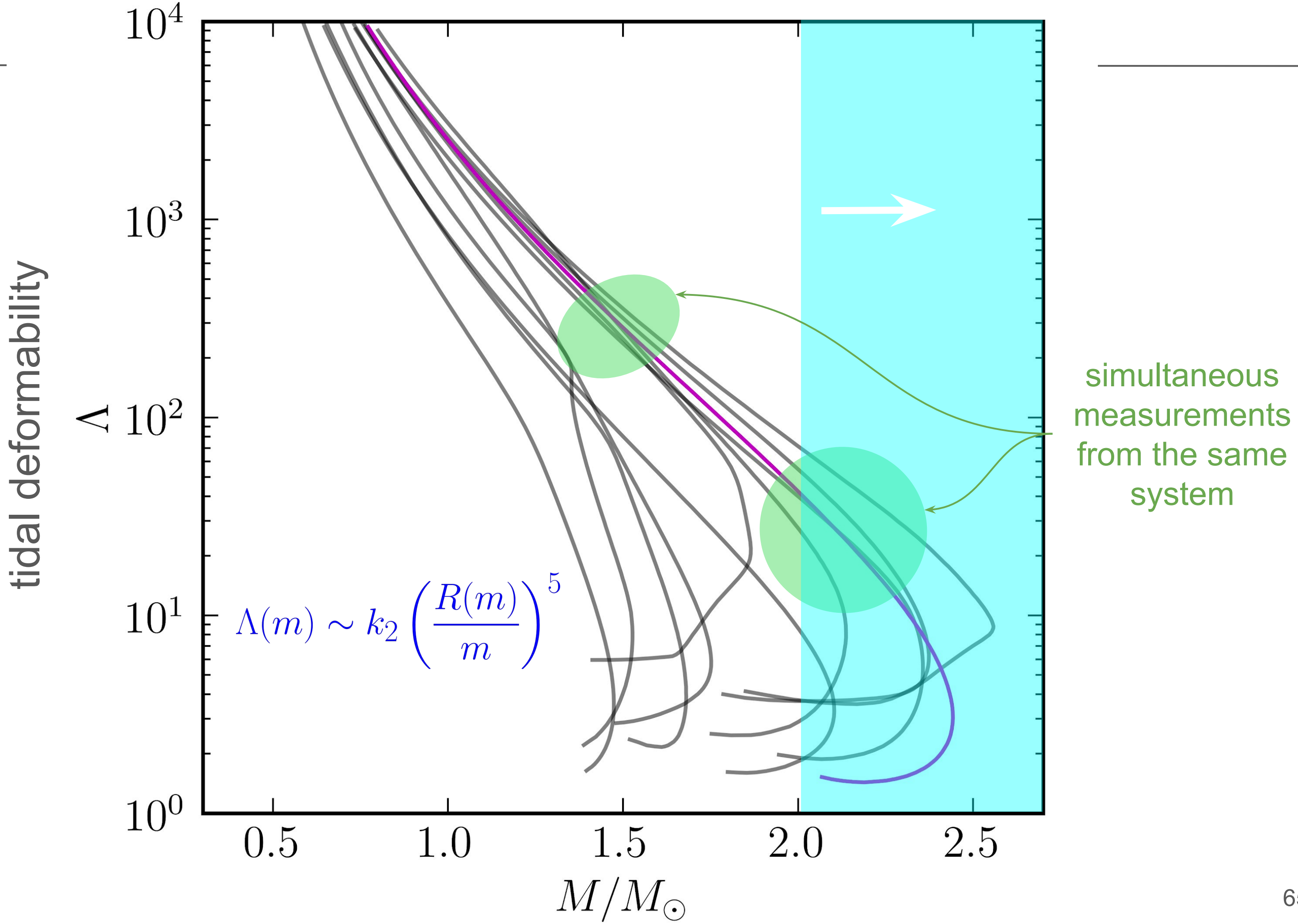

Probing the Edges of the “Mass Gap”

Barr+ (2024) Abbott+**Essick**+ (2017) Abbott+**Essick**+ (2020) Abbott+**Essick**+ (2020) Abbott+**Essick**+ (2021)

outlier detection

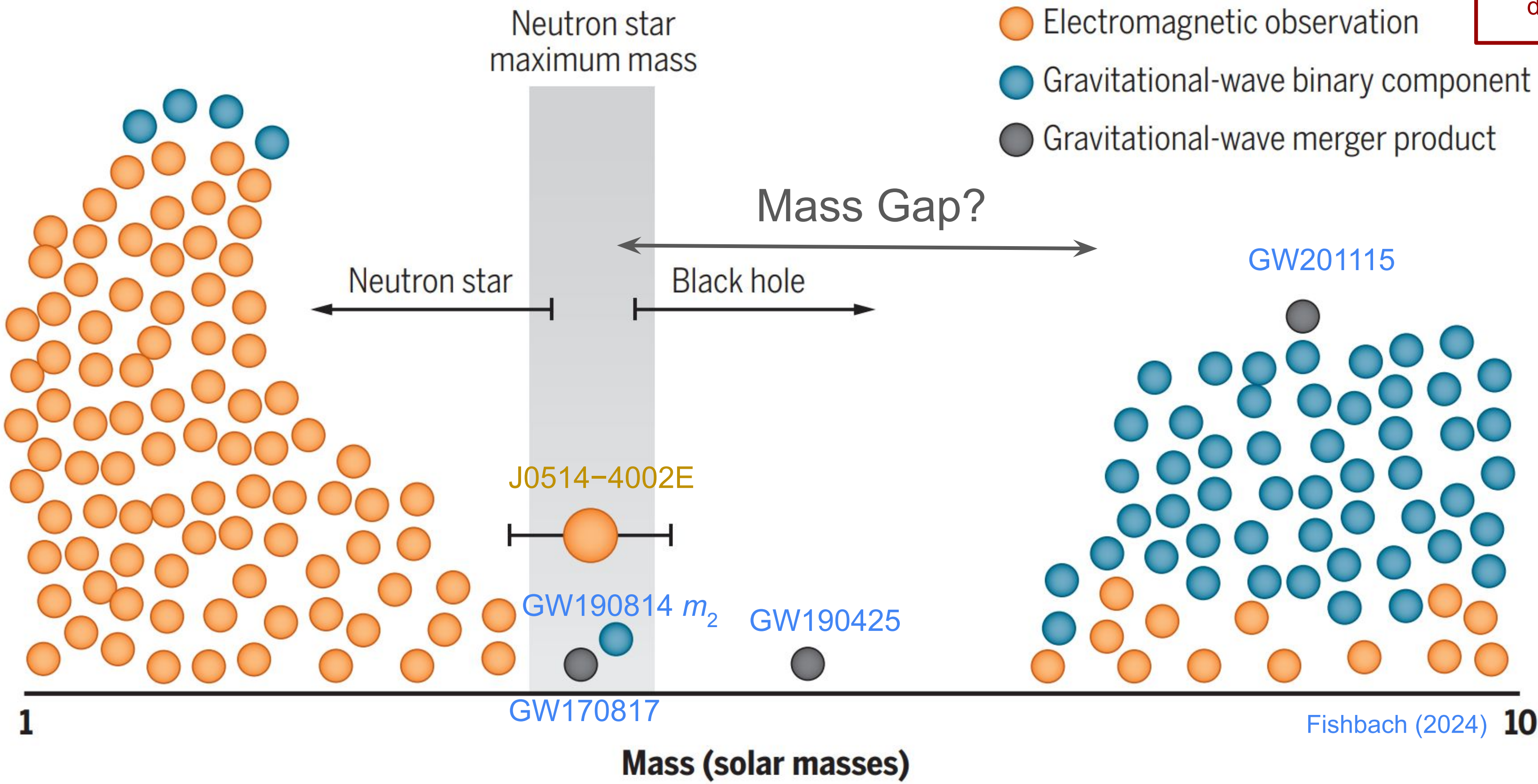

Fishbach (2024)

Accounting for Selection Effects (Malmquist Bias)

Fishbach, **Essick**+ (2020)
Farah+**Essick**+ (2022)

maximum likelihood model from O1+O2+O3a+(O3b NSBHs)

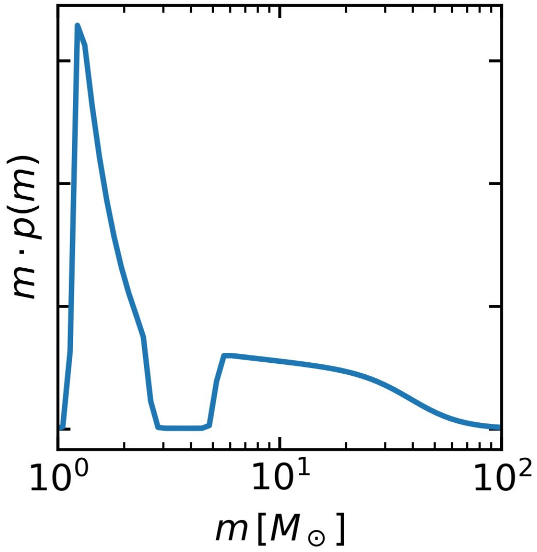

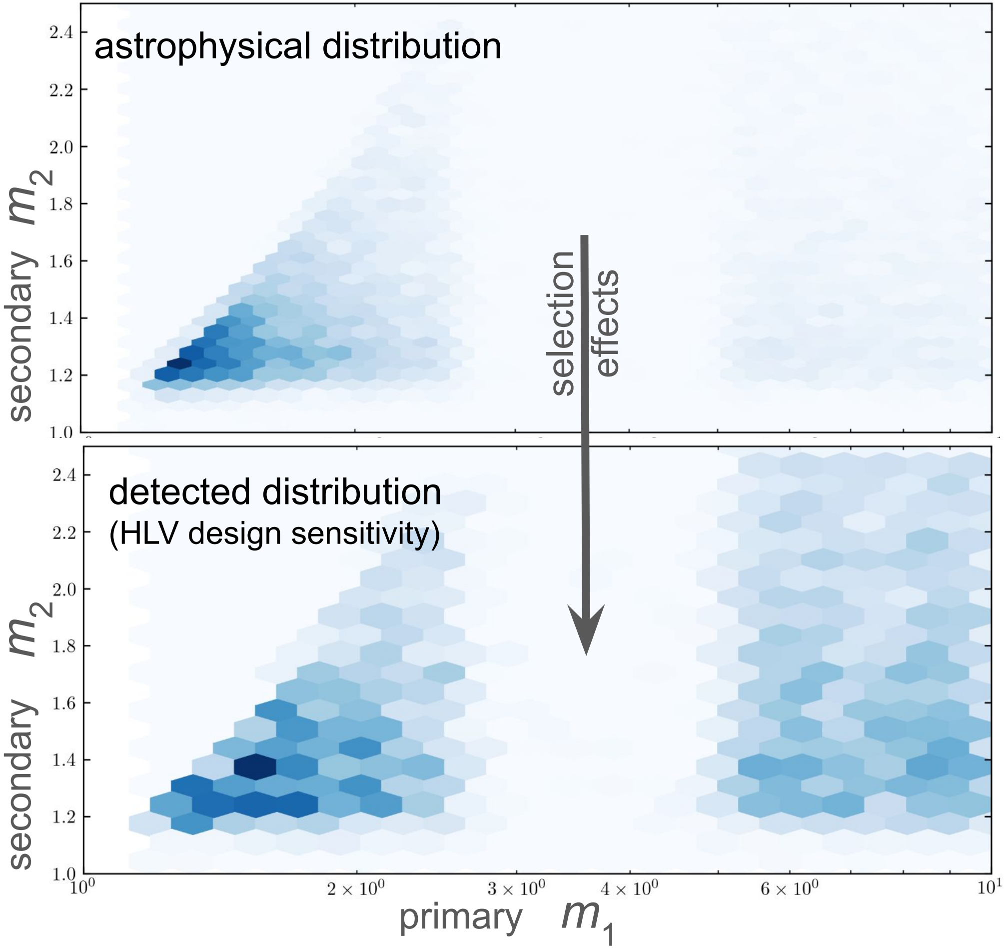

monte carlo uncertainty

search sensitivity

causal inference

Identified Features within the Mass Distribution

Fishbach, **Essick**+ (2020)
Farah+**Essick**+ (2022)

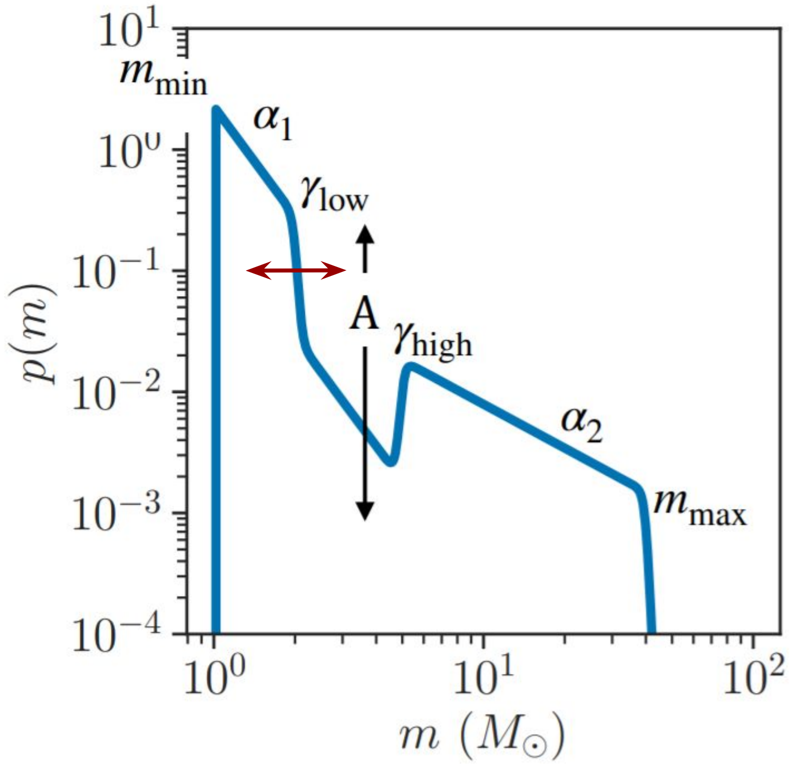

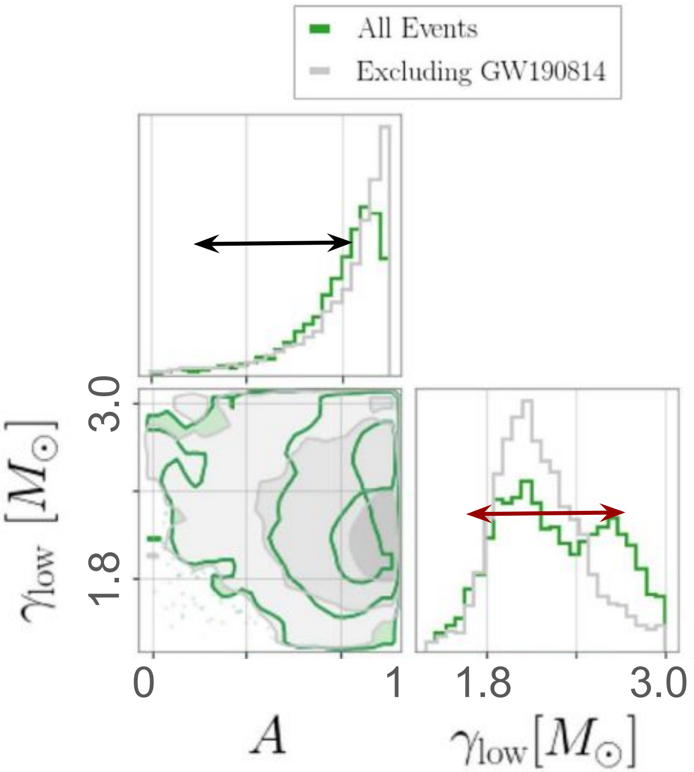

outlier detection

GW astrology

flexible pop models

Inference of the NS EoS: what is the EoS?

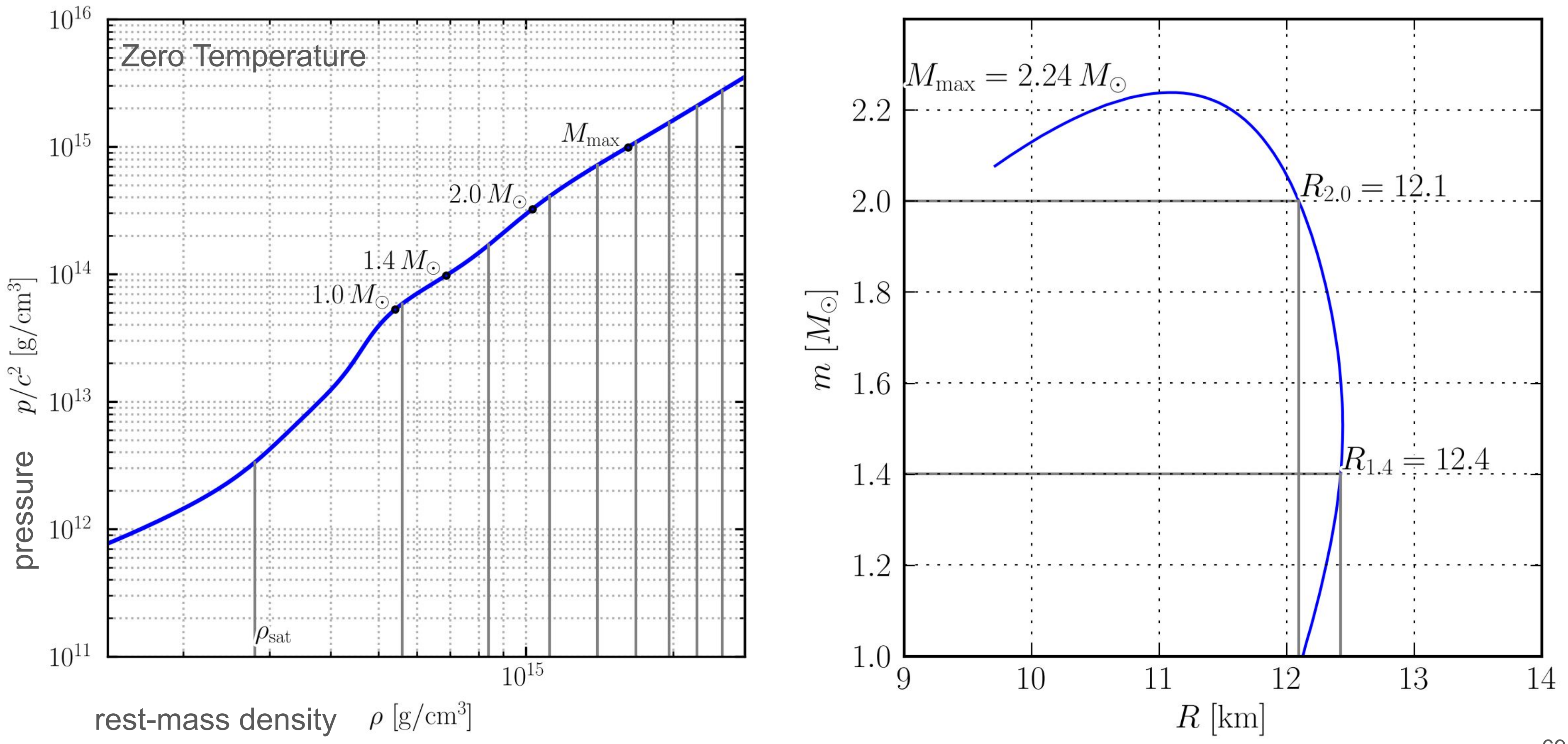

Distinguishing between NSs and BHs

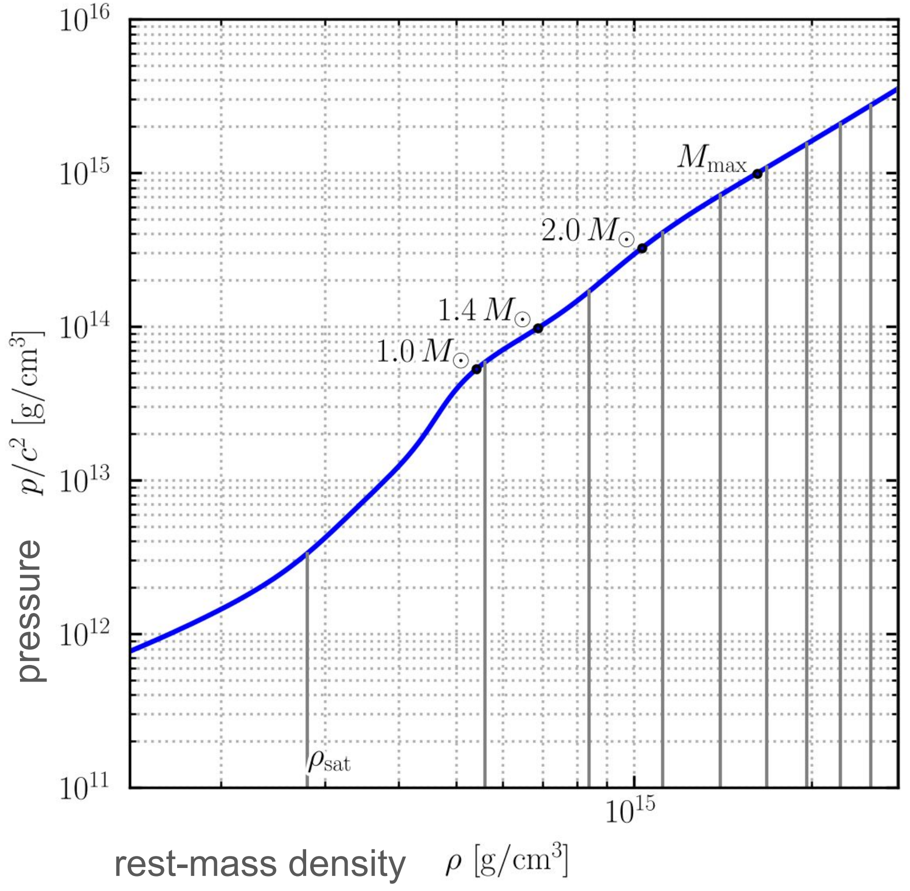

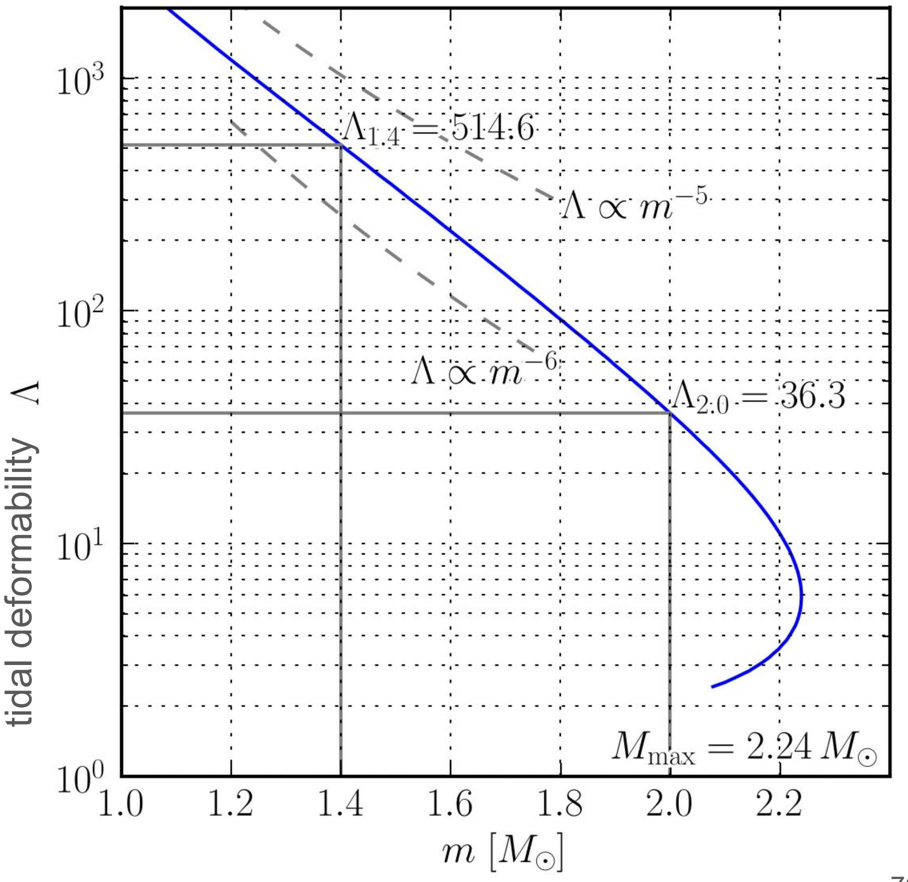

Distinguishing between NSs and BHs: effective tidal signal

Leading-order adiabatic tidal term

$$\tilde{\Lambda} = \frac{16}{13}\left(\frac{(m_1 + 12m_2)m_1^4\Lambda_1 + (m_2 + 12m_1)m_2^4\Lambda_2}{(m_1 + m_2)^5}\right)$$

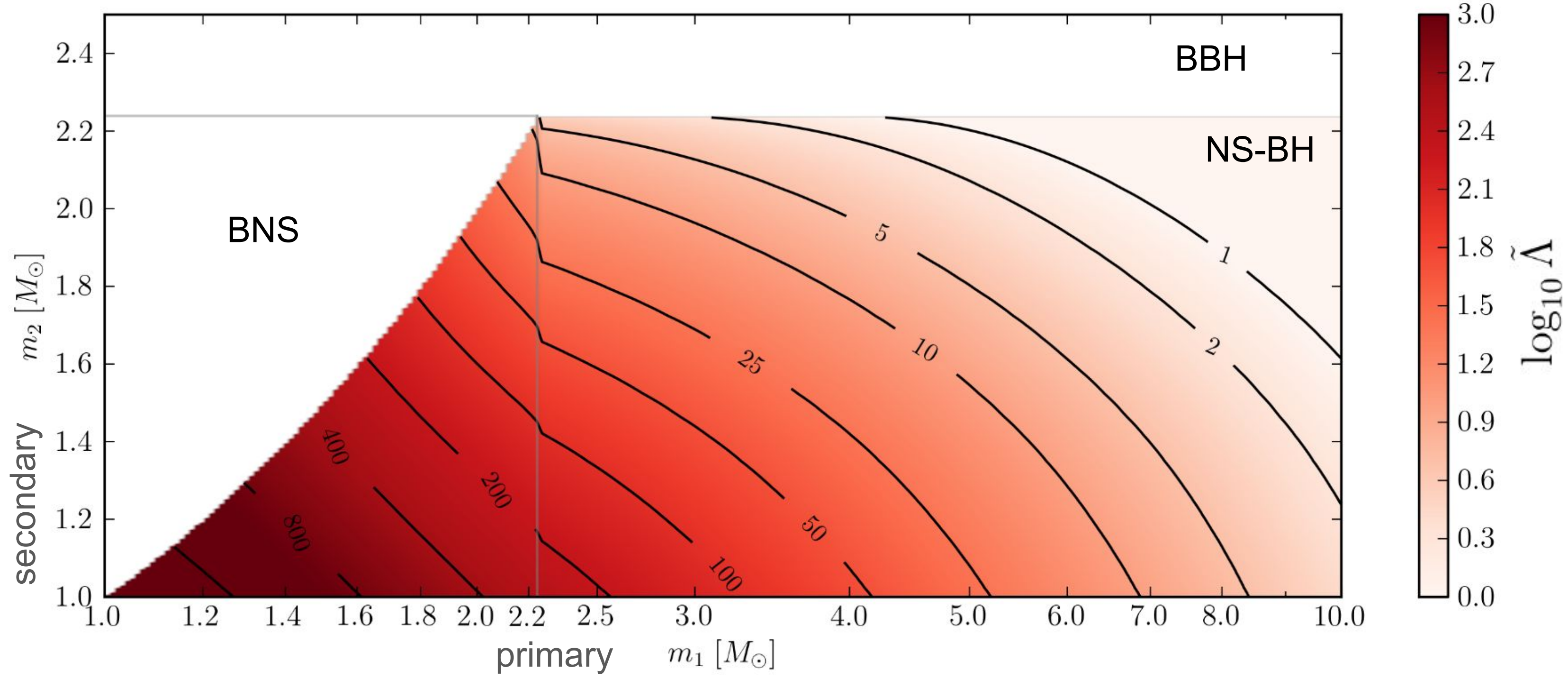

Distinguishing between NSs and BHs

Fisher Matrix : simplistic PN phasing, aLIGO design sensitivity, **SNR=10**, wide priors on spins, mass ratio
→ “best case” scenario (Cramer-Rao bound) that strictly holds only in the high-SNR limit

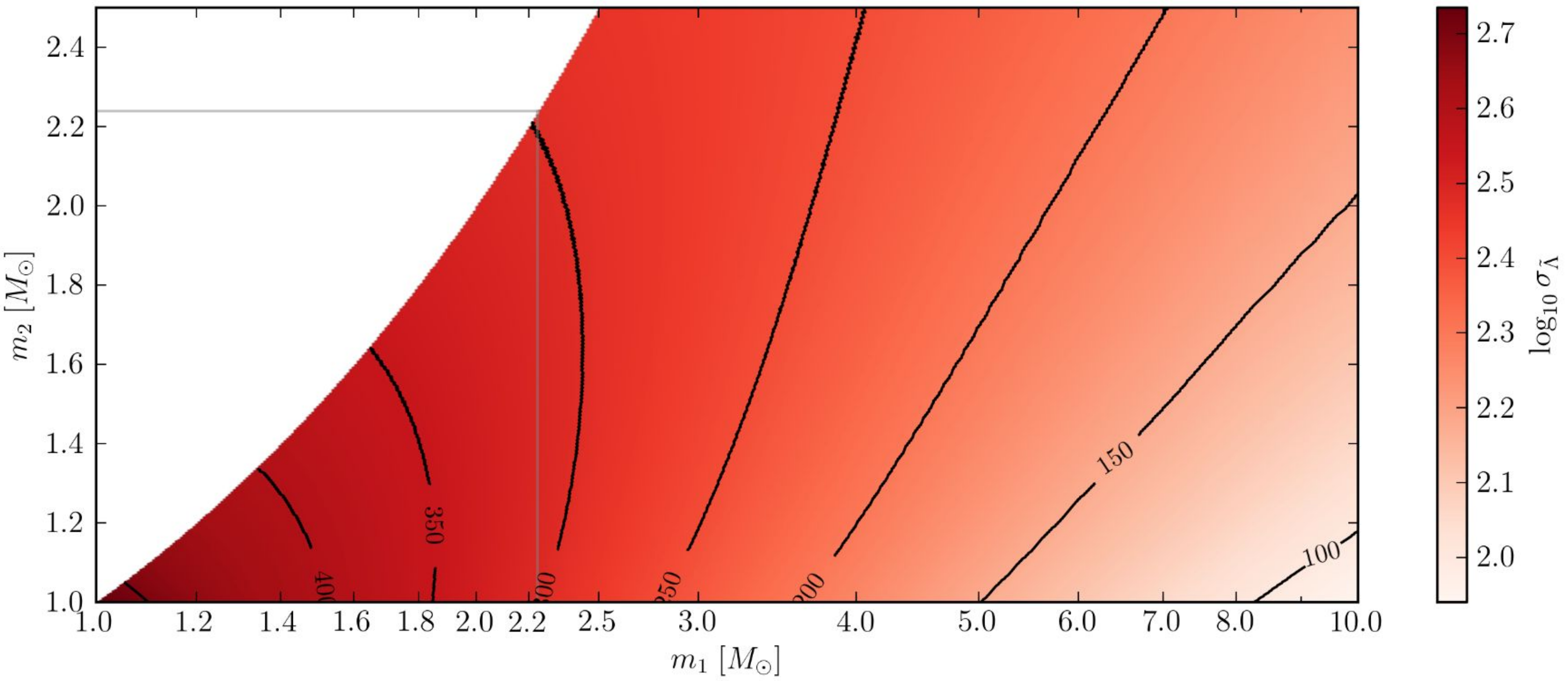

Distinguishing between NSs and BHs: precision of individual measurements

It will be nearly impossible to distinguish between NS and BH based on tidal deformability at high masses

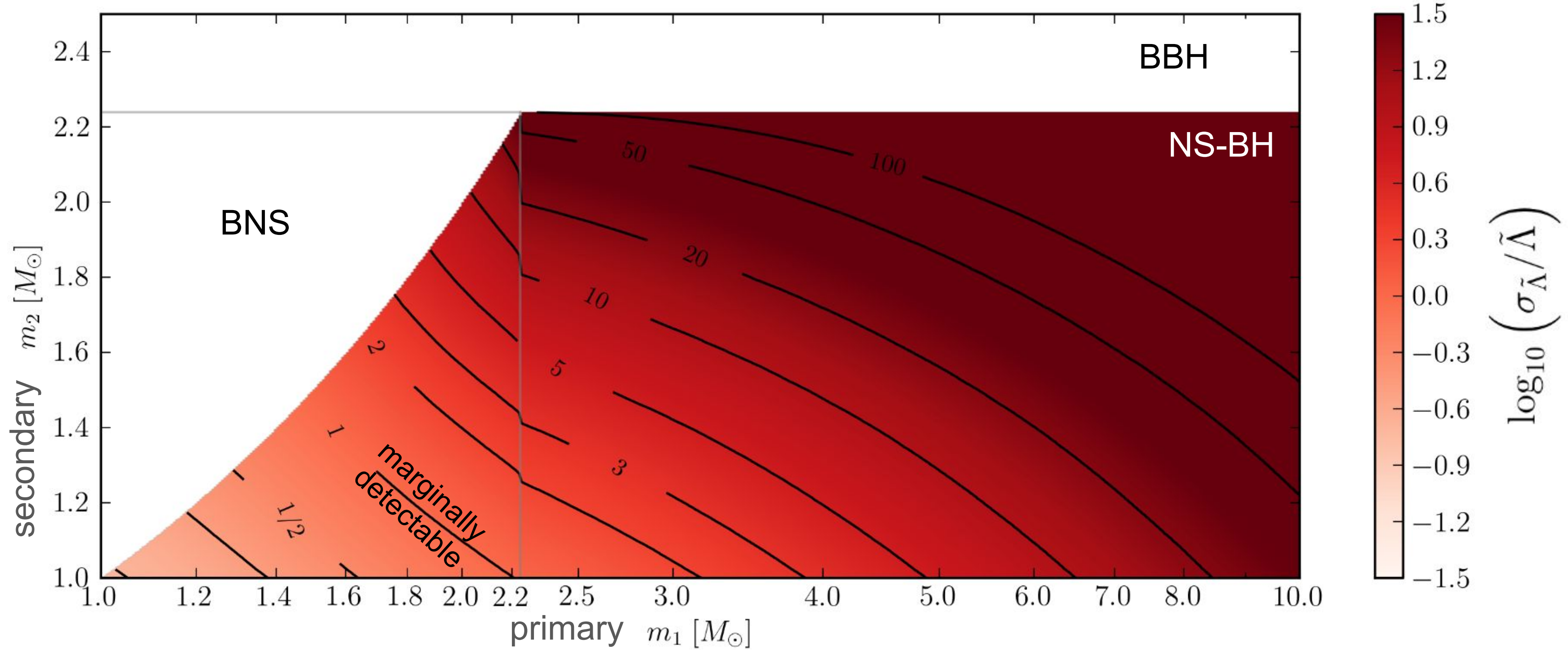

Distinguishing between NSs and BHs Masses & Spins

Essick & Landry (2020)

We can still check for consistency between mass, spin, and EoS accounting for uncertainty in the

object's mass and spin
(including uncertainty in the population)

properties of NSs

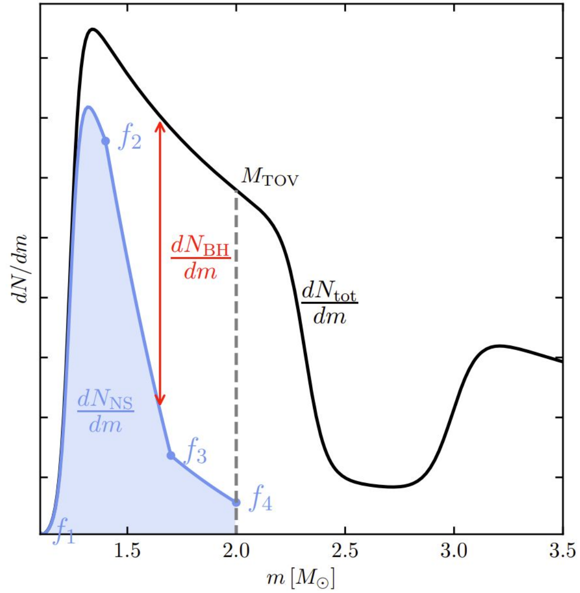

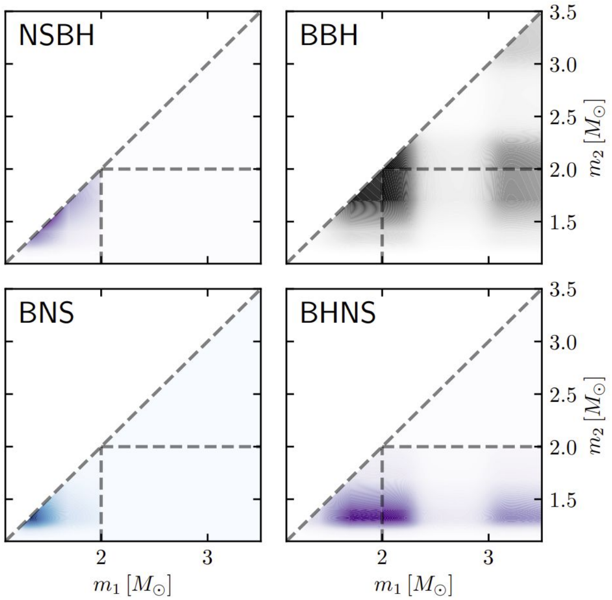

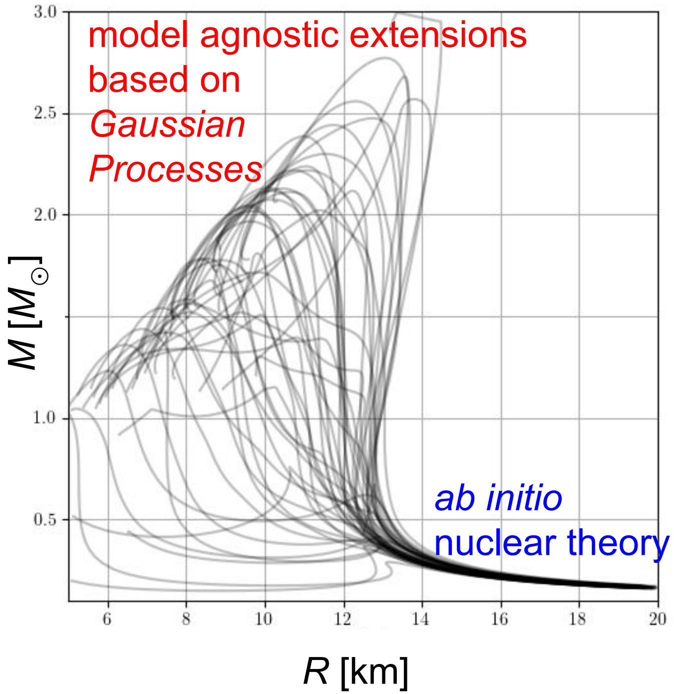

Distinguishing between NSs and BHs

Essick & Landry (2020)

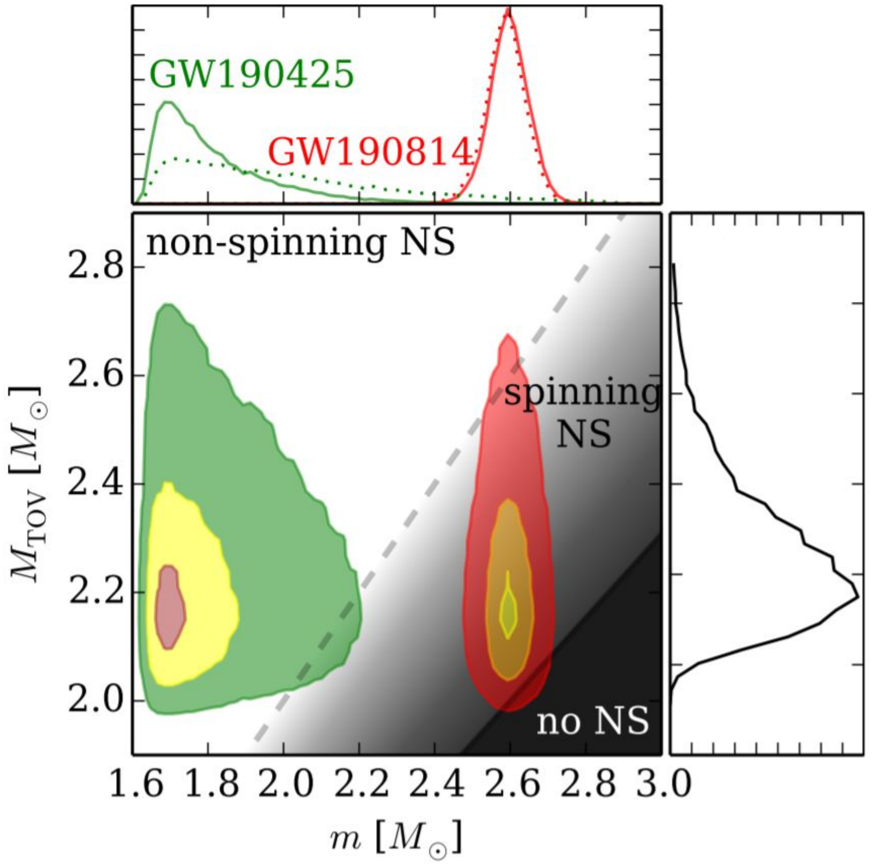

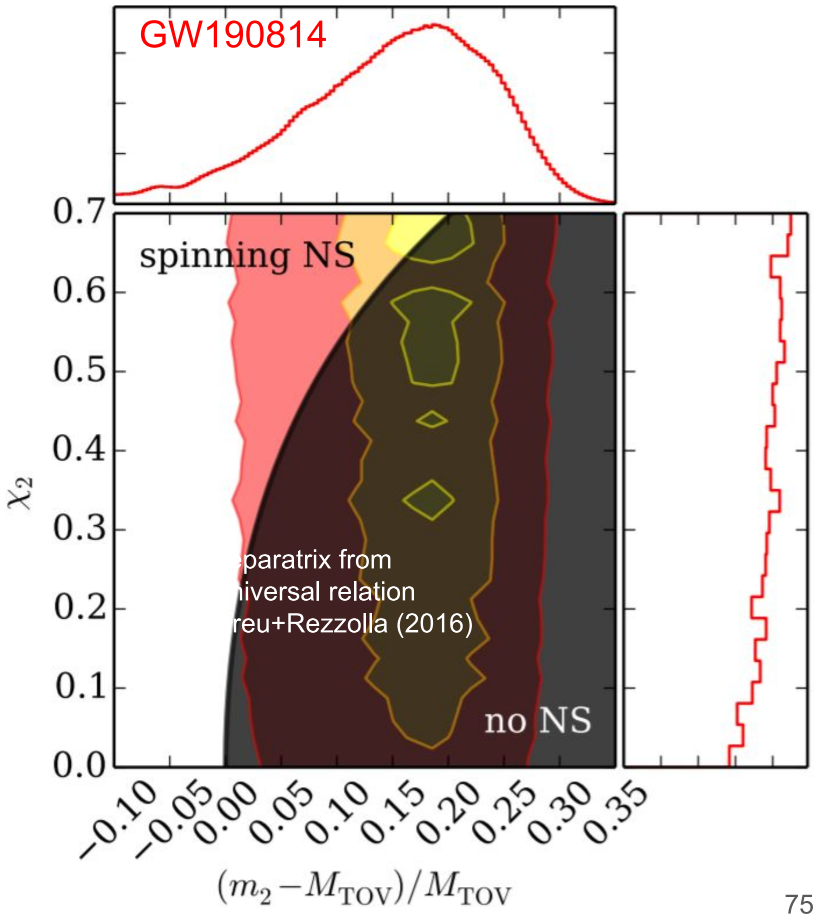

Distinguishing between NSs and BHs Masses & Spins

Essick & Landry (2020) Abbott+Essick+ (2020) Abbott+Essick+ (2021)

We can still check for **consistency between mass, spin, and EoS** with GW200115 (NSBH from Abbott+**Essick**+ 2023)

mass distribution disfavors equal-mass binaries

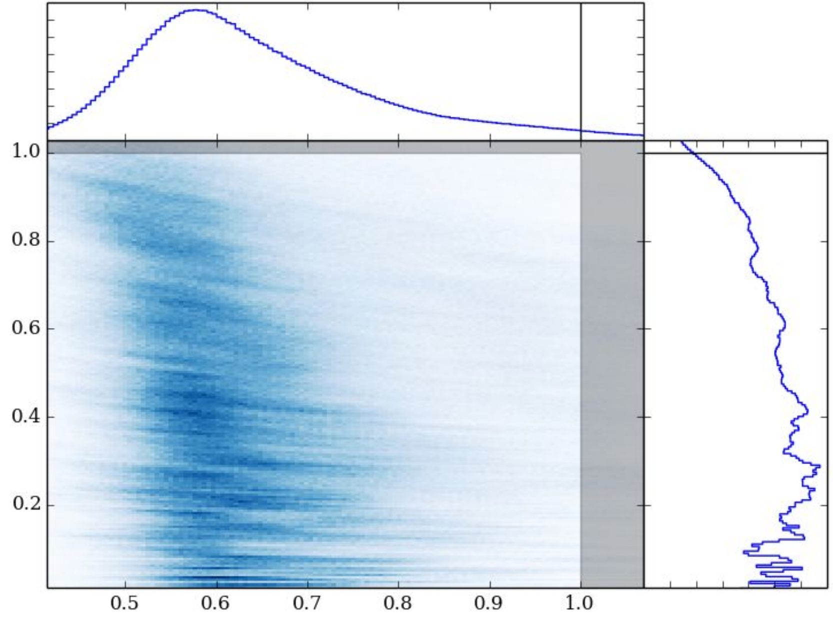

$s\,/\,s_{max}(M_{TOV}, R_{TOV})$

$m\,/\,M_{max}(M_{TOV}, s)$

mass distribution favors equal-mass binaries

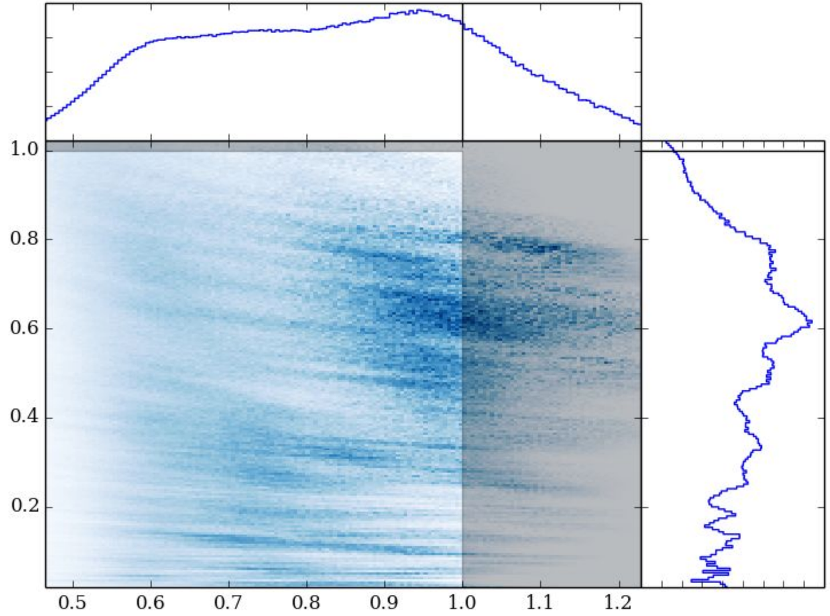

$m\,/\,M_{max}(M_{TOV}, s)$

Inference of the NS EoS: hierarchical Bayesian inference

Essick & Fishbach (2023)

hierarchical inference

We use a hierarchical model of the data-generation process

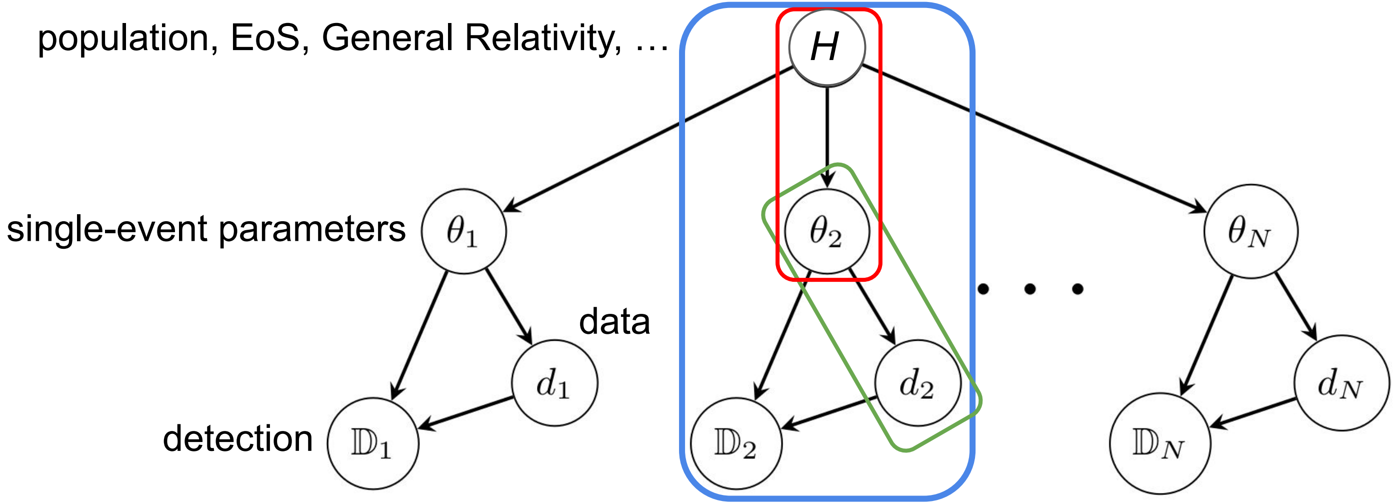

or, equivalently,

$$p(\{\mathbb{D}_i, d_i, \theta_i\}|N, H) = \prod_i^N \boxed{P(\mathbb{D}_i|d_i, \theta_i)\boxed{p(d_i|\theta_i)}\boxed{p(\theta_i|H)}}$$

likelihood prior

Inference of the NS EoS: phase transitions

Legred+**Essick**+ (2021)

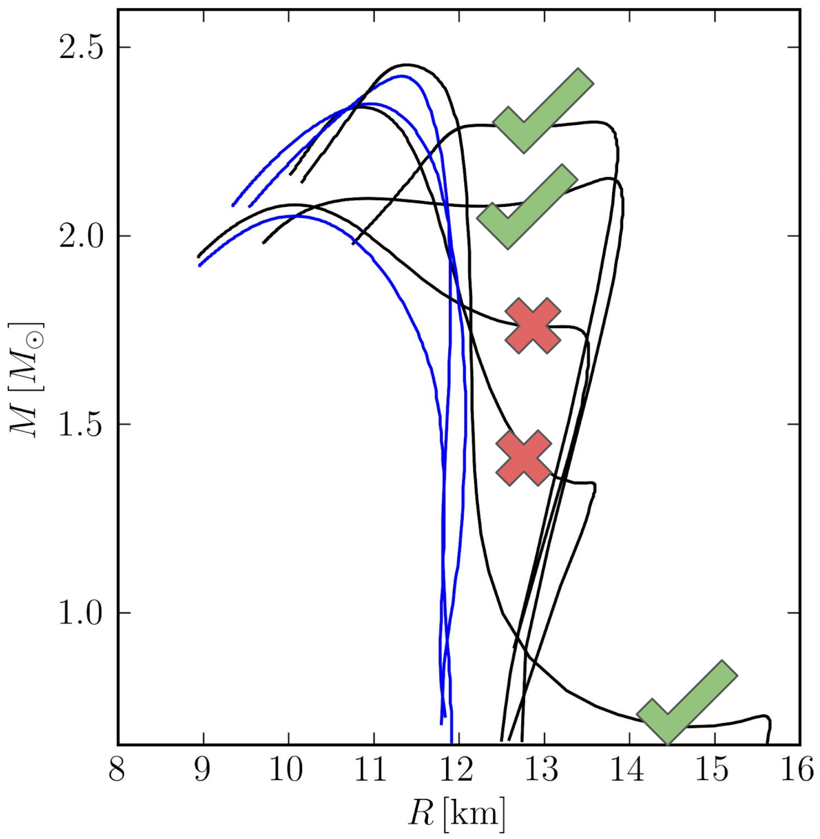

Data		max $\mathcal{L}^{n>1}_{n=1}$	$\mathcal{B}^{n>1}_{n=1}$	max $\mathcal{L}^{c_s^2>c^2/3}_{c_s^2\le c^2/3}$	$\mathcal{B}^{c_s^2>c^2/3}_{c_s^2\le c^2/3}$
w/PSRs		1.00	0.120 ± 0.002	1.0	10.2 ± 0.5
w/o J0740+6620		0.97	0.220 ± 0.007	50.8	2220 ± 790
w/J0740+6620	Miller+	0.60	0.146 ± 0.005	26.7	1000 ± 340
	Riley+	0.94	0.185 ± 0.006	72.7	2450 ± 1820

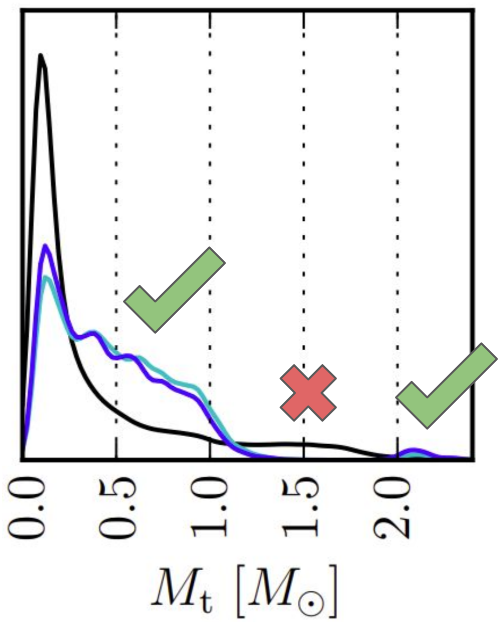

Inference of the NS EoS: phase transitions

Essick+ (2023)

the sudden appearance of new (degenerate) degrees of freedom produces a sharp drop in the sound speed (c_s)
→ *"loss of pressure support"*

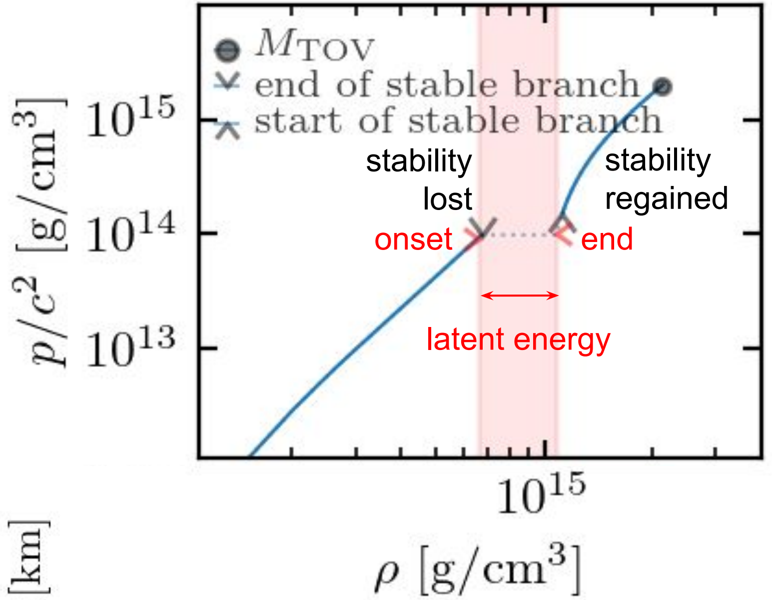

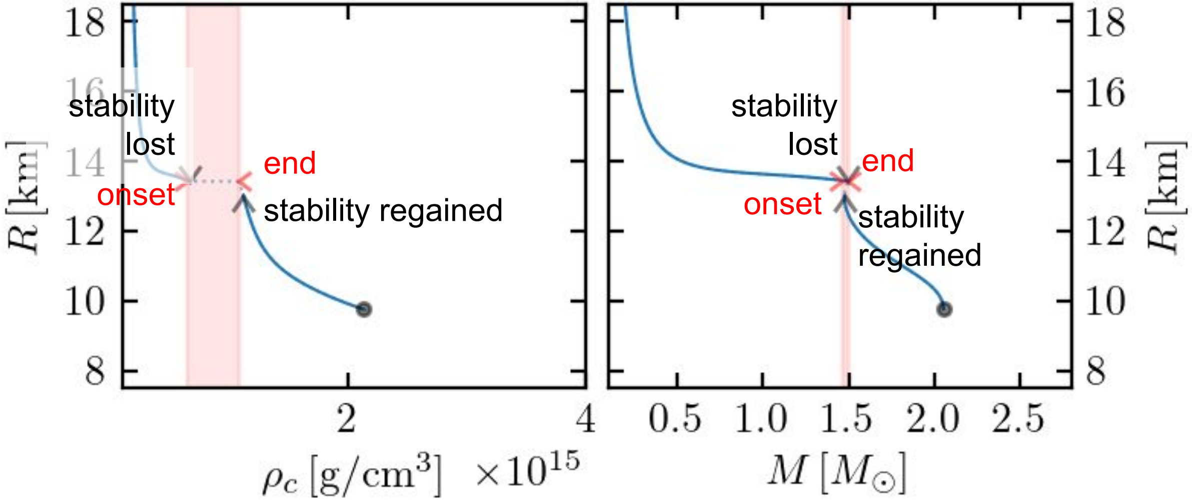

Inference of the NS EoS: phase transitions

Essick+ (2023)

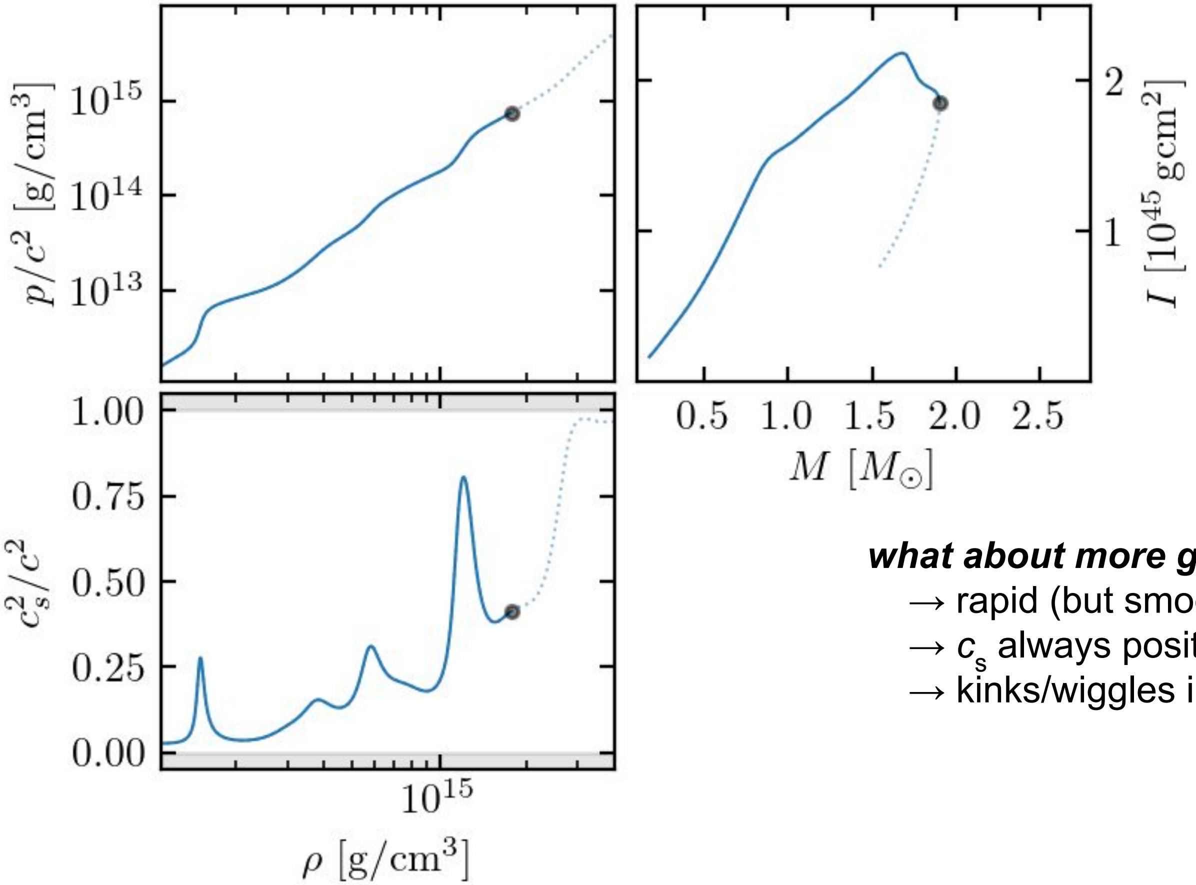

what about more general phenomenology?

→ rapid (but smooth) changes in c_s?

→ c_s always positive definite?

→ kinks/wiggles in stellar sequence but no loss of stability?

Inference of the NS EoS: phase transitions

Essick+ (2023)

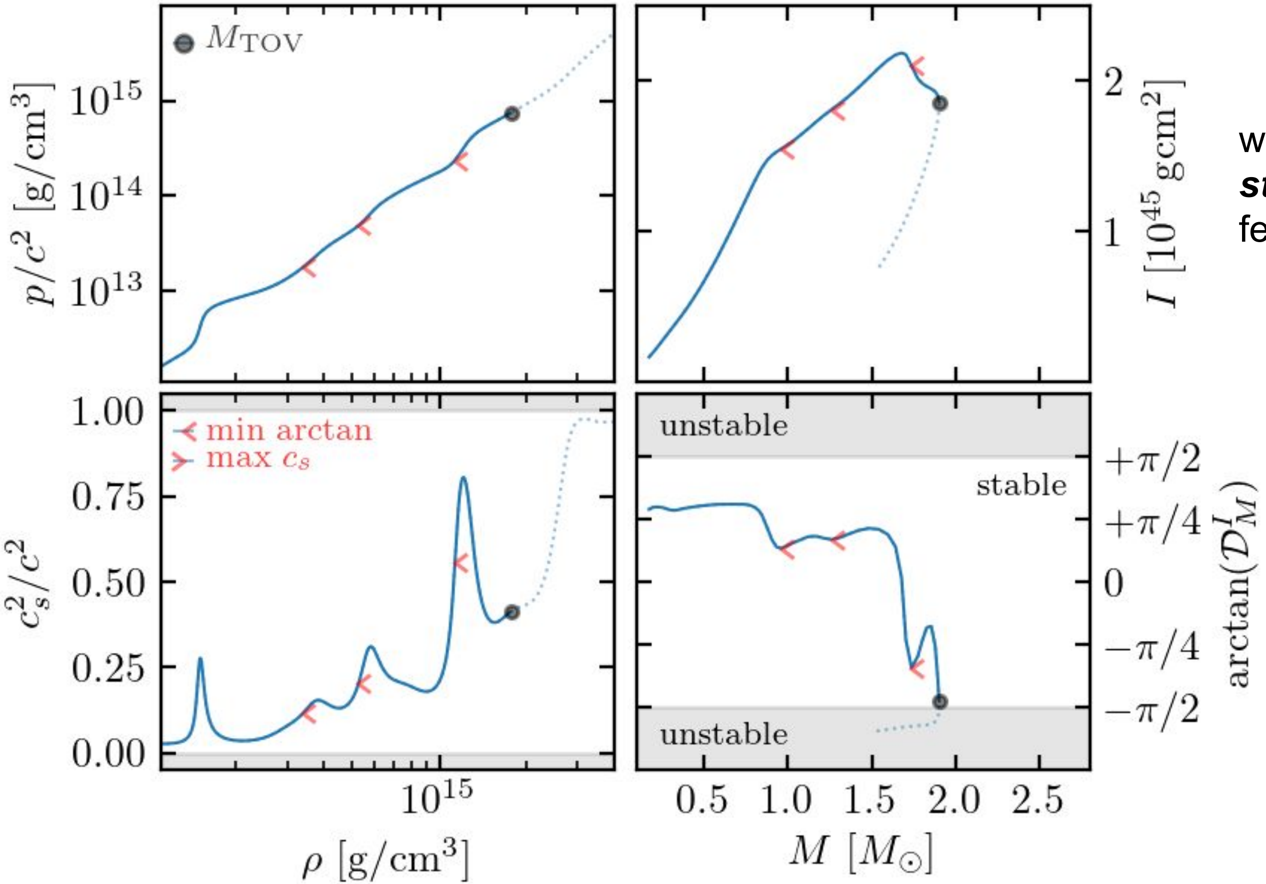

we search for ***features based on stellar properties*** and connect these to features in c_s

$$\mathcal{D}^I_M \equiv \frac{d\log I/d\log p_c}{d\log M/d\log p_c}$$

Inference of the NS EoS: phase transitions

Essick+ (2023)

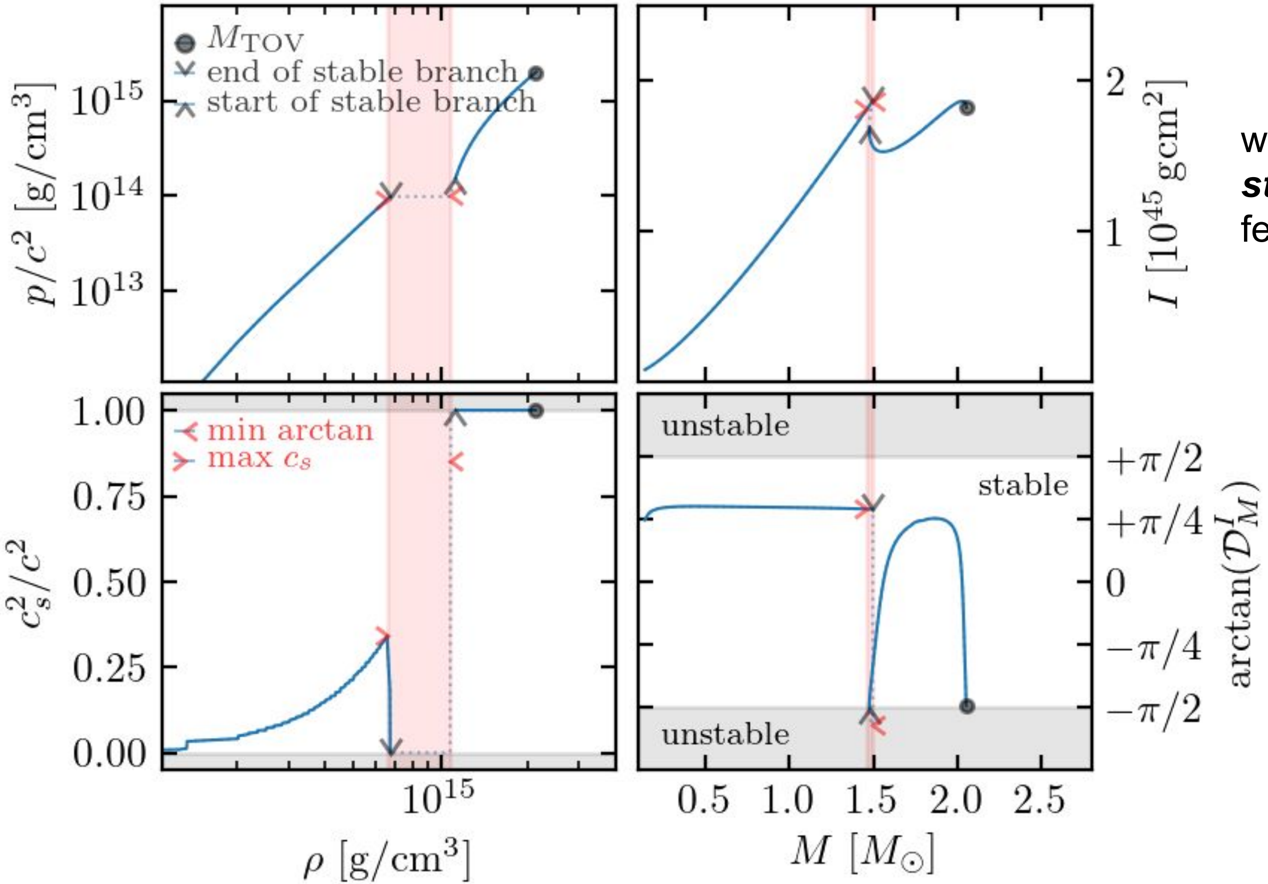

we search for ***features based on stellar properties*** and connect these to features in c_s

local minima → ***end*** of phase trans

and do so more precisely than where stability is regained

Inference of the NS EoS: phase transitions

Essick+ (2023)

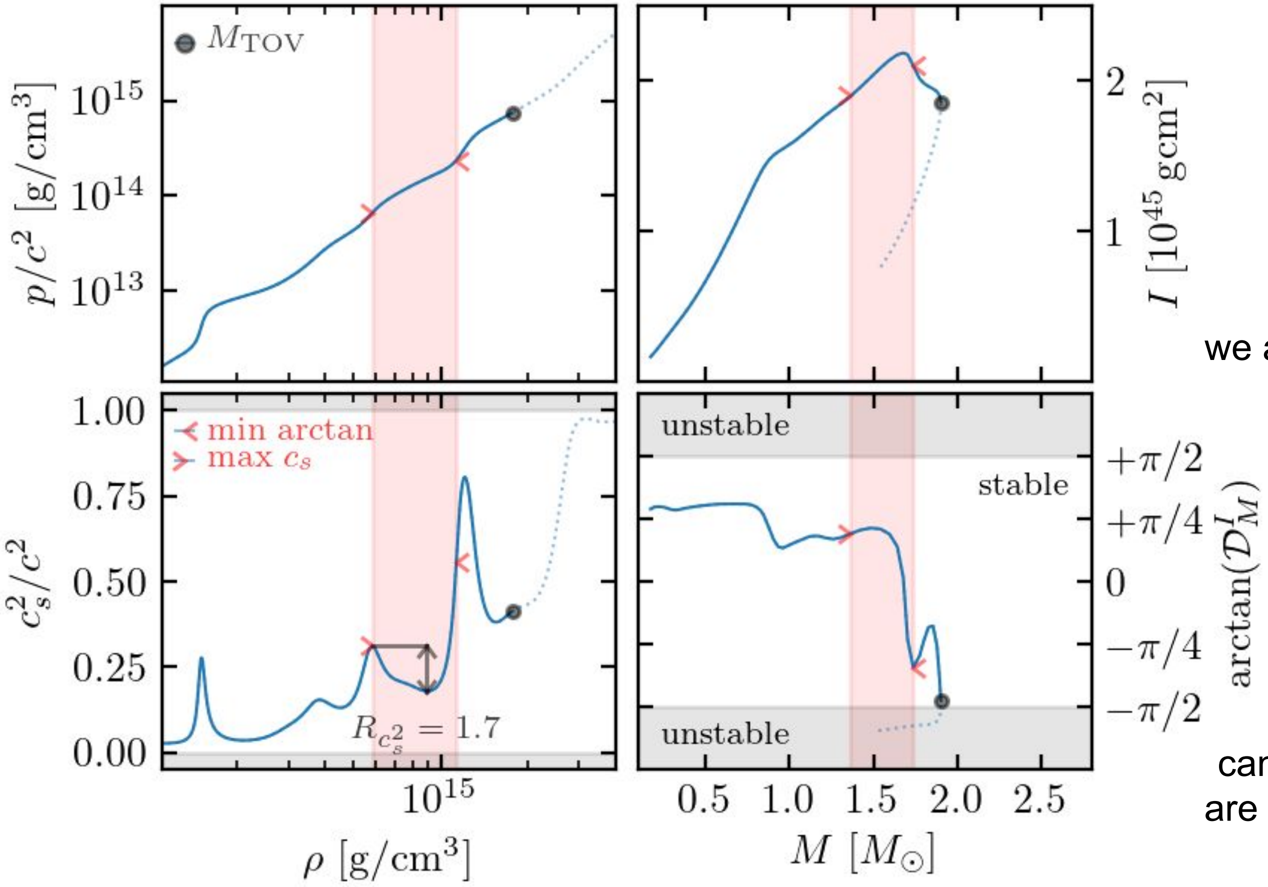

we associate a ***local minimum*** (***end***) with the most recent preceding ***"running maximum" in c_s*** (***onset***)

candidate ***running maxima in c_s*** (***onset***) are accepted only if they are followed by a ***large drop in c_s***

Inference of the NS EoS: phase transitions

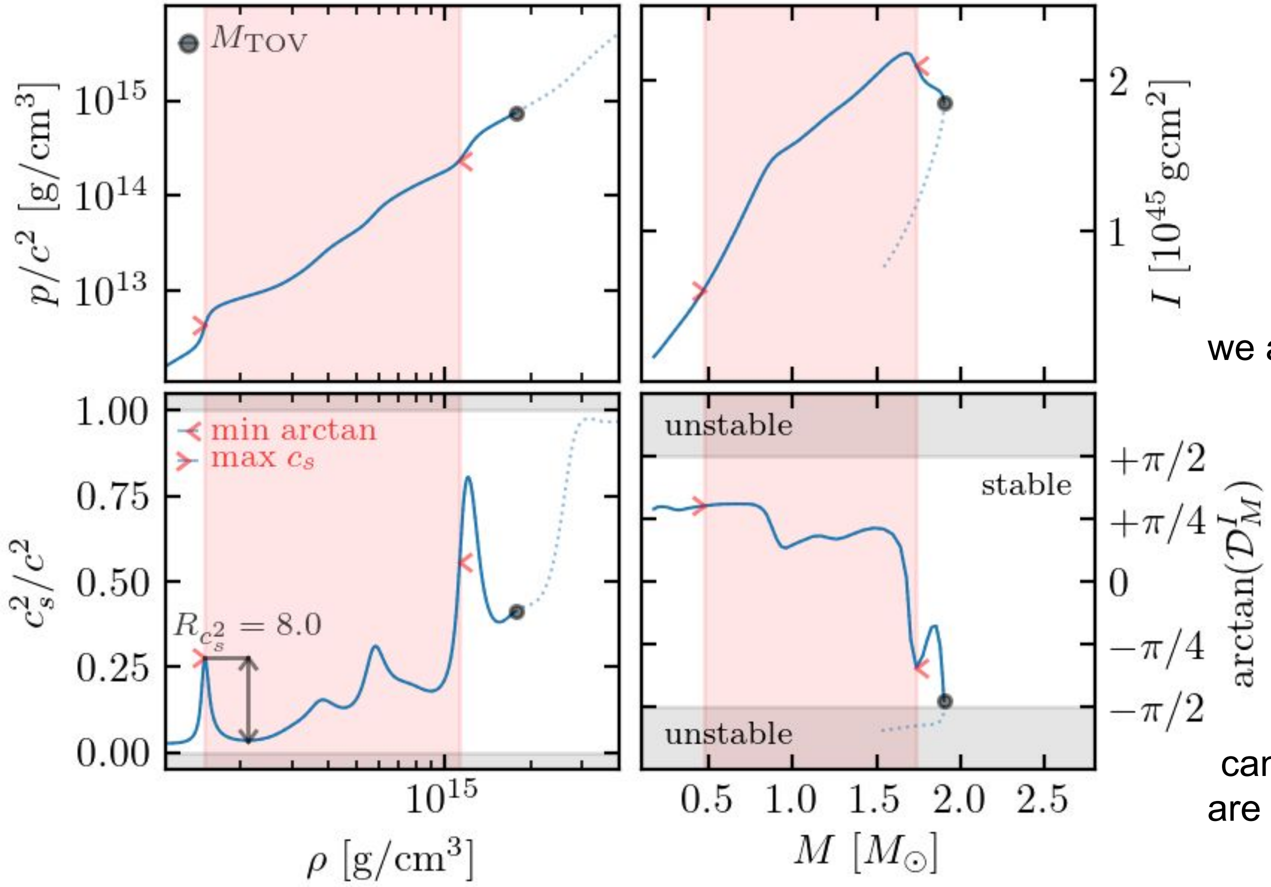

we associate a ***local minimum*** (***end***) with the most recent preceding ***"running maximum" in c_s*** (***onset***)

candidate ***running maxima in c_s*** (***onset***) are accepted only if they are followed by a ***large drop in c_s***

Inference of the NS EoS: phase transitions

Essick+ (2023)

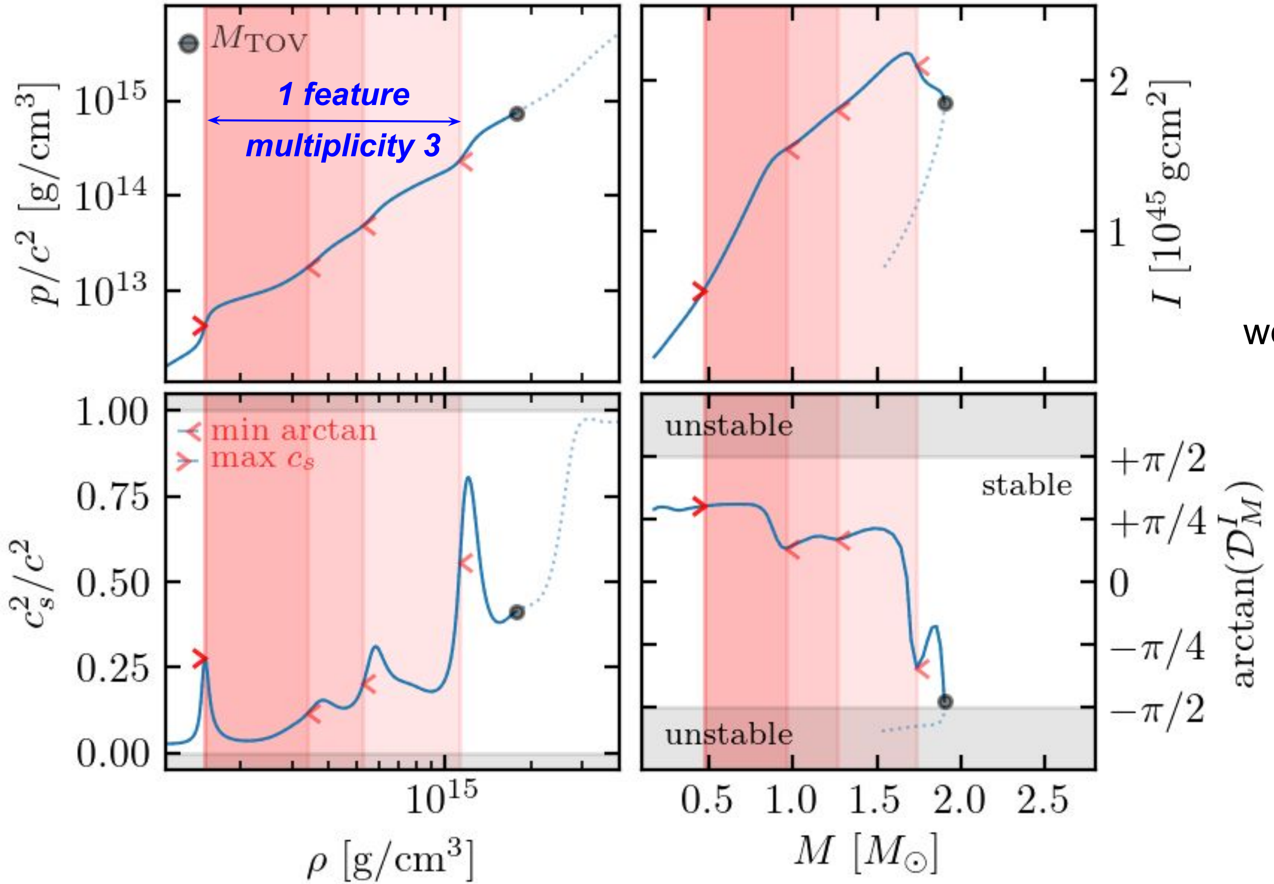

we iterate until all ***local minimum*** (***end***) *have an associated* ***"running maximum" in c_s*** (***onset***)

this EoS has
1 feature
with
multiplicity 3

Inference of the NS EoS: phase transitions

masses from J0348, J0740
LIGO-Virgo-KAGRA GWs from GW170817, GW190425
NICER X-ray Timing from J0030, J0740

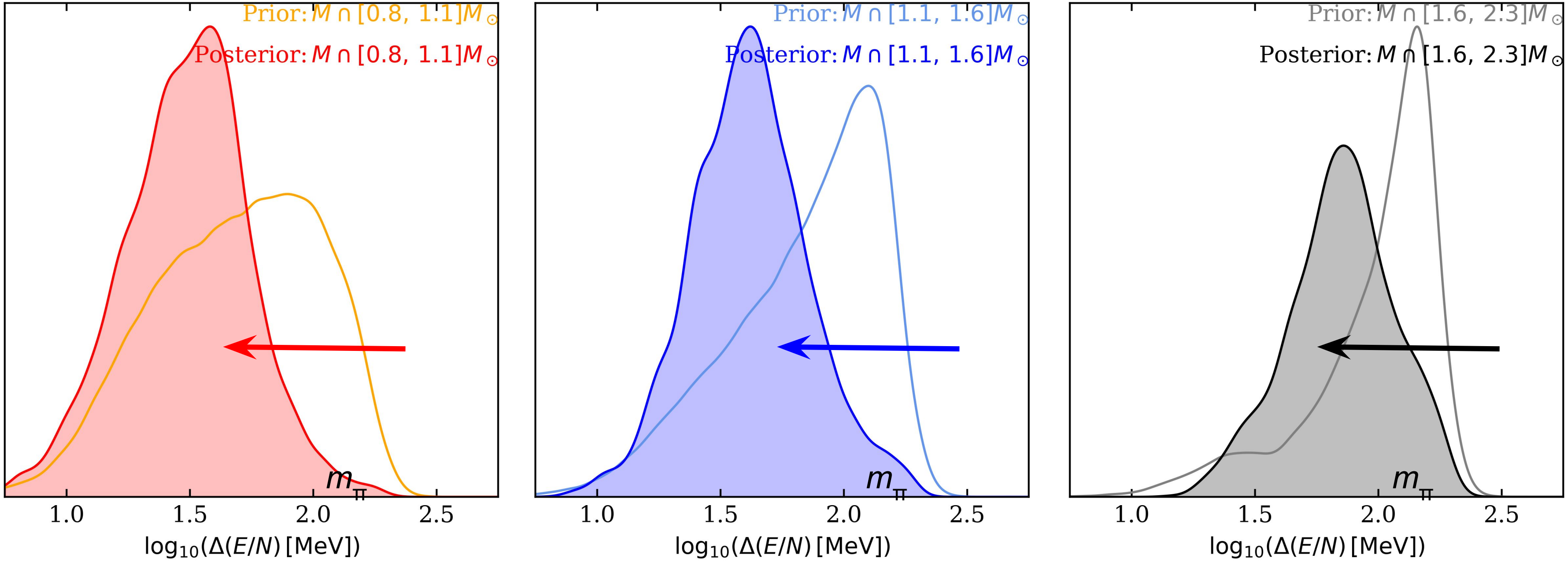

Inference of the NS EoS: phase transitions

Essick+ (2023)

masses from J0348, J0740
LIGO-Virgo-KAGRA GWs from GW170817, GW190425
NICER X-ray Timing from J0030, J0740

M $[M_\odot]$	Stable Branches			$\min \Delta(E/N)$ [MeV]	$\mathcal{D}_M^I$ Features		
	$\max \mathcal{L}_{n=1}^{n\geq 2}(\mathrm{PGX})$	$\mathcal{B}_{n=1}^{n\geq 2}(\mathrm{PGX})$	$\mathcal{B}_{n=1}^{n\geq 2}(\mathrm{GX}\|\mathrm{P})$		$\max \mathcal{L}_{n=0}^{n\geq 1}(\mathrm{PGX})$	$\mathcal{B}_{n=0}^{n\geq 1}(\mathrm{PGX})$	$\mathcal{B}_{n=0}^{n\geq 1}(\mathrm{GX}\|\mathrm{P})$
0.8–1.1	0.47	0.362 ± 0.036	2.219 ± 0.162	10	0.57	1.222 ± 0.020	0.684 ± 0.011
				50	0.49	0.366 ± 0.011	0.588 ± 0.016
				100	0.26	0.117 ± 0.008	0.292 ± 0.021
1.1–1.6	0.14	0.030 ± 0.006	0.291 ± 0.055	10	0.57	1.043 ± 0.020	0.552 ± 0.010
				50	0.49	0.463 ± 0.013	0.552 ± 0.010
				100	0.26	0.152 ± 0.009	0.267 ± 0.017
1.6–2.3	0.20	0.147 ± 0.028	0.120 ± 0.026	10	0.52	1.012 ± 0.035	0.385 ± 0.013
				50	0.49	0.898 ± 0.034	0.385 ± 0.013
				100	0.29	0.383 ± 0.023	0.256 ± 0.016

Inference of the NS EoS: no systematics with nonparametrics

Essick+ (2023)

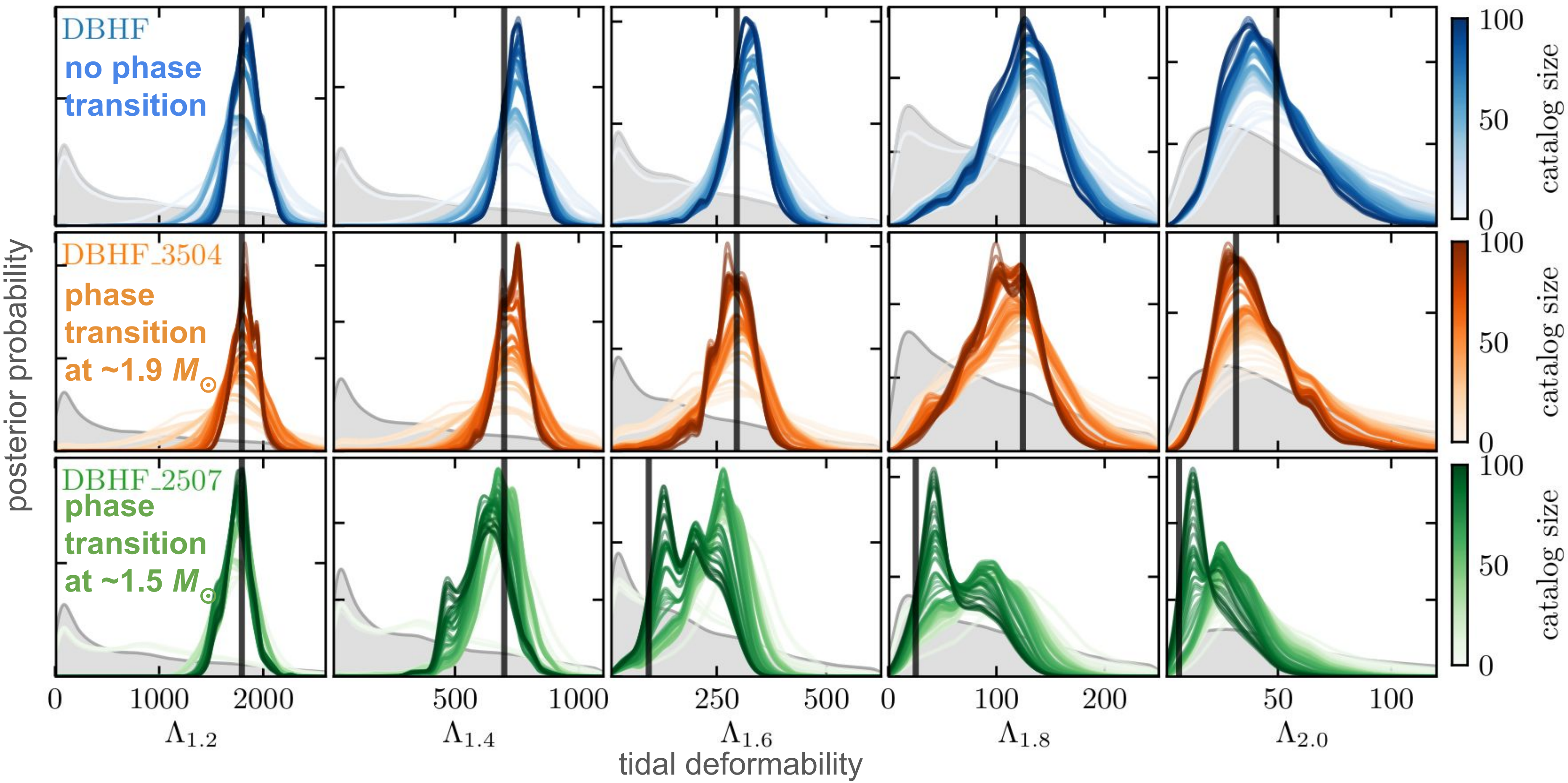

Future Prospects: phase transitions

Essick+ (2023)

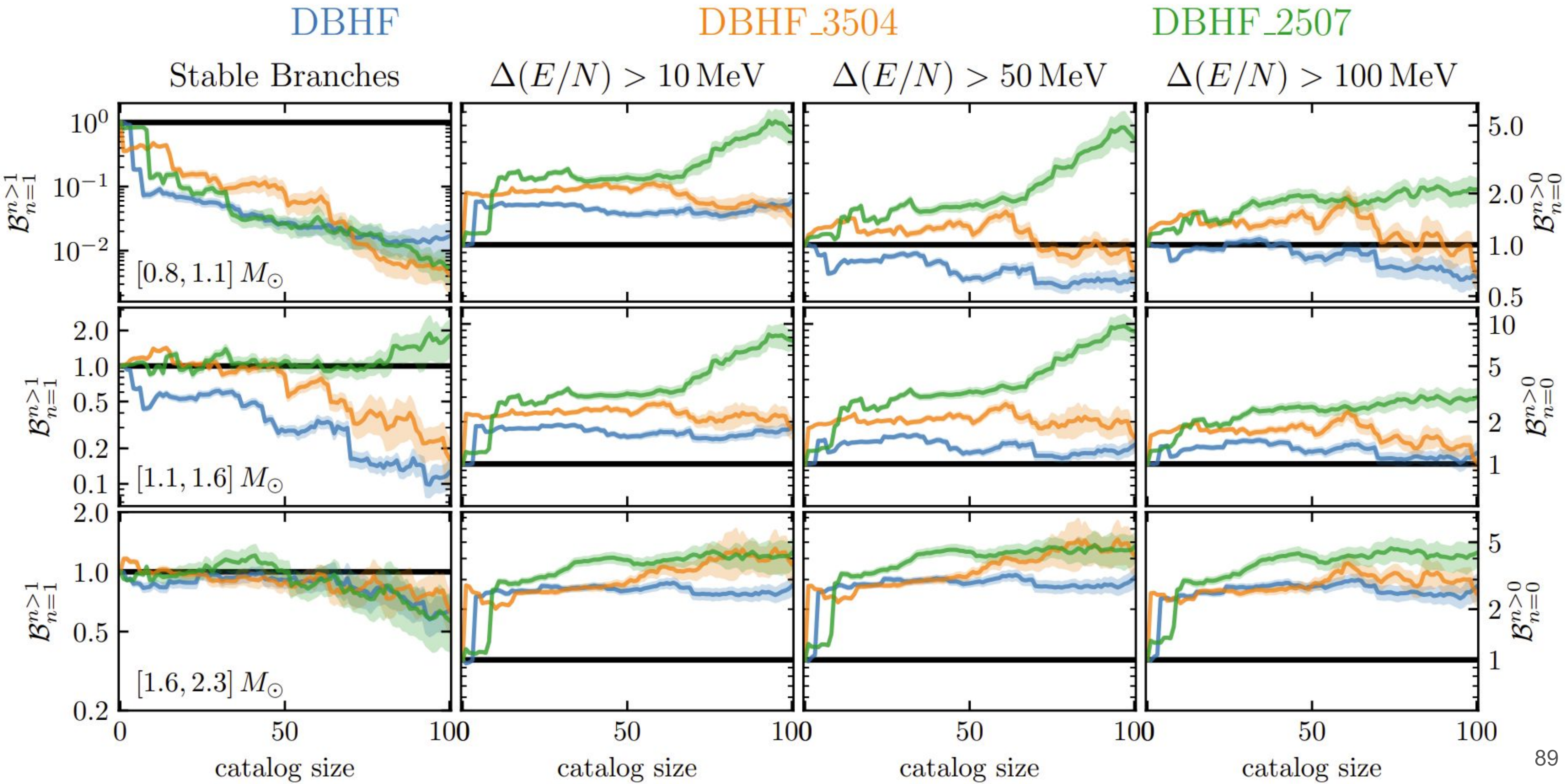

Future Prospects

At a ***fixed SNR***, ***measurement of tides is worse***

- low-freq sensitivity increases more than high-freq sensitivity for “nominal” CE (e.g., Essick 2022)

- detectors may be tuned to target tidal effects Srivastava+ (2022)

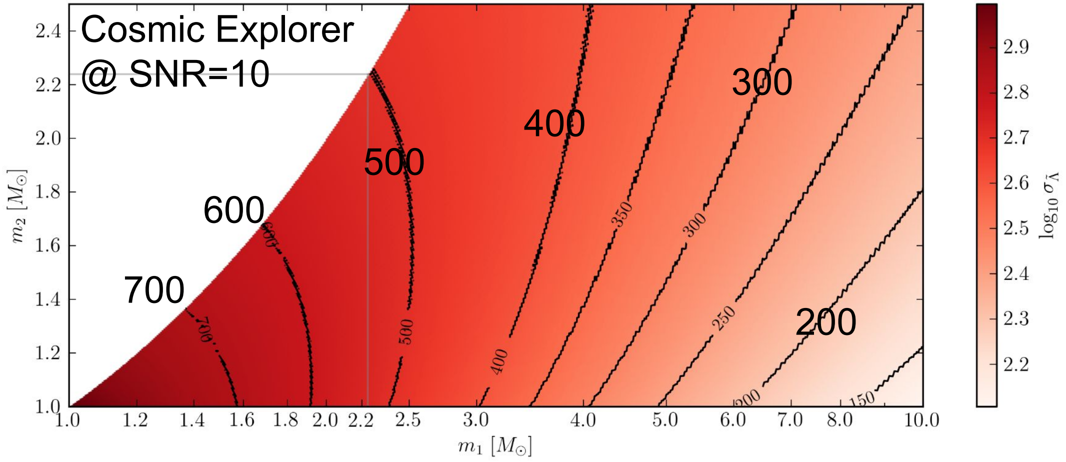

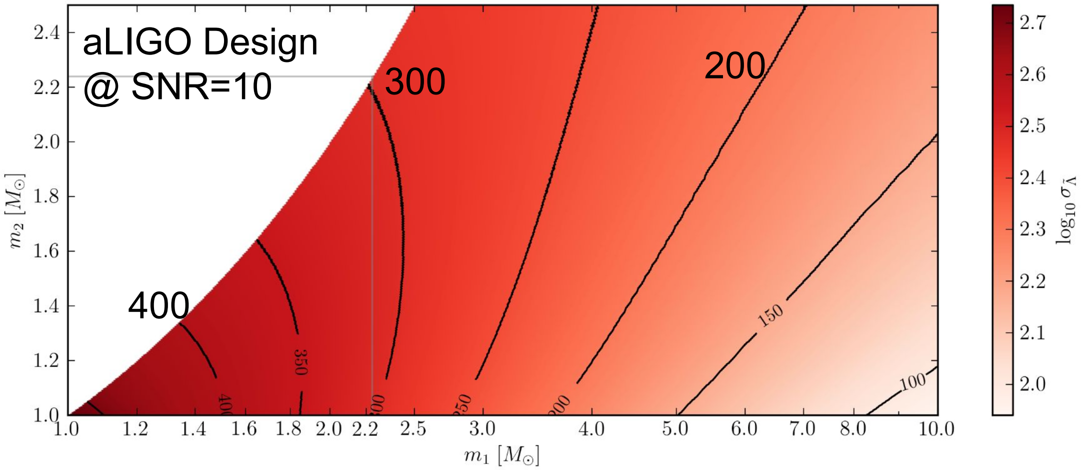

Each individual source will have a higher SNR in 3G than in aLIGO.

→ will the proportion of high-SNR signals be larger in 3G detectors?

Future Prospects

Most low-mass events in 3G will still be near the detection threshold (compare to Vitale 2016)

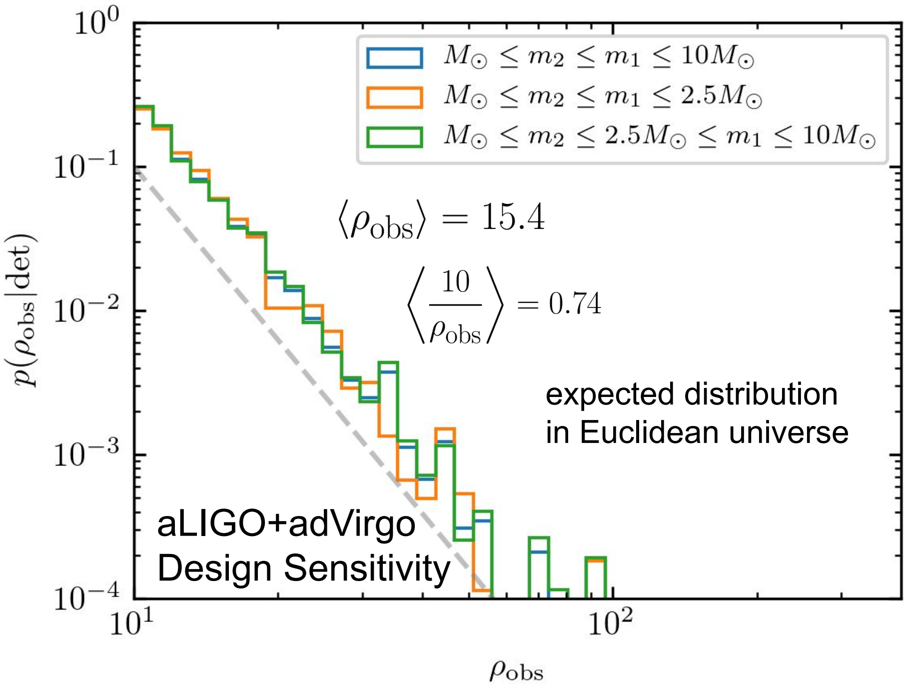

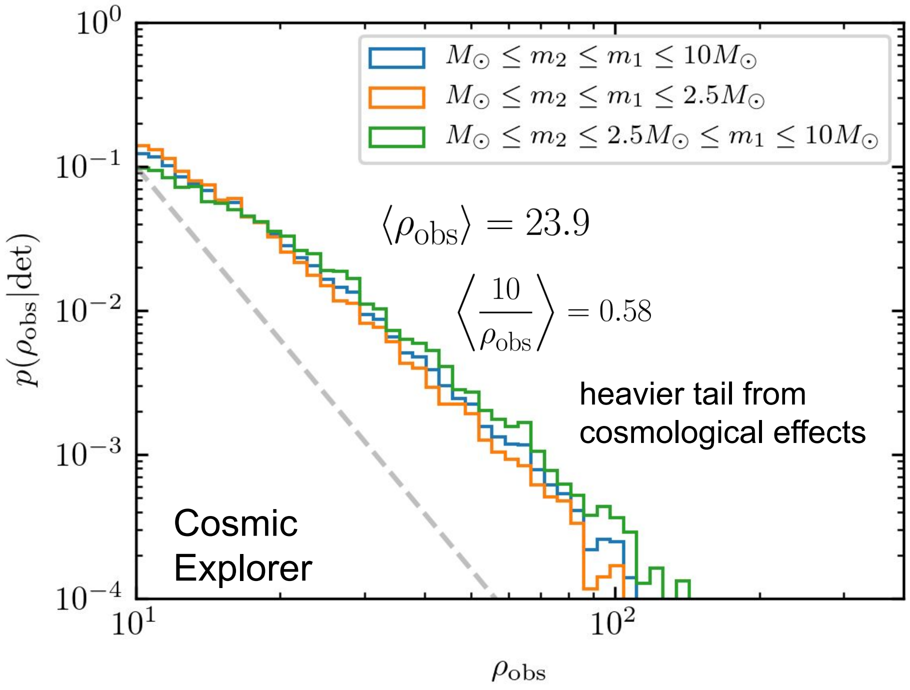

For the average event, increased SNR with CE will ***not*** overcome the decreased precision in adiabatic tidal measurements

Semianalytic GW Sensitivity Estimates

Essick (2023)

maximization over template bank

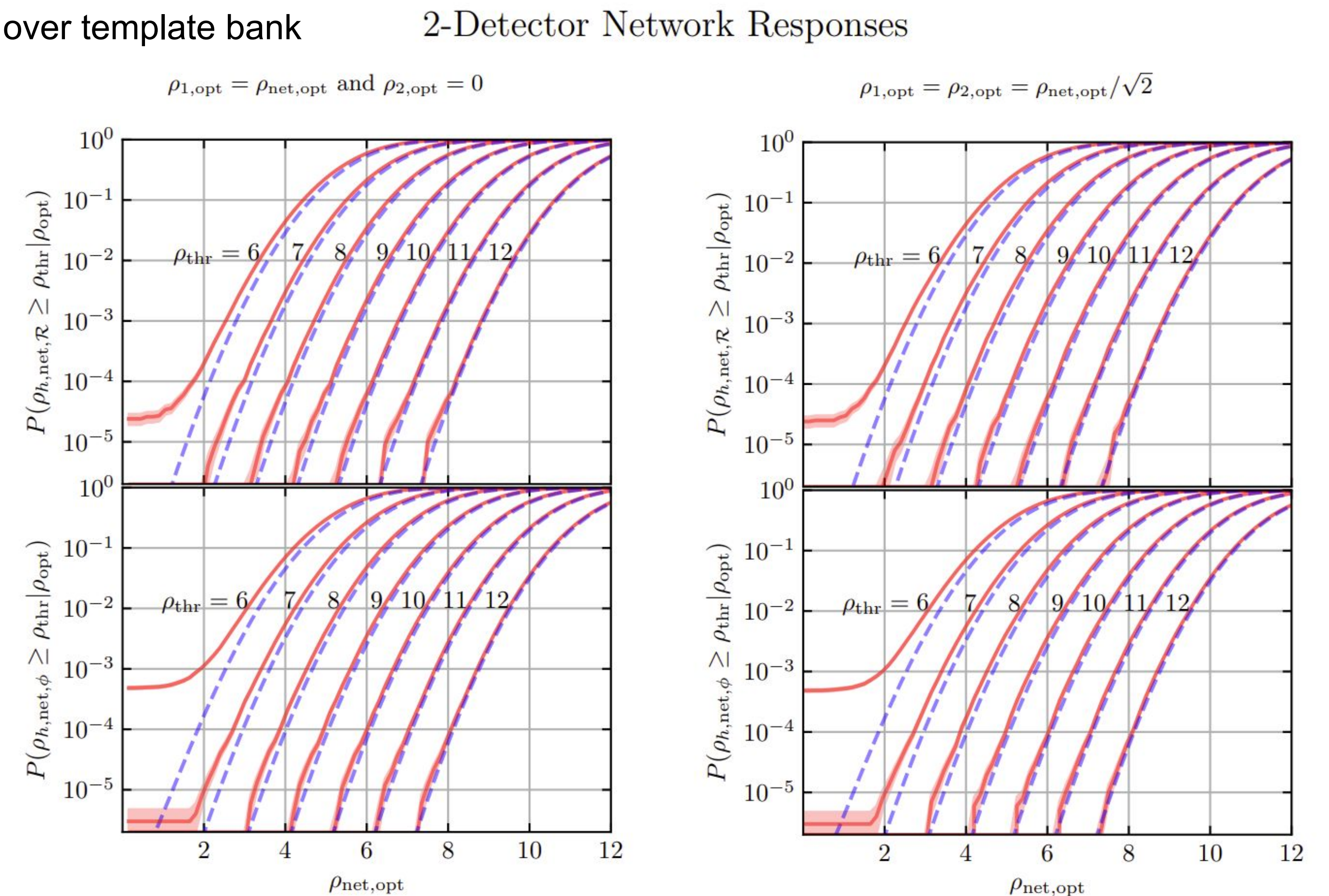

Semianalytic GW Sensitivity Estimates

Optimal vs. Observed SNR

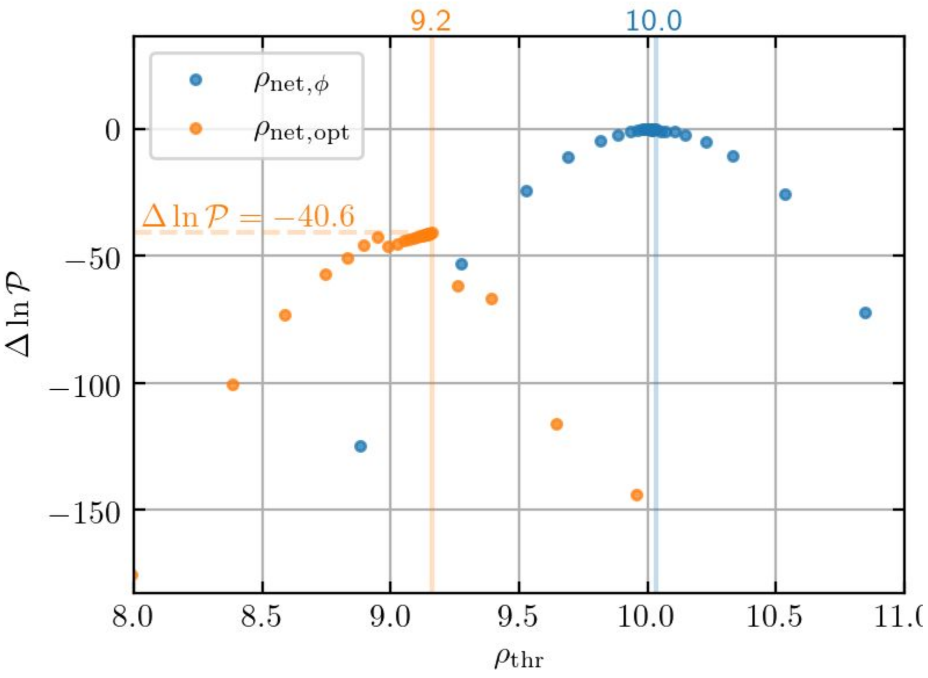

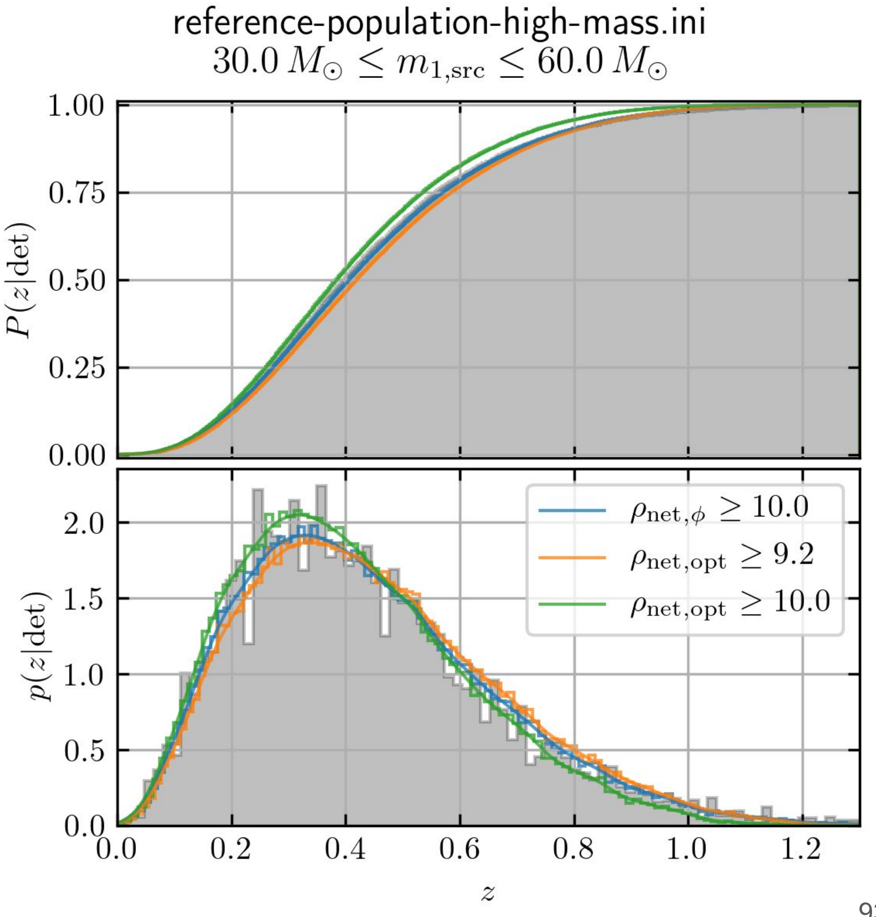

Semianalytic GW Sensitivity Estimates

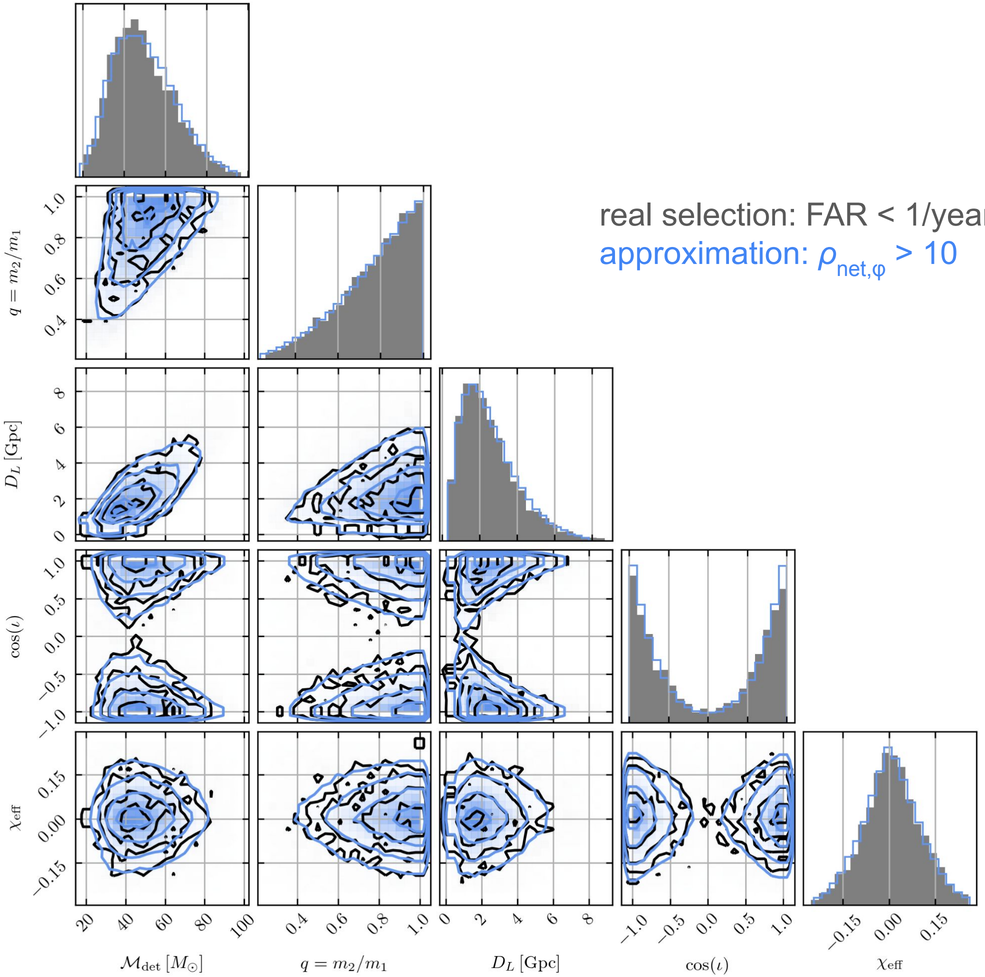

real selection: FAR < 1/year

approximation: $\rho_{\mathrm{net},\varphi}$ > 10

Semianalytic GW Sensitivity Estimates

Essick (2023)

SNR is not a sufficient statistic

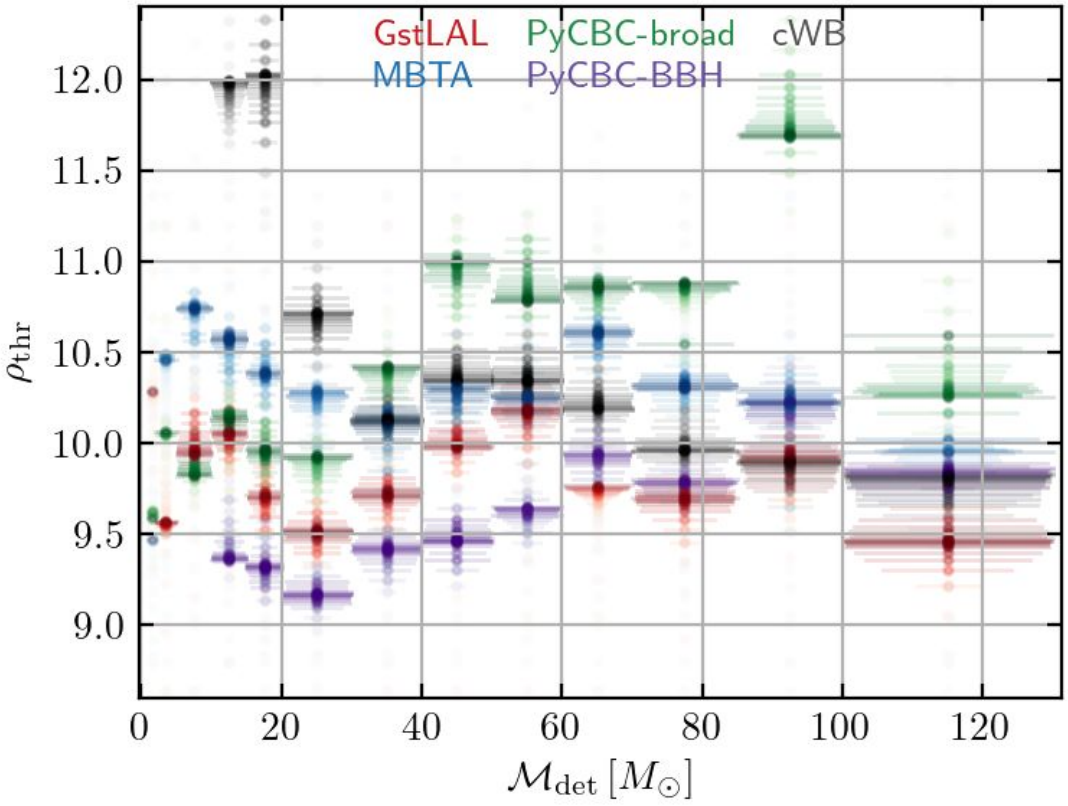

Semianalytic GW Sensitivity Estimates

Essick (2023)

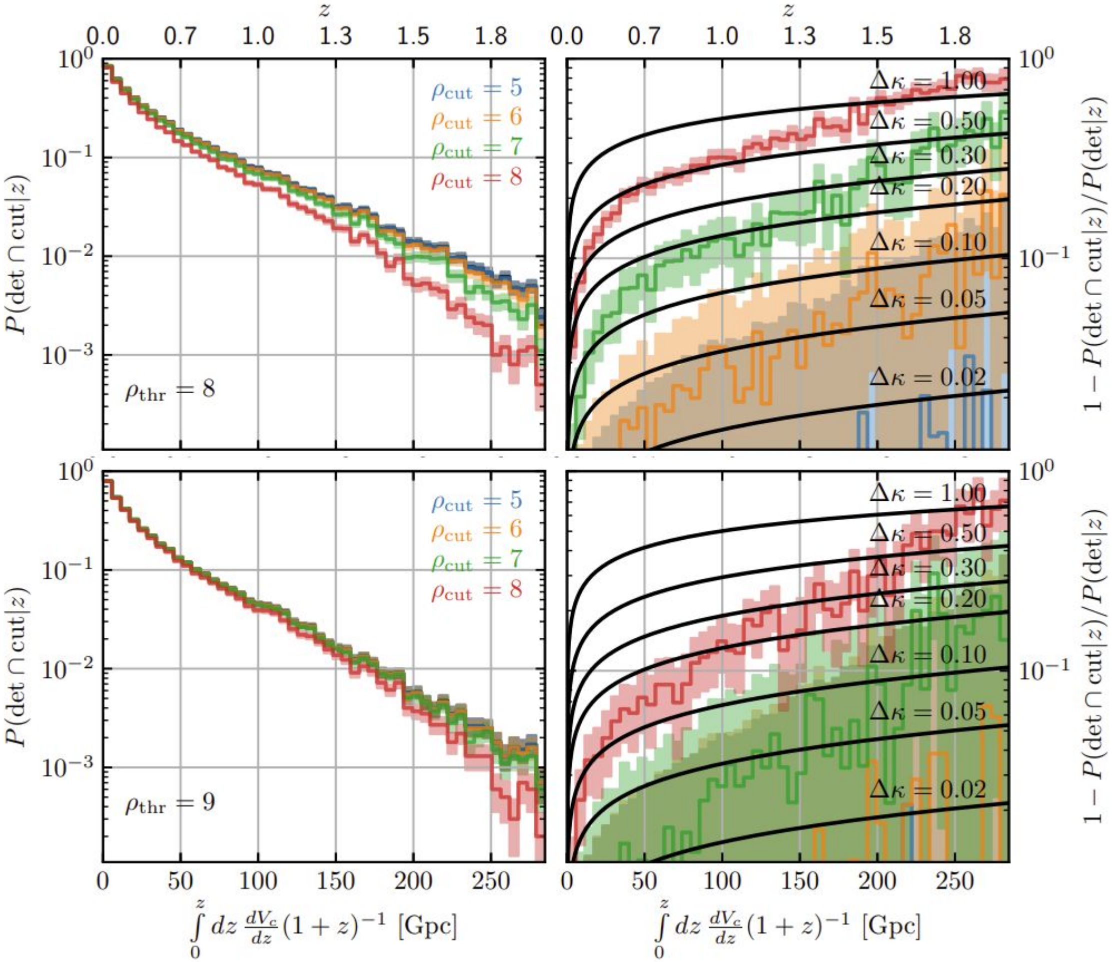

Selection Effects for EM Follow-up to GW Candidates

Chen, **Essick+** (2017)

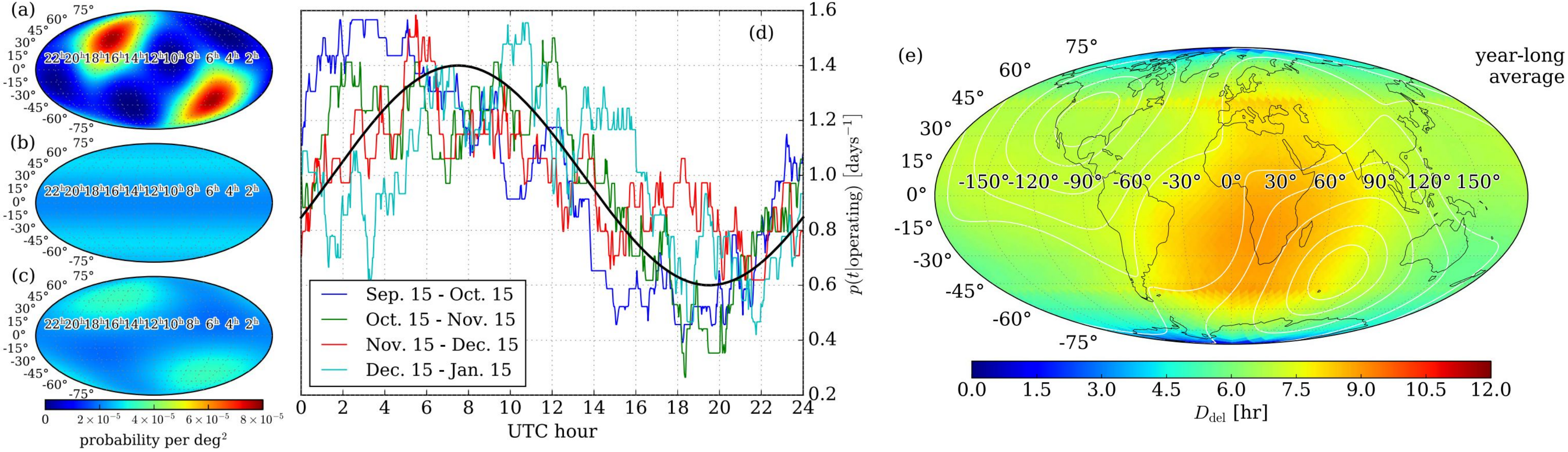

Coarse-Grained Hierarchical Likelihood

Essick+ (2022)

Consider the following: *we only wish retain a limited amount of information about an event* (i.e., it is in a particular region of single-event parameter space)

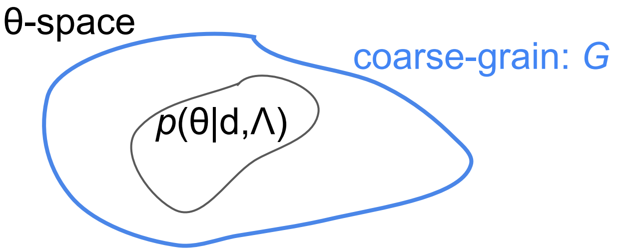

$$\int d\theta\, p(\theta|d,\Lambda)\Theta(\theta \in G) \sim 1 \qquad \forall\, \Lambda$$

Then we can insert the indicator function into the hierarchical model without affecting the distribution

$$p(\{d_i\}|\{\mathbb{D}_i\}, N, \Lambda) \propto \left[\frac{\int d\theta\, P(\mathbb{D}_i|d_i)p(d_i|\theta)p(\theta|\Lambda)\Theta(\theta \in G)}{P(\mathbb{D}|\Lambda)}\right] \prod_{j\neq i}^{N} \frac{\int d\theta\, p(d_j|\theta)p(\theta|\Lambda)}{P(\mathbb{D}|\Lambda)}$$

and finally marginalize over d_i to "forget" everything about the event except that it came from *G*

$$p(\{d_{j\neq i}\}, \theta_i \in G|\{\mathbb{D}_i\}, N, \Lambda) = [P(\theta_i \in G|\mathbb{D}_i, \Lambda)] \prod_{j\neq i}^{N} \frac{\int d\theta\, p(d_j|\theta)p(\theta|\Lambda)}{P(\mathbb{D}|\Lambda)}$$

Coarse-Grained Hierarchical Likelihood

Essick+ (2022)

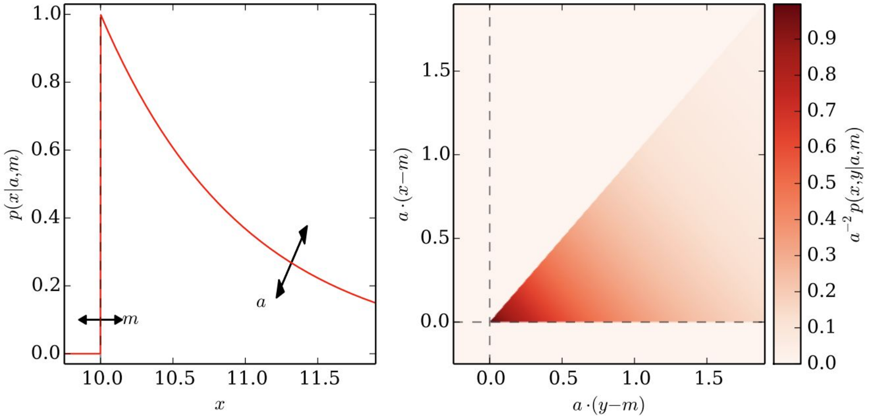

for a simple population model, replacing a simple “leave-one-out” analysis with a coarse-grain is able to correctly identify outliers while retaining meaningful posterior calibration (i.e., passes the *p*-*p* test)

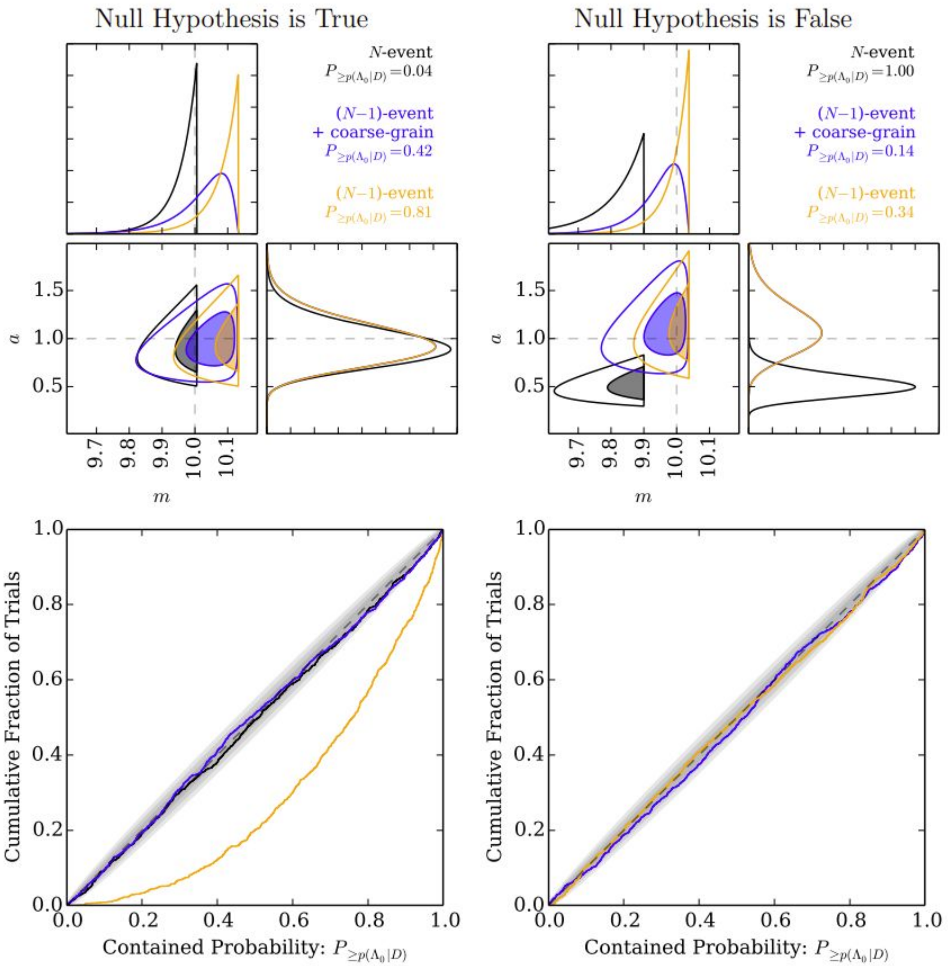

Coarse-Grained Hierarchical Likelihood

worked example: GW190814 in the context of GWTC-3's "main BBH" population

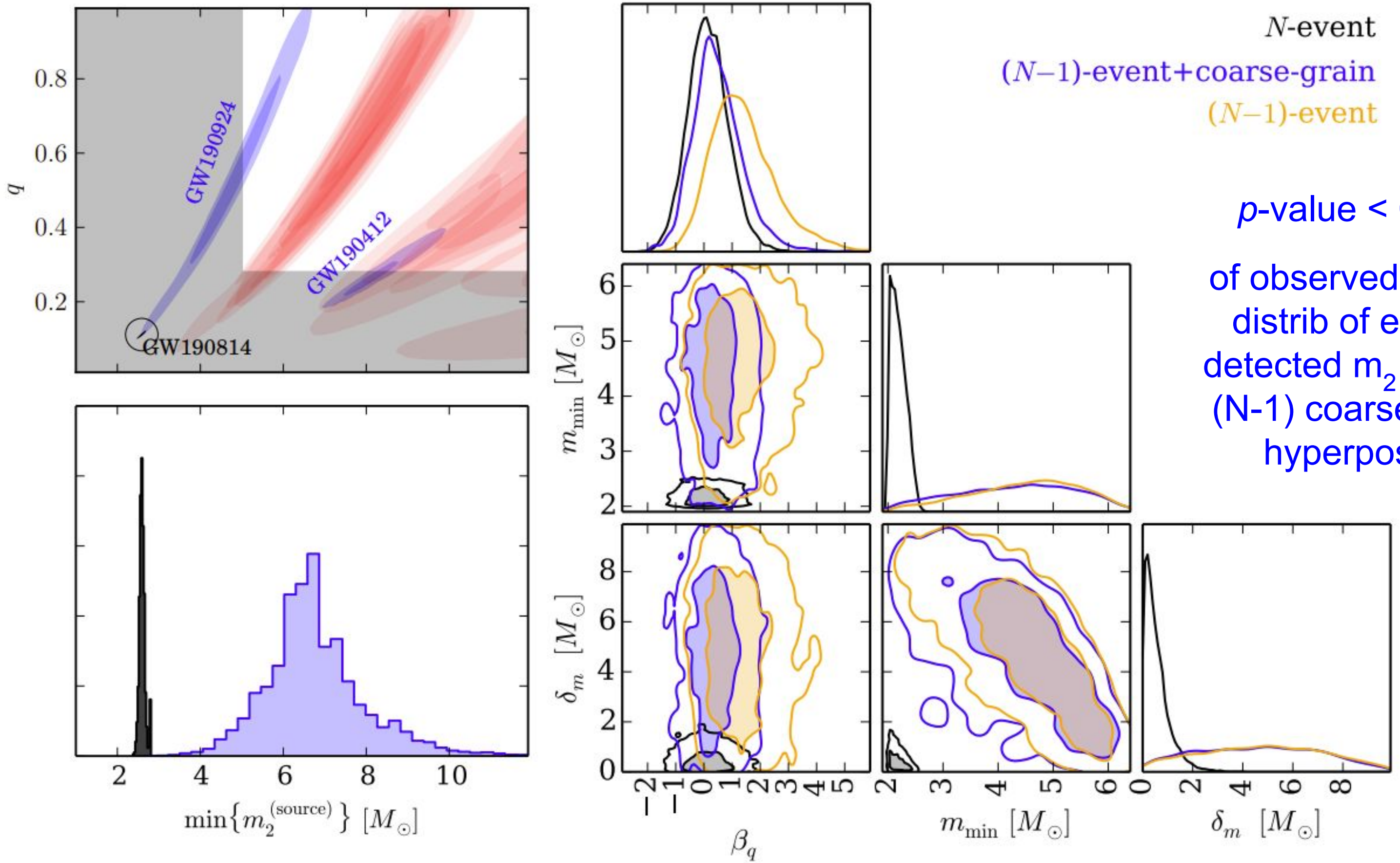

p-value < 0.056%

of observed m_2 given distrib of expected detected m_2 based on (N-1) coarse-grained hyperposterior

Coarse-Grained Hierarchical Likelihood

Essick+ (2022)

GW190412 *p*-value = 22%

GW190521 *p*-value = 20%

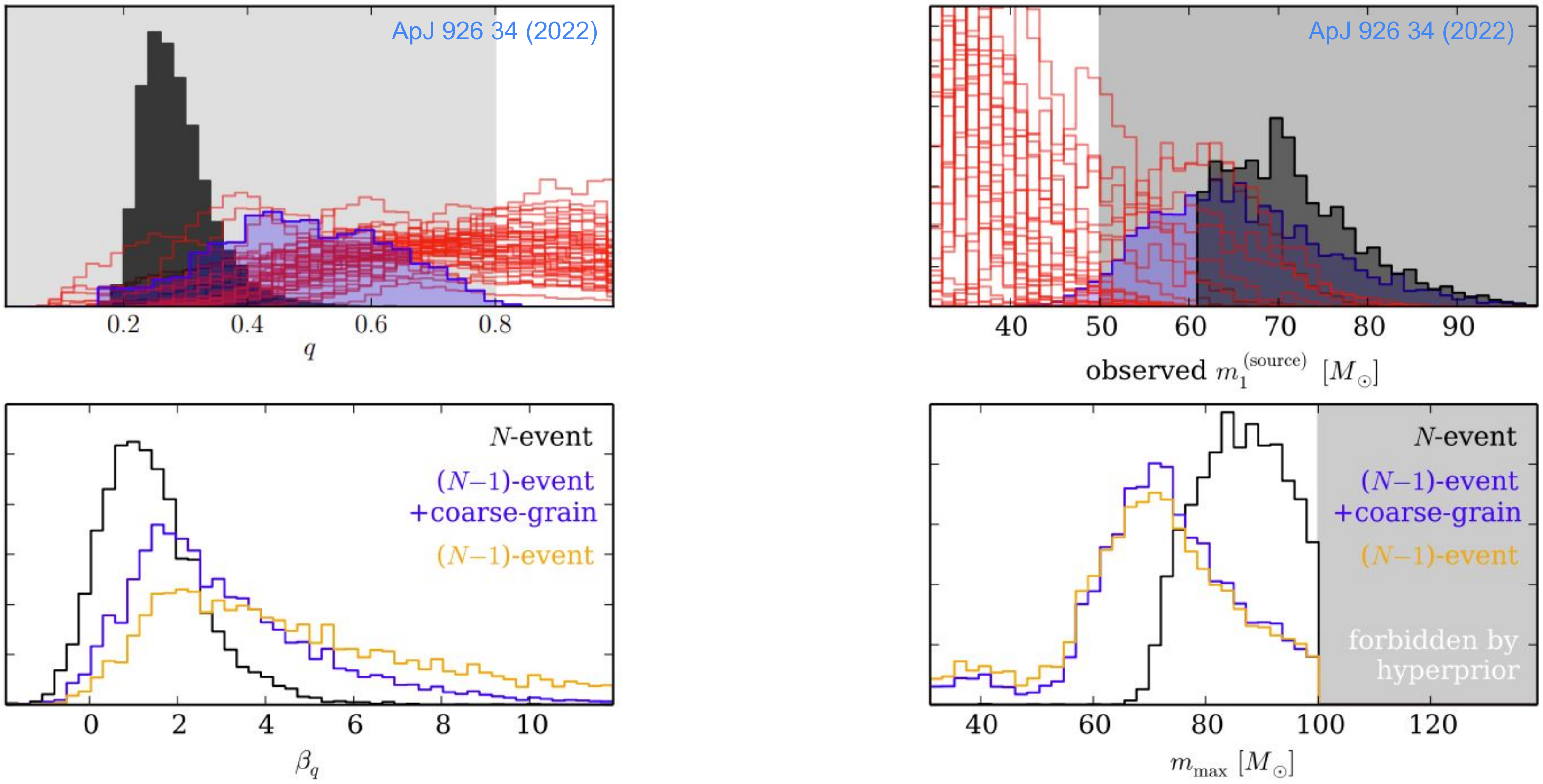

Consistency Between Detection and Noise

Our hierarchical model is

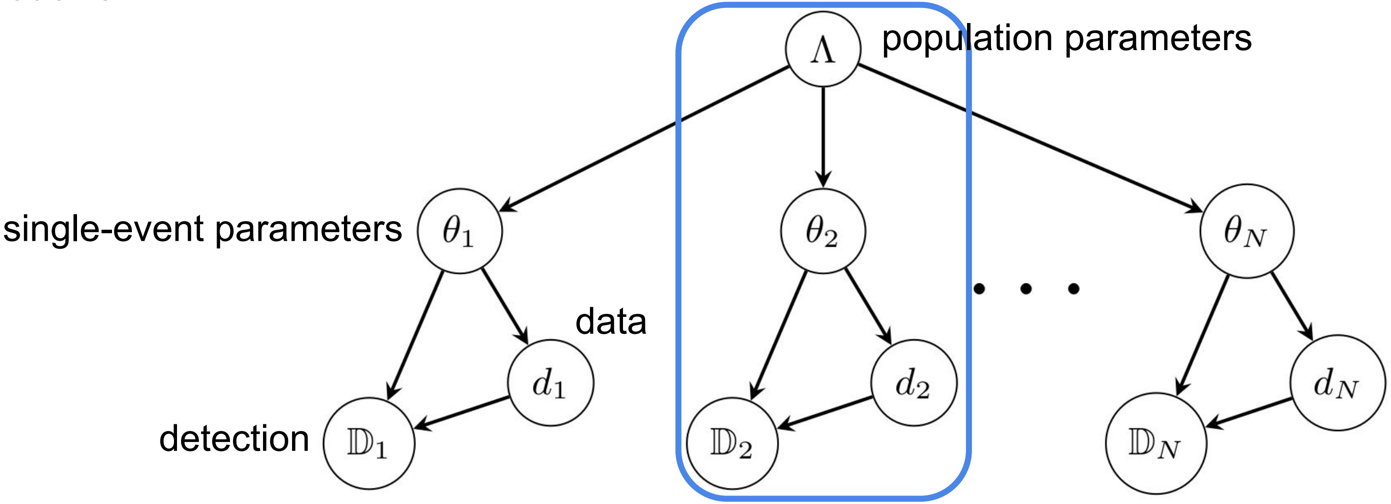

or, equivalently,

$$p(\{\mathbb{D}_i, d_i, \theta_i\}|N, \Lambda) = \prod_i^N \boxed{P(\mathbb{D}_i|d_i, \theta_i)p(d_i|\theta_i)p(\theta_i|\Lambda)}$$

Consistency Between Detection and Noise

Essick & Fishbach (2023)

Physical $P(\mathbb{D}|d,\theta) = P(\mathbb{D}|d)$

$(\mathbb{D} \perp \theta \mid d)$

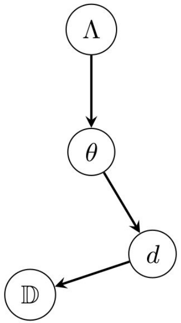

term-by-term cancellation

$$p(\Lambda|\{d_i,\mathbb{D}_i\},N) = \frac{p(\Lambda)\prod_i^N \left[P(\mathbb{D}_i|\Lambda)^{-1}\int d\theta\, \boxed{P(\mathbb{D}_i|d_i)}\, p(d_i|\theta)p(\theta|\Lambda)\right]}{\int d\Lambda p(\Lambda)\prod_i^N \left[P(\mathbb{D}_i|\Lambda)^{-1}\int d\theta\, \boxed{P(\mathbb{D}_i|d_i)}\, p(d_i|\theta)p(\theta|\Lambda)\right]}$$

$$\boxed{\propto p(\Lambda)P(\mathbb{D}|\Lambda)^{-N}\prod_i^N \int d\theta\, p(d_i|\theta)p(\theta|\Lambda)}$$

standard expression

$$P(\mathbb{D}|\Lambda) = \int d\theta\, p(\theta|\Lambda)\int dd P(\mathbb{D}|d)p(d|\theta)$$
$$= \int d\theta\, p(\theta|\Lambda)P(\mathbb{D}|\theta)$$

physical detection processes only have access to the data

Unphysical $P(\mathbb{D}|d,\theta) = Q(\mathbb{D}|\theta)$

$(\mathbb{D} \perp d \mid \theta)$

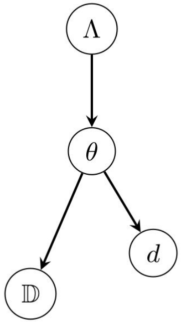

no cancellation

$$q(\Lambda|\{d_i,\mathbb{D}_i\},N) = \frac{p(\Lambda)\prod_i^N \left[Q(\mathbb{D}_i|\Lambda)^{-1}\int d\theta\, \boxed{Q(\mathbb{D}_i|\theta)}\, p(d_i|\theta)p(\theta|\Lambda)\right]}{\int d\Lambda p(\Lambda)\prod_i^N \left[Q(\mathbb{D}_i|\Lambda)^{-1}\int d\theta\, \boxed{Q(\mathbb{D}_i|\theta)}\, p(d_i|\theta)p(\theta|\Lambda)\right]}$$

$$\boxed{\propto p(\Lambda)\prod_i^N \int d\theta\, p(d_i|\theta)q(\theta|\mathbb{D},\Lambda)}$$

fitting the “detected distribution”

$$q(\theta|\mathbb{D},\Lambda) = \frac{Q(\mathbb{D}|\theta)p(\theta|\Lambda)}{Q(\mathbb{D}|\Lambda)}$$

incorrectly models detection as independent of the data given the event’s true parameters

Consistency Between Detection and Noise

Essick & Fishbach (2023)

Physical $P(\mathbb{D}|d,\theta) = P(\mathbb{D}|d)$

$(\mathbb{D} \perp \theta \mid d)$

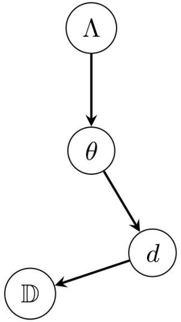

these assumptions are only compatible when

- d is one-to-one with θ — i.e., perfect measurements
- D is independent of both d and θ — e.g., everything is detectable

Unphysical $P(\mathbb{D}|d,\theta) = Q(\mathbb{D}|\theta)$

$(\mathbb{D} \perp d \mid \theta)$

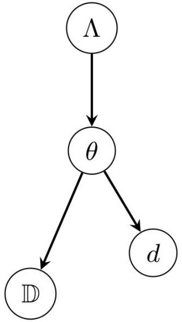

Consistency Between Detection and Noise

Essick & Fishbach (2023)

Fitting the “detected distribution” and then dividing by *P*(D|θ)

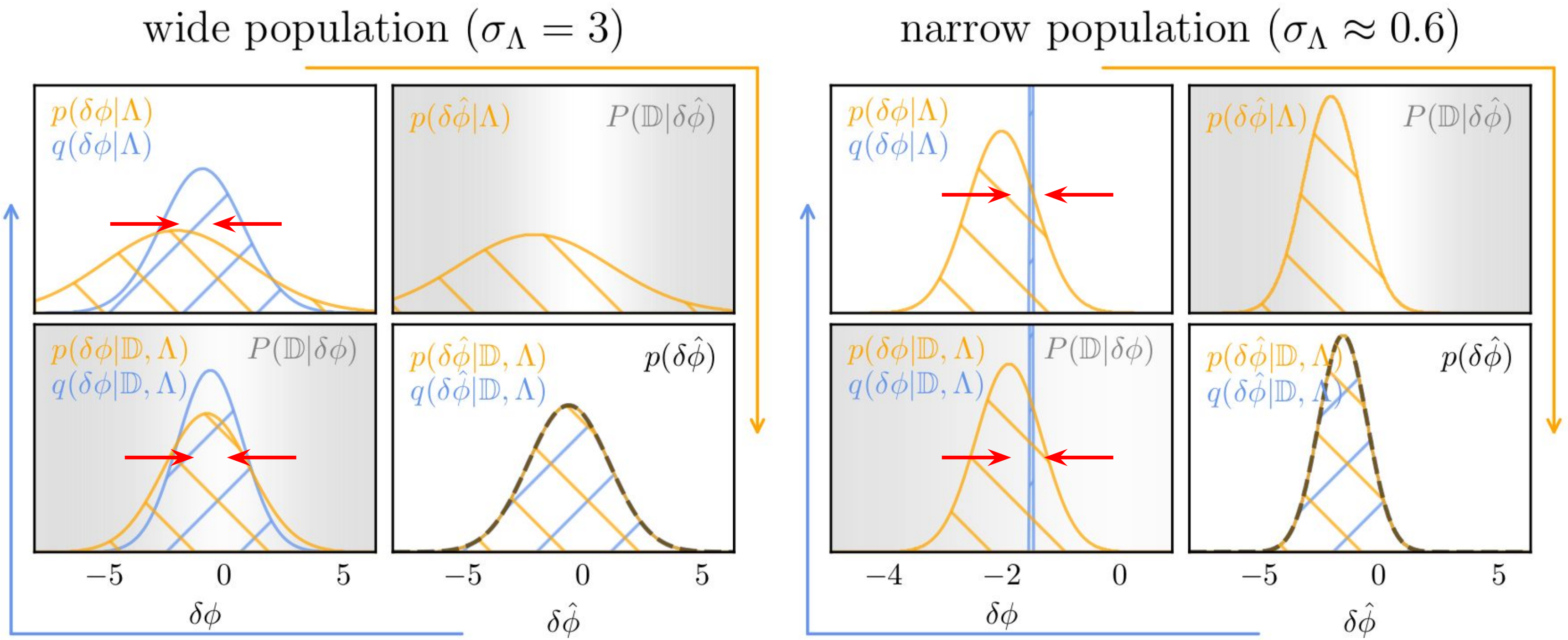

$$p(\delta\phi|\Lambda) = \mathcal{N}(\mu_\Lambda, \sigma_\Lambda^2) \qquad p(\delta\hat{\phi}|\delta\phi) = \mathcal{N}(\delta\phi, \sigma_o^2) \qquad P(\mathbb{D}|\delta\hat{\phi}) = \exp\left(-\frac{(\delta\hat{\phi} - \mu_D)^2}{\sigma_D^2}\right)$$

fitting the "detected distribution" (via the *unphysical DAG*) does ***not*** recover the correct "detected distribution" even when the model can perfectly match the true "detected distribution" (derived under the *physical DAG*)

deterministic selection

$$p(\theta|\Lambda) = (2\pi\sigma_\Lambda^2)^{-1/2} \exp\left(-\frac{(\theta - \boxed{\mu_\Lambda})^2}{2\boxed{\sigma_\Lambda^2}}\right)$$

$$p(d|\theta) = (2\pi\sigma_o^2)^{-1/2} \exp\left(-\frac{(d-\theta)^2}{2\sigma_o^2}\right)$$

$$P(\mathbb{D}|d) = \Theta(\boxed{d_{\mathrm{min}}} \leq d)$$

parameters allowed to vary within *unphysical DAG*'s fit for

$$\boxed{p(\theta|\mathbb{D},\Lambda) = \frac{p(\theta|\Lambda) \int_{d_{\mathrm{min}}}^{\infty} \mathrm{d}d\, p(d|\theta)}{P(\mathbb{D}|\Lambda)}}$$

Astrophysical distribution obtained by dividing by analytic model of detection probability

$$p(\theta|\Lambda) = \frac{p(\theta|\mathbb{D},\Lambda)}{P(\mathbb{D}|\theta)} P(\mathbb{D}|\Lambda)$$